Who Bears Climate-Related Physical Risk?*†

David Wylie,[1∓] Natee Amornsiripanitch,[1] John Heilbron[2], Kevin Zhao[2]

[1]Federal Reserve Bank of Philadelphia,
10 Independence Mall, Philadelphia, PA 19106, USA
[2]Office of Financial Research
717 14th Street NW, Washington, DC 20220, USA

[∓]To whom correspondence should be addressed; E-mail: david.wylie@phil.frb.org.

Abstract

This paper combines data on current and future property-level physical risk from major climate-related perils (severe convective storm, inland floods, hurricane storm surge, hurricane wind, winter storms, and wildfires) that single-family residences (SFRs) face with data on local economic characteristics to study the geographic and demographic distribution of such risks in the contiguous United States. Current (circa 2021) expected damage to SFRs from climate-related perils is approximately $39 billion per year and will rise to $48 billion by 2050 under a "middle-of-the-road" emissions scenario. Severe convective storms are the leading contributor to expected damage, however the riskiest areas are predominantly areas facing hurricane and/or inland flood risk on the Gulf and South Atlantic coasts. Higher current physical risk is associated with lower household incomes, lower labor market participation rates, lower education attainment, higher in-migration, higher increase in expected physical risk by 2050, and lower belief in climate change. Overall, the results suggest that climate risk mitigation policies are likely to be progressive now and into the future.

*The views expressed in this paper are solely those of the authors and do not necessarily reflect the views of the Federal Reserve Bank of Philadelphia, the Federal Reserve Board, the Federal Reserve System, the Office of Financial Research, or the U.S. Department of the Treasury. Any errors or omissions are the responsibility of the authors. No statements here should be treated as legal or investment advice.

†This paper subsumes Section 2 of the OFR Brief "The Uneven Distribution of Climate Risk and Discounts", which also documented cross-sectional heterogeneity in climate risk factors using CoreLogic data.

Introduction

For the majority of American homeowners, housing is, by far, the largest component of their net worth [1]. An open question in the climate risk literature is who bears the current and future climate-related physical risk to residential properties? Since floods are among the most damaging natural disasters related to climate change, the physical risk literature has mostly focused on flood risk [2–4]. However, flooding is just one of several disasters posing current and future risk [5]. Therefore, studies that focus exclusively on floods cannot yield a comprehensive picture of the magnitude and distribution of climate-related physical risk (see Supplementary Information Section E for full discussion of contribution to literature).

We fill this gap by using novel data on current (circa 2021) and future property-level physical risk from six major climate-related perils (severe convective storms, winter storms, inland floods, wildfires, hurricane wind, and hurricane storm surge) that single-family residences (SFRs) face in the contiguous U.S. The physical risk data are produced by CoreLogic, a major commercial catastrophic risk modeler and property data vendor used by private industry and government. CoreLogic's proprietary models incorporate natural hazard information with detailed structure and property characteristics to generate structure-level estimates of loss for climate-related perils.

Our analysis is based on property-level average annual loss (AAL), provided under current conditions and 2050 conditions. AAL is the expected annual loss to the structure generated by simulating many possible iterations of a given year and then calculating the average loss across all iterations. Thus, AALs account for the magnitude of damage resulting from events of different severity as well as the likelihood of events of different severities occurring. CoreLogic reports AALs as share of total insurable value (TIV), which can be understood as the replacement cost of the structure.

Combining the property-level physical risk data with property-specific transactions data, local economic conditions data from the American Community Survey (ACS), and county-level data on climate change beliefs allows us to paint a more comprehensive picture of the magnitude and the (geographic and demographic) distribution of climate-related physical risk in the U.S. In addition, we can identify the specific climate-related perils that are likely to be the costliest now and in the future. The knowledge of the distribution of climate-related physical risk along different dimensions informs policymakers on the segments of the U.S. population that are likely to benefit from policies that aim to mitigate such risks and whether such policies are likely to be regressive or progressive with respect to key socioeconomic characteristics such as income and education attainment, a proxy for earning potential [6].

Results

What is the level and composition of current physical risk?

We estimate the all-peril average AAL among our sample of 97 million SFRs in the contiguous U.S. is 0.17% of TIV and $401, in dollar terms. Thus, national annual expected losses total $39 billion. In Table 1, we show the contribution of the six climate-related perils to expected losses (using AAL measured as percent of TIV). Severe convective storm is the leading contributor, accounting for about one-third of expected losses. This is largely a result of the ubiquity of severe convective storms. Nearly every SFR in the contiguous U.S. has some severe convective storm risk.

Inland flood is the next largest contributor, followed by hurricane wind. Both perils have the potential to impact a very similar number of SFRs, but inland flood is more damaging on average, as evidenced by larger average AALs among SFRs with non-zero risk. This is driven by the long right tail of the distribution of expected losses from inland flood – SFRs at the 99^{th} percentile of inland flood expected losses face expected losses of 2.46% of TIV compared

to 0.60% of TIV for hurricane wind. The other flood-related peril, hurricane storm surge, is the only other peril to have that wide of a range of AALs. However, hurricane storm surge's contribution to national expected losses is limited because 95% of SFRs face no hurricane storm surge risk.

Wildfire is the smallest contributor to national expected losses due to a combination of relatively small geographic reach and relatively low AAL, conditional on facing non-zero wildfire risk. Wildfire surpasses hurricane storm surge when measuring AALs in dollars due to greater SFR structure value in wildfire-exposed areas (see Supplementary Table 1).

What is the geography of current physical risk?

The decile of tract average AAL (measured as percent of TIV) is mapped in Fig. 1(a). The least risky areas – colored in dark blue – are largely in the western U.S. Over 85% of the tracts in the lowest decile of tract average AAL are in the Pacific region, which includes California, Washington, and Oregon. The Pacific region has relatively low severe convective storm risk and does not have any modeled hurricane-related risk (see Supplementary Tables 1 and 7).

The riskiest areas – colored in dark red – are clustered, to different extents, in parts of California, the central U.S., Appalachia, and the Gulf and Atlantic coasts. The predominant peril in each of these areas differs – wildfire in California, severe convective storm in the central U.S., inland flood in Appalachia, and hurricane-related risk along the Gulf and Atlantic Coasts (see Fig. 2). The states with largest shares of tracts in the top risk decile are all coastal states: Florida (22%), Texas (17%), and Louisiana (12%).

The riskiest tracts are distinctive both in terms of their magnitude of expected damage and their peril composition. As shown in Fig. 1(b), the distribution of tract average AALs is right-skewed. Tracts in the top decile of expected losses are over five times as risky as the median tract and more than twice as risky as tracts in the ninth decile, on average. Tracts in the top

decile face a substantially higher level of risk compared with other tracts, largely because of hurricane - and inland flood-related damage – those perils comprise over 80% of expected losses in the top decile tracts. Despite severe convective storm accounting for the greatest share of expected damage across the country, expected damage in the riskiest areas of the U.S. is driven by hurricane and flood risk.

In fact, if we examine the very top of the risk distribution, the differences in magnitude and composition of risk become even starker. Tracts in the top 1% of the distribution have an average more than 14 times as large as the median tract AAL. Nearly all of the expected losses in these very risky tracts is attributable to hurricane and flood risk (see Supplementary Table 2). Among the top 1% riskiest tracts, 30% are in Louisiana, 26% are in Florida, 12% are in Texas, and 8% are in Mississippi. Nearly half of the tracts are in either the New Orleans-Metairie (28%), Miami-Fort Lauderdale (12%), or Gulfport-Biloxi (7%) metro areas.

In Supplementary Fig. 1, we plot the tract-level average AALs in terms of dollars, by the percentile of tract average AAL. We estimate that the top 1% of tracts in terms of expected losses in dollars account for 10% of total expected dollar losses in the U.S.; the top 10% of tracts account for 40% of total expected dollar losses.

Who demographically bears current physical risk?

Table 2 shows select tract characteristics by AAL decile based on the 2019 American Community Survey (ACS) five-year estimates. Tracts in the highest-risk decile have, on average, lower education attainments, lower household incomes, lower prime age (25 to 54) labor force participation rates, and higher non-seasonal vacancy rates, a proxy of neighborhood quality [7]. The differences between the highest-risk decile and the fifth decile are substantial: 18% lower higher education attainment rate, 16% lower household income, 5% lower prime age labor participation rate, and 74% greater non-seasonal vacancy rate. The differences are even greater

between the highest-risk decile and the lowest-risk decile.

Urban status is a contributor to the pattern shown in Table 2. Urban tracts face less physical risk, on average, than rural tracts as illustrated by the fact that the share of tracts that are urban core tracts decreases across tract AAL deciles, while the share of rural tracts increases. However, the differences in tract characteristics remain qualitatively and quantitatively similar when we limit the analysis to only urban core tracts (see Supplementary Table 3), so the empirical pattern that we observe in Table 2 is not explained by the degree of urbanization.

To further investigate the peril-specific drivers of the regressivity of physical risk, we look at tract average AALs broken down by peril for each decile of median household income. Fig. 3(a) shows a near-linear decrease in expected losses from the lowest to highest tract income deciles. The highest-income decile faces only about two-thirds of the risk that the lowest income decile faces, on average. Notably, the share of AAL that comes from inland flood increases substantially as we move down the income deciles. In fact, in the bottom quintile income tracts, inland floods are the primary contributor to average expected losses. We see similar patterns when examining educational attainment, labor force participation rate, and vacancy rate (see Fig. 3(b)-(d)).

Additionally, the pattern in local economic characteristics we observe appears to be driven more by cross-metro than intra-metro differences. The income difference between high- and low-risk tracts attenuates when we sort tracts within metropolitan statistical area (MSA) average AAL deciles (see Supplementary Table 4). The prime age labor force participation rate, vacancy rate, and educational attainment patterns show similar attenuation. We do see larger White population share in riskier areas using the within-MSA sort.

Next, we investigate whether climate-related physical risk is correlated to changes in tract characteristics from 2010 to 2019 across current average tract AAL deciles. Table 3 shows larger increases in the vacancy rate, larger decreases in prime age labor force participation,

and smaller increases in education attainment in tracts in the upper AAL deciles. The gap in economic conditions between high- and low-risk areas appears to be increasing over time. The empirical patterns suggest that climate-related physical risk itself and/or the realization of such risk may be important determinants of economic performance, but it is not the focus of the current paper to evaluate the potential causal nature of the relationship or potential mechanisms [8].

While we do see smaller average 2010–2019 total population change in riskier areas, we do not find evidence that, in aggregate, people are migrating away from higher- risk areas during that period. The results in Supplementary Table 5 suggest net movement into higher risk areas based on tracts' all-peril AAL. While our analysis does not lend itself to a causal claim regarding the marginal impact of climate-related physical risk on migration, our analysis does indicate that such risk is not sufficiently influential for migration decisions such that, in aggregate, people are moving away from risky areas [9].

Finally, we examine how beliefs about climate change are related to physical risk faced across the contiguous U.S. Due to data limitations, we perform this analysis at the county level. We find that counties with the greatest physical risk were least likely to believe global warming is happening (see Supplementary Table 6). We also find that a more muted, but directionally similar pattern when counties are sorted by the share of respondents who say they have been personally affected by global warming. Together, the results suggest that neither personal experience of climate-related events nor the estimated current physical risk are determining whether people believe that climate change is happening. One potential contributor to these observed patterns is political beliefs, which has been shown to be related to beliefs about climate change [10].

What does future physical risk look like?

Climate-related physical risk is expected to increase in the future because of climate change [11]. Future climate scenarios are characterized by Representative Concentration Pathways (RCPs), which depict different trajectories of greenhouse gas emissions that then affect different climate-related outcomes. Under the middle-of-the-road scenario, RCP 4.5, we estimate that expected losses for SFRs in the contiguous U.S. will increase by 3.8 basis points of TIV by 2050. This represents a 22% increase on the current average AAL of 0.17% of TIV (see Table 4). Under a more severe emissions scenario, RCP 8.5, we estimate an average increase in expected losses of 5.6 basis points of TIV, a 33% increase.

In dollar terms, we estimate expected damages will increase by 24% to $48 billion under RCP 4.5 and by 36% to $53 billion under RCP 8.5. These estimates are based on the 2021 inventory of SFRs and therefore represent the change in expected dollar losses that are attributable exclusively to the change in risk from the six climate-related perils.

On a percentage increase basis, hurricane storm surge will undergo the largest increase in risk by 2050. Expected damage from hurricane storm surge will increase by about 75% by 2050 under RCP 4.5 and, under the more severe RCP 8.5, it will more than double. The perils exhibiting the next largest growth in expected damages are wildfire and severe convective storm.

The largest increases in AAL will occur in the regions where current AALs are the greatest. Fig. 4(a) plots the tract-average change in AAL by the tract-average current AAL. There is a clear positive relationship — higher-risk tracts today will, on average, experience greater increases in physical risk.

The changes in AAL in current highest risk decile areas are driven more by hurricane-related risk than they are in the lower-risk deciles areas, where severe convective storm makes up a larger share of the projected change. The strong positive relationship between current risk and future risk is robust to uncertainty surrounding the relationship between climate change and

the intensity of severe convective storms, which is considered the least well understood peril, in terms of how climate change will impact it in the future [11, 12]. Fig. 4(b) shows a version of Fig. 4(a) without severe convective storm. We see that the relationship between current risk and the change in risk is largely unchanged.

Discussion

In this analysis, we provide a comprehensive accounting of the climate-related physical risk to SFRs in the contiguous U.S. However, our study has several notable limitations. Because of data limitations, we cannot make claims about the expected damage to other property types (e.g., multifamily residential properties, commercial properties, public infrastructure, etc.). Additionally, we are not capturing non-property or indirect losses, such as loss of business, hardship costs, mortality costs, or the cost of potential lost future growth [13]. Last, we do not differentiate between the proportion of the cost that will be borne by insurance companies and the proportion of the cost that will be borne by homeowners [14].

Our distributional analysis provides insights into where and who bear the physical risk. Geographically, the safest areas tend to be in the western U.S. while the riskier areas tend to be in the southeastern and central parts of the country. Within those riskier areas, it is the hurricane- and flood- exposed areas on the Gulf and South Atlantic Coasts that face the greatest risk, along with some inland flood exposed areas, like parts of Appalachia. Severe convective storms are estimated to be the largest contributor to expected losses across the U.S., but the areas with the largest expected losses are largely hurricane- and flood-exposed areas. Demographically, we find that low-income, less educated, low labor market participation, and low-amenity areas face the greatest physical risk. Inter-metro differences in local economic conditions across the distribution of physical risk appear larger than intra-metro differences.

Altogether the results suggest that areas that are relatively less economically vibrant face

the greatest risk of disruption from climate-related perils. The correlation between current physical risk and the estimated future change in risk suggests the current relationship between physical risk and local economic conditions will remain into the future. Thus, policies that aim to decrease the underlying physical risk (e.g., slowing global temperature increases) and/or mitigate the impacts of these climate-related perils will likely be progressive now, and into the future [15]. With insurance markets in place, realized damages are likely to manifest in the form of higher insurance premiums and disruption to general economic activities in the affected areas. However, as insurance companies pull out of risky markets, realized damages are likely to fall fully on homeowners, or, in the case of rental SFRs, on a combination of homeowners and renters [16]. Lack of insurance coverage has already been the reality in some inland areas that face considerable flood risk but have low flood insurance take-up because the area is not designated by FEMA as a Special Flood Hazard Area [17, 18]. The concerns regarding low flood insurance take-up is heightened by the fact that inland flooding is the most regressive peril in our analysis and FEMA's analysis suggests the insurance gap is more pronounced for low-income households [19].

While a full investigation of the mechanisms driving the regressivity of climate-related physical risk is beyond the scope of this paper, we do offer a few possibilities for further exploration. First, the income pattern we observe is consistent with climate-related physical risk being viewed as a "bad amenity" by households [20, 21]. Second, the strength of the inter-metro differences we observe is consistent with lower income households being priced out of more expensive metro areas that tend to face less physical risk. Barriers to new housing development (e.g., regulatory and physical constraints) in safer regions may be of particular importance [22, 23]. Lastly, the relationship between beliefs about climate change and physical risk suggests that people may have beliefs about climate change that differ from the empirical measure of risk we employ. Therefore, the regressivity of climate-related physical risk may be partly driven by

the correlation between income, education attainment, and access to accurate information. Further research is needed to evaluate these potential mechanisms.

Methods

Estimates of Average Annual Loss

The AALs used in this analysis are sourced from CoreLogic, which is a major commercial catastrophic risk modeler and property data vendor. CoreLogic's climate risk data is used in private industry as well as by several government agencies [24]. For example, CoreLogic's inland flood and storm surge models were recently used in the Federal Emergency Management Agency's (FEMA's) "Risk Rating 2.0", which revamped the National Flood Insurance Program's (NFIP's) rate-setting procedures to better align charged insurance premiums with property-specific risk [25]. Other users of CoreLogic's climate risk data include the Department of Veteran's Affairs, the Department of the Treasury, and several large banks conducting climate impact analyses. These banks include Flagstar Bank, US Bank, UBS, Bank of Montreal, and Stancorp [26, 27]. CoreLogic's climate risk estimates have also been employed in recent academic research on insurance markets and climate change [28].

CoreLogic provides AAL estimates for approximately 190 million structures in the contiguous United States. AALs are expected losses, meaning they represent the loss per year averaged over many possible iterations of that year. Mathematically, the AAL is the area under the exceedance probability curve, which, for every possible loss amount, provides a likelihood that the loss amount will be met or exceeded for a given structure. Importantly for our multiperil analysis, AALs are additive because they are expectations. CoreLogic's AALs are ground-up losses, meaning they represent gross losses to the structure and contents prior to applying any insurance policy terms (e.g., deductible). The AALs generated by CoreLogic's loss modeling are expressed as a share of total insurable value (TIV), and therefore range from 0 to 1 for

any single peril and structure. TIV can be thought of as the replacement cost of the structure; however, note that the TIV is not used directly in generating the AAL estimate. In other words, AAL is not generated by first estimating the expected annual loss in dollars and then dividing by the TIV.

This paper uses AALs based on current conditions (circa 2021) and on conditions in 2050 under two different greenhouse gas emissions pathways: Representative Concentration Pathways (RCPs) 4.5 and 8.5, as specified in the Intergovernmental Panel on Climate Change's Fifth Assessment Report (IPCC AR5) [29]. Our main 2050 risk estimates are based on RCP 4.5, which depicts a "middle-of-the-road" climate scenario. RCP 4.5 is associated with a global mean surface temperature increase of 0.9–2.0 degrees Celsius by the mid-21st century (relative to 1986–2005), while the more severe business-as-usual scenario, RCP 8.5, is associated with an increase of 1.4–2.6 degrees Celsius. In terms of global mean sea level rise, the increase by the mid-21st century under RCP 8.5 is expected to be about 15% larger than it would be under RCP 4.5 [30].

The AALs are generated by CoreLogic's proprietary climate, hazard, and vulnerability models (see Supplementary Information Section F for CoreLogic's modeling documentation). Inputs to CoreLogic's modeling consist of natural hazard information and "industry-leading property data" [31]. These models account for future changes to environmental conditions, but they do not incorporate any changes to development. All 2050 AAL estimates are based on the current stock of structures.

Since AALs are slow-moving measures, we interpret the current AALs as being relatively constant between 2019 and 2021. Therefore, in sections where we merge in other data sources to study the correlation between current AALs and other variables of interest (e.g., local economic conditions, migration patterns, and so on), we use data ranging from 2019 to 2021. Where possible, we perform robustness checks to show that the results are qualitatively and quantitatively

similar across data year choices.

It is important to note that the AAL estimates are model-generated and, hence, they inherently contain a degree of uncertainty around the point estimates that we use in our analyses. The sources of uncertainty include CoreLogic's modeling choices and the choice of historical data sets used to feed the models. We cannot assess the degree of uncertainty because CoreLogic does not provide the necessary data.

Validating AAL estimates is difficult because the ground truth is unknown. CoreLogic performs validation exercises on its model output to test reasonableness. While specific validation analyses vary by peril, they typically involve comparison with data on historical events and, if available, damages from those events (see Supplementary Information Section F for full description of CoreLogic's validation exercises). In our own validation exercise, we find our national expected loss total to be reasonable when compared with long-run historical losses recorded in the Spatial Hazard Events and Losses Database for the United States (SHELDUS). The SHELDUS comparison and full methodology is discussed in Supplementary Information Section A. Using SHEDLUS data we also show that expected loss estimates based on CoreLogic's AALs have predictive value above using past realized disaster (see Supplementary Information Section B). Additionally, as a robustness check on our distributional analyses, we show that tract-level averages based on CoreLogic's AALs correlate moderately well with tract-level averages based on AAL estimates from a different risk modeler for a subset of perils (see Supplementary Information Section C). Agreement between the two sets of tract-level estimates is strongest at the top end of the risk distribution.

Perils

We focus on AALs for six climate-related perils provided by CoreLogic: inland floods, hurricane wind, hurricane storm surge, severe convective storms, winter storms, and wildfires. We

selected these perils because they are likely to be affected by future environmental changes brought on by climate change. By this logic, we ignore data on earthquake-related perils. The perils are defined to be mutually exclusive and consistent with insurance industry practices. For example, water damage resulting from hurricane wind tearing off part of a roof and allowing for rainfall to enter the home would be considered hurricane wind damage and would be covered under a standard homeowner's insurance policy. However, water damage resulting from a stream overflowing because of hurricane precipitation would be considered inland flooding damage and would not be covered under a standard homeowner's insurance policy.

The peril descriptions from CoreLogic are as follows:

1. **Inland Flooding** – Inundation caused by (1) water in an existing waterway (river, stream, or pond) rising overtop the normal banks and spreading onto adjacent land, (2) ponding of rainwater in low-lying areas, and/or (3) coastal flooding from unusually high tides, strong onshore winds, and storm surge associated with a landfalling strong storm (other than a hurricane). Water depth, flow velocity, building age, first floor height, construction type, occupancy type, number of stories, and presence of a basement are considered in determining damage.

2. **Hurricane Wind** – Damage caused by sheer force of hurricane wind (>74 mph one-minute sustained wind speed at landfall) and any resulting water damage from precipitation entering the structure. The peak gust, flood depth and velocity, structure type, occupancy type, and total value of the exposure are considered in determining damage.

3. **Hurricane Storm Surge** – Inundation caused by hurricane-force winds (>74 mph) pushing shallow coastal waters in such a way that the sea level rises. Powerful storms can cause up to 30 feet of storm surge. Storm surge flood depth and velocity can depend on factors like variations in astronomical tides, flood defense systems, and first floor eleva-

tion of building. Storm surge flood depth and velocity, structure type, occupancy type, and total value of the exposure are considered in determining damage.

4. **Severe Convective Storm** – Damage caused by one of three different types of storms: tornadoes, hailstorms, or straight-line winds (e.g., squall or derecho). The hazard intensity, structure type, occupancy, building material, cladding, and height of structure are considered in determining damage.

5. **Winter Storm** – Damage caused by winter storm precipitation and prolonged cold temperatures. Types of damage include roof damage due to snow accumulation, frozen and ruptured pipes, and ice dams on roofs and gutters causing flooding from melting snow. Snow depth, snow and ice thickness, wind speed, as well as structure and occupancy types are considered in determining damage.

6. **Wildfire** – Damage caused by fire and smoke from combustion of vegetative fuel. Fire behavior is modeled considering available fuel load, topography of area, prevailing weather conditions, and fire suppression factors, including firefighting resources. Structure type, occupancy type, age of structure, number of stories, vegetation clearance, roofing fire class, and the presence of fire resistive windows or siding are considered in determining damage.

Some of the perils are not modeled for the entire contiguous U.S. Hurricane wind and hurricane storm surge are only modeled for states on the Gulf and Atlantic coasts. Wildfires are only modeled for the western U.S. and Florida. Nonmodeled areas are considered to have negligible risk, according to CoreLogic. Consequently, when aggregating the AALs over the different perils, we consider structures in non-modeled areas to have an AAL of zero for the geographically limited perils.

Sample Construction

The analyses in this paper are based on property-level estimates of AAL. Thus, we do not aggregate over all structures in the CoreLogic data. Instead, we select one structure per property. If a primary structure is identifiable, we use that structure. If the primary structure is unknown, we take the structure with the largest AAL.

We then use CoreLogic's property tax assessment data to identify properties that are single-family residences (SFRs). To determine SFR status, we use the CoreLogic-standardized land use code. For tax year 2021, we identify about 96.7 million SFRs in the contiguous US.

To generate tract-level average AALs, we identify each property's census tract by performing a spatial join of the chosen properties (using structure-specific coordinates) and 2010-vintage census tracts. We find that 70,558 out of the total 72,247 land area tracts in the contiguous US have at least one SFR. Then, for each property, we sum the AALs over all perils and calculate the average all-peril AAL for properties in the tract. Among the 70,558 tracts, we exclude about 4% of the tracts that had fewer than 30 non-missing AAL values for SFRs. These are either tracts with a very small number of SFRs or tracts where data limitations prevented CoreLogic from providing an AAL estimate for most properties. Together, these excluded tracts contain about 0.2 million SFRs. We are left with 67,487 tracts in the final sample covering 96.5 million SFRs

Census Tract Characteristics

Census tract characteristics are produced using 2019 five-year American Community Survey (ACS) estimates. The 2019 ACS was chosen because of the economic activities and migration patterns that were driven by the COVID-19 pandemic [32]. However, migration and economic shocks related to COVID-19 do not materially affect our conclusions. All the results shown in Table 2 are quantitatively and qualitatively similar when we use the 2021 ACS five-year

estimates, as opposed to the 2019 ACS five-year estimates [33].

The 2019 ACS fields used were:

1. Median Household Income (B19013_001)
2. Total Households (B17017_001)
3. Total Households – Income in the Past 12 Months Below Poverty Level (B17017_002)
4. Population 25 Years and Over (B15003_001)
5. Population 25 Years and Over – Bachelor's Degree (B15003_022)
6. Population 25 Years and Over – Master's Degree (B15003_023)
7. Population 25 Years and Over – Professional Degree (B15003_024)
8. Population 25 Years and Over – Doctorate Degree (B15003_025)
9. Male: 25 to 29 Years: In Labor Force (B23001_025)
10. Male: 30 to 34 Years: In Labor Force (B23001_032)
11. Male: 35 to 44 Years: In Labor Force (B23001_039)
12. Male: 45 to 54 Years: In Labor Force (B23001_046)
13. Female: 25 to 29 Years: In Labor Force (B23001_111)
14. Female: 30 to 34 Years: In Labor Force (B23001_118)
15. Female: 35 to 44 Years: In Labor Force (B23001_125)
16. Female: 45 to 54 Years: In Labor Force (B23001_132)

17. Male: 25 to 29 years (B01001_011)

18. Male: 30 to 34 years (B01001_012)

19. Male: 35 to 39 years (B01001_013)

20. Male: 40 to 44 years (B01001_014)

21. Male: 45 to 49 years (B01001_015)

22. Male: 50 to 54 years (B01001_016)

23. Female: 25 to 29 years (B01001_035)

24. Female: 30 to 34 years (B01001_036)

25. Female: 35 to 39 years (B01001_037)

26. Female: 40 to 44 years (B01001_038)

27. Female: 45 to 49 years (B01001_039)

28. Female: 50 to 54 years (B01001_040)

29. Housing Units (B25002_001)

30. Housing Units — Vacant (B25002_003)

31. Vacant Housing Units – For Seasonal, Recreational, or Occasional Use (B25004_006)

32. Total Population (B03002_001)

33. Total Population – Not Hispanic or Latino: White Alone (B03002_003)

34. Total Population – Not Hispanic or Latino: Black or African American Alone (B03002_004)

35. Total Population – Hispanic or Latino (B03002_012)

36. Total Population – Hispanic or Latino: White Alone (B03002_013)

Urban/Rural Tract Classification

Tracts are designated as urban core, suburban, or rural based on 2010 Census Urban Areas and Core-Based Statistical Area (CBSA) definitions. A tract is classified as "urban core" if the tract centroid intersects with a Census "Urbanized Area" (not "Urban Cluster"). A tract is defined as "suburban" if it is located within a Census CBSA or Census Urban Cluster but not within a Census Urbanized Area. All tracts outside CBSAs are considered "rural".

Generating Tract Characteristics by Average AAL Decile

In Table 2, we examine tract characteristics by tract average AAL deciles. We do this as follows. First, we sort our sample of 67,487 tracts into deciles based on the tract average AAL. Second, we winsorize the distribution of the tract characteristics at 0.01 and 0.99 within each AAL decile to mitigate the influence of extreme values. Last, we take averages of the tract characteristics within each decile.

Generating AALs in Dollars

We use the following procedure to convert the property-level CoreLogic AALs, which are expressed as a share of TIV, to dollar values.

We employ several different data sources to estimate AAL in dollars. We first use a combination of CoreLogic public records and the Zillow Home Value Index (ZHVI) to calculate home values for each SFR in the contiguous US. For SFRs where we observe an arm's length transaction in the CoreLogic public records data, we use the latest observed transaction and impute the 2021 home value using the ZHVI, which we transform from ZIP code- to tract-level

using the Housing and Urban Development (HUD) crosswalk. We are able to impute the 2021 home value from transaction data for just over half of the SFRs in our data. We winsorize the imputed values at the 1st and 99th percentile and we top code the values at $10 million to address extreme outliers. For the vast majority of the remaining SFRs, we use the December 2021 tract-level ZHVI value as the home value. For the small set of remaining SFRs, we use the county-level average home value. The national average and median home value from our estimates are $385,000 and $276,000, respectively.

Next, we isolate structure value from the home value estimate to use as a proxy for the replacement cost (i.e. TIV) of the property. We use structure value estimates in lieu of replacement cost estimates due to data availability. While structure value and replacement cost are not conceptually identical, we believe they are similar enough to produce reliable estimates. We isolate structure value by merging in land value share of home value estimates from Davis et al. (2021). Davis et al. provides, to our knowledge, the most granular estimates of land value measures – they provide tract-level estimates for over three-quarters of tracts in the United States [34]. When a tract-level measure is not available, we use the most granular option available among ZIP code-, county-, or state-level measure.

We then calculate the AAL in dollars for each SFR as AAL*Home Value*(1 – Land Share of Home Value).

Net Migration by Tract AAL Decile

We examine net migration between 2010 and 2019 for areas of different climate risk levels using the anonymized FRBNY Consumer Credit Panel /Equifax data (CCP) (see Supplementary Table 5). The CCP is a 5% random sample that is representative of all U.S. individuals who have a credit history. It is widely used in consumer finance research, but it has also been used in several studies of mobility and migration [35]. We use the CCP because its size (about 10 million

borrowers per year) enables us to generate more granular migration estimates than some other sources of migration data allow. For example, ACS data only provide county-level flows based on five years of pooled data. We provide a county-level comparison of those sources below to help validate our CCP-derived migration estimates in Supplementary Information Section D.

Using the CCP, we generate census tract-level net migration estimates and then group tracts by the same AAL deciles that are used in the main analyses. The migration estimation proceeds as follows.

1. Identify individuals in the CCP who have a different reported street address and ZIP code in year t compared with year t-1 for t = 2010 to t = 2019 and generate counts by 2000 census block. The CCP provides a scrambled address where the trailing characters are affected by small variations such as whether "Unit" or "Apt" is used. To deal with this issue, we only use the first five characters of the scrambled address in conjunction with the ZIP code to avoid falsely identifying movers that result from small variations in address syntax.

2. Merge counts with the National Historical Geographic Information System (NHGIS) 2000–2010 block crosswalk to convert to 2010 census geography definitions. Using the weights provided in the crosswalk, we allocate each 2000 block migration count to a 2000 block to a 2010 block pair. Then we aggregate to the 2010 block level.

3. Aggregate counts to the 2010 tract level.

4. Multiply counts by 22 because the CCP is a 5% nationally representative sample among those with credit histories. We multiply by 22 instead of 20 to account for individuals without credit histories. We implicitly assume that the migration pattern of individuals who lack credit histories is similar to that of individuals who have credit histories.

5. Scale migration counts by 2010 tract population.

6. Group tracts by AAL decile and winsorize the distribution of net migration at 1st and 99th percentiles within each decile.

7. Calculate average net migration as share of 2010 population within AAL tract deciles.

We also consider migration within MSAs to investigate if people are moving to or away from riskier areas within their original MSA. In this case, we generate AAL deciles within the MSAs instead of across all tracts. We also calculate the average net migration among movers who moved within the same MSA, excluding the relatively small percentage of movers who move across different MSAs. All results are qualitatively and quantitatively similar when we use 2021 as the ending period.

Climate Change Beliefs Survey Data

Climate change beliefs survey data is sourced from the Yale Climate Opinion Map 2021, which is based on the methodology developed in Howe et al. (2015) [36]. We draw on county-level results for two survey questions:

1. "Recently, you may have noticed that global warming has been getting some attention in the news. Global warming refers to the idea that the world's average temperature has been increasing over the past 150 years, may be increasing more in the future, and that the world's climate may change as a result. What do you think: Do you think that global warming is happening?" RESPONSES: Yes, No, Don't Know.

2. "How much do you agree or disagree with the following statement: "I have personally experienced the effects of global warming"?" RESPONSES: Strongly agree, Somewhat agree, Somewhat disagree, Strongly disagree.

In the first question we use the share of respondents who responded “Yes”. In the second question, we use the share of respondents who responded, “Strongly agree” or “Somewhat agree”.

We combine the county-level beliefs data with county-level AALs generated by averaging the property AAL of every SFR in the county.

References

1. *2022 Survey of Consumer Finances* 2023. www.federalreserve.gov/econres/scfindex.htm.
2. Wing, O. E. J. *et al.* Inequitable patterns of US flood risk in the Anthropocene. *Nature Climate Change* **12,** 891–921 (2022).
3. Gourevitch, J. D. *et al.* Unpriced climate risk and the potential consequences of overvaluation in US housing markets. *Nature Climate Change* **13,** 250–257 (2023).
4. Ouazad, A. & Kahn, M. E. *Mortgage Securitization Dynamics in the Aftermath of Natural Disasters: A Reply* 2023. arXiv: 2305.07179.
5. IPCC. in *Climate Change 2023. Contribution of Working Groups I, II and III to the Sixth Assessment Report of the Intergovernmental Panel on Climate Change* (eds Lee, H. & Romero, J.) (2023).
6. Taber, C. R. The Rising College Premium in the Eighties: Return to College or Return to Unobserved Ability? *The Review of Economic Studies* **68,** 665–691 (2001).
7. Branas, C., Keddem, S., Sellman, J. & Cannuscio, C. More than just an eyesore: local insights and solutions on vacant land and urban health. *Journal of urban health : bulletin of the New York Academy of Medicine* **90,** 412–426 (2013).
8. Boustan, L. P., Kahn, M. E., Rhode, P. W. & Yanguas, M. L. The effect of natural disasters on economic activity in US counties: A century of data. *Journal of Urban Economics* **118,** 103257 (2020).
9. Indaco, A. & Ortega, F. *Adapting to Climate Risk? Local Population Dynamics in the United States* Discussion Paper 15982 (IZA Institute of Labor Economics, 2023).
10. Baldauf, M., Garlappi, L. & Yannelis, C. Does Climate Change Affect Real Estate Prices? Only If You Believe In It. *The Review of Financial Studies* **33,** 1256–1295 (2020).
11. Jay, A. K. *et al.* in *Fifth National Climate Assessment* (eds Crimmins, A. *et al.*) (U.S. Global Change Research Program, Washington, DC, USA, 2023).
12. National Academies of Sciences, Engineering, and Medicine. *Attribution of Extreme Weather Events in the Context of Climate Change* (The National Academies Press, Washington, DC, 2016).
13. Hsiang, S. *et al.* Estimating economic damage from climate change in the United States. *Science* **356,** 1362–1369 (2017).
14. Oh, S. S., Sen, I. & Tenekedjieva, A.-M. *Pricing of Climate Risk Insurance: Regulation and Cross-Subsidies* Working Paper 2022-064 (Federal Reserve Board, 2022).
15. Acemoglu, D., Johnson, S. & Robinson, J. A. in *Handbook of Economic Growth* (eds Aghion, P. & Durlauf, S. N.) (Elsevier, 2005).

16. Wagner, K. R. H. Designing insurance for climate change. *Nature Climate Change* **12,** 1070–1072 (12 2022).

17. Kousky, C. Financing Flood Losses: A Discussion of the National Flood Insurance Program. *Risk Management and Insurance Review* **21,** 11–32 (2018).

18. Billings, S. B., Gallagher, E. A. & Ricketts, L. Let the rich be flooded: The distribution of financial aid and distress after hurricane harvey. *Journal of Financial Economics* **146,** 797–819 (2022).

19. FEMA. *An Affordability Framework for the National Flood Insurance Program* (FEMA, 2018).

20. Roback, J. Wages, Rents, and the Quality of Life. *Journal of Political Economy* **90,** 1257–1278 (1982).

21. Rosen, S. in *Current Issues in Urban Economic* (eds Mieszkowski, P. & Straszheim, M.) (Johns Hopkins University Press, Baltimore, 1979).

22. Saiz, A. The Geographic Determinants of Housing Supply. *The Quarterly Journal of Economics* **125,** 1253–1296 (2010).

23. Gyourko, J. & Molloy, R. in *Handbook of Regional and Urban Economics* chap. 19 (Elsevier, 2015).

24. CoreLogic. *Modeling a Secure Future for Real Estate Portfolios With Climate Risk Analytics* Accessed April 2024. https://www.corelogic.com/intelligence/case-studies/climate-risk-modeling-future-for-real-estate-portfolios/.

25. FEMA. *National Flood Insurance Program Risk Rating 2.0 Methodology and Data Sources* (FEMA, 2021). https://www.fema.gov/sites/default/files/documents/fema_risk-rating-2.0-methodology-data-sources_3-2021.pdf.

26. Email correspondence with representatives from CoreLogic. June 2024.

27. Flagstar. *Climate Scenario Change Analysis* Accessed July 2024. https://www.flagstar.com/esg/environmental/climate-change-scenario-analysis.html.

28. Boomhower, J., Fowlie, M., Gellman, J. & Plantinga, A. *How Are Insurance Markets Adapting to Climate Change? Risk Selection and Regulation in the Market for Homeowners Insurance* Working Paper 32625 (National Bureau of Economic Research, June 2024). http://www.nber.org/papers/w32625.

29. IPCC. in *Climate Change 2014: Synthesis Report. Contribution of Working Groups I, II and III to the Fifth Assessment Report of the Intergovernmental Panel on Climate Change* (eds Pachauri, R. & Meyer, L.) (2014).

30. Hayhoe, K. *et al.* in *Fourth National Climate Assessment, Volume II* (eds Reidmiller, D. *et al.*) (U.S. Global Change Research Program, Washington, DC, USA, 2018).

31. CoreLogic. *Climate Risk Analytics* Accessed April 2024. www.corelogic.com/data-solutions/property-data-solutions/climate-risk-analytics.

32. Bloom, N., Davis, S. J. & Zhestkova, Y. COVID-19 Shifted Patent Applications toward Technologies That Support Working from Home. *AEA Papers and Proceedings* **111,** 263–66 (2021).

33. Coven, J., Gupta, A. & Yao, I. JUE Insight: Urban flight seeded the COVID-19 pandemic across the United States. *Journal of Urban Economics* **133,** 103489 (2023).

34. Davis, M. A., Larson, W. D., Oliner, S. D. & Shui, J. The price of residential land for counties, ZIP codes, and census tracts in the United States. *Journal of Monetary Economics* **118,** 413–431 (2021).

35. DeWaard, J., Johnson, J. & Whitaker, S. Internal migration in the United States: A comprehensive comparative assessment of the Consumer Credit Panel. *Demographic Research* **41,** 953–1006 (2019).

36. Howe, P. D., Mildenberger, M., Marlon, J. R. & Leiserowitz, A. Geographic variation in opinions on climate change at state and local scales in the USA. *Nature Climate Change* **5,** 596–603 (2015).

Tables

Table 1. Current Average Annual Loss (AAL) for Single-Family Residences (SFRs), by Peril

Peril	Average AAL (% of TIV)	Percent of All-Peril AAL	Average AAL in Dollars	Percent of SFRs with >0 AAL	Average AAL Among SFRs with >0 AAL	AALs Among SFRs with >0 AAL					
						p10	*p25*	*median*	*p75*	*p90*	*p99*
Severe Convective Storm	0.06%	33.0%	121	99.8%	0.06%	*	0.01%	0.04%	0.08%	0.12%	0.26%
Inland Flood	0.05%	28.3%	101	47.6%	0.10%	*	*	0.01%	0.03%	0.13%	2.46%
Hurricane Wind	0.03%	18.4%	81	48.0%	0.07%	*	*	0.02%	0.07%	0.19%	0.60%
Winter Storm	0.02%	10.7%	42	86.4%	0.02%	*	0.01%	0.02%	0.03%	0.04%	0.09%
Hurricane Storm Surge	0.01%	5.5%	25	5.2%	0.18%	*	*	0.01%	0.11%	0.50%	2.16%
Wildfire	0.01%	4.1%	30	27.2%	0.03%	*	*	*	0.01%	0.05%	0.45%
All	0.17%	100.0%	401	99.8%	0.17%	0.03%	0.06%	0.10%	0.15%	0.27%	1.60%

Note: The table shows summary statistics of AAL by peril for SFRs in the contiguous US. AAL is presented as percentage of total insurable value (TIV) unless otherwise noted. Asterisks indicate values greater than 0% but less than 0.005%. Dollar values are in 2021 dollars.

Table 2. 2019 Census Tract Characteristics by Tract Average Current AAL Decile

	Mean (Standard Error)									
	Decile of Tract Average Current AAL (measured as % of TIV)									
Description	**1**	**2**	**3**	**4**	**5**	**6**	**7**	**8**	**9**	**10**
Percent White	45.2	56.7	65.4	64.0	66.1	68.6	68.3	66.5	63.4	62.3
	(0.3)	(0.4)	(0.4)	(0.4)	(0.3)	(0.3)	(0.3)	(0.3)	(0.4)	(0.4)
Percent with Bachelor's Degree or Higher	34.4	33.3	31.4	31.9	31.8	31.0	29.8	27.2	26.1	26.1
	(0.3)	(0.2)	(0.2)	(0.2)	(0.2)	(0.2)	(0.2)	(0.2)	(0.2)	(0.2)
Median Household Income	84,244	78,522	72,682	73,289	72,185	70,578	68,947	65,684	63,161	60,906
	(477)	(481)	(433)	(418)	(401)	(386)	(384)	(362)	(344)	(331)
Home Value	838,602	491,514	353,840	388,196	353,773	333,720	343,697	317,659	282,167	343,244
	(6,983)	(4,767)	(3,005)	(3,267)	(2,934)	(2,658)	(3,296)	(2,950)	(2,436)	(3,869)
Percent Prime Age Labor Force Participation	82.7	82.4	82.5	82.6	83.0	82.8	82.3	81.3	80.4	78.9
	(0.1)	(0.1)	(0.1)	(0.1)	(0.1)	(0.1)	(0.1)	(0.1)	(0.1)	(0.1)
Percent Vacant (Excluding Seasonal Units)	5.0	7.6	8.2	7.9	8.3	8.2	8.7	9.4	10.1	11.3
	(0.04)	(0.09)	(0.08)	(0.07)	(0.07)	(0.07)	(0.07)	(0.07)	(0.07)	(0.08)
Percent of Tracts Rural	0.5	2.3	3.9	4.3	4.8	7.0	9.1	11.7	12.7	12.5
Percent of Tracts Urban Core	90.1	76.5	69.5	68.6	64.5	59.5	54.2	49.3	50.1	50.9

Note: Census tract average characteristics by tract-level average current AAL decile. Home Values are as of 2021. Dollar values are in 2021 dollars.

Table 3. Change in Census Tract Characteristics (2010–2019) by Tract Average Current AAL Decile

	Mean (Standard Error)									
	Decile of Tract Average Current AAL									
Description	**1**	**2**	**3**	**4**	**5**	**6**	**7**	**8**	**9**	**10**
Change in Percent with Bachelor's Degree or Higher	4.2	3.7	3.8	3.9	3.9	3.8	3.5	3.3	2.8	3.3
	(0.1)	(0.1)	(0.1)	(0.1)	(0.1)	(0.1)	(0.1)	(0.1)	(0.1)	(0.1)
Percent Change Median Household Income	9.5	4.3	4.1	4.3	4.0	4.3	4.9	5.4	4.3	4.3
	(0.2)	(0.2)	(0.2)	(0.2)	(0.2)	(0.2)	(0.2)	(0.2)	(0.2)	(0.3)
Change in Percent Prime Age Labor Force Participation	0.7	0.1	0.2	0.1	0.0	-0.2	-0.4	-0.4	-0.7	-0.5
	(0.1)	(0.1)	(0.1)	(0.1)	(0.1)	(0.1)	(0.1)	(0.1)	(0.1)	(0.1)
Change in Percent Vacant (Excluding Seasonal Units)	-0.9	-0.6	-0.4	-0.1	-0.2	-0.2	-0.1	0.2	0.4	0.2
	(0.1)	(0.1)	(0.1)	(0.1)	(0.1)	(0.1)	(0.1)	(0.1)	(0.1)	(0.1)
Percent Change in Total Population	8.4	7.0	4.6	4.7	5.5	6.3	6.9	6.6	6.9	5.5
	(0.2)	(0.2)	(0.2)	(0.2)	(0.2)	(0.2)	(0.2)	(0.2)	(0.3)	(0.2)

Note: Average change in select census tract characteristics by tract average current AAL decile.

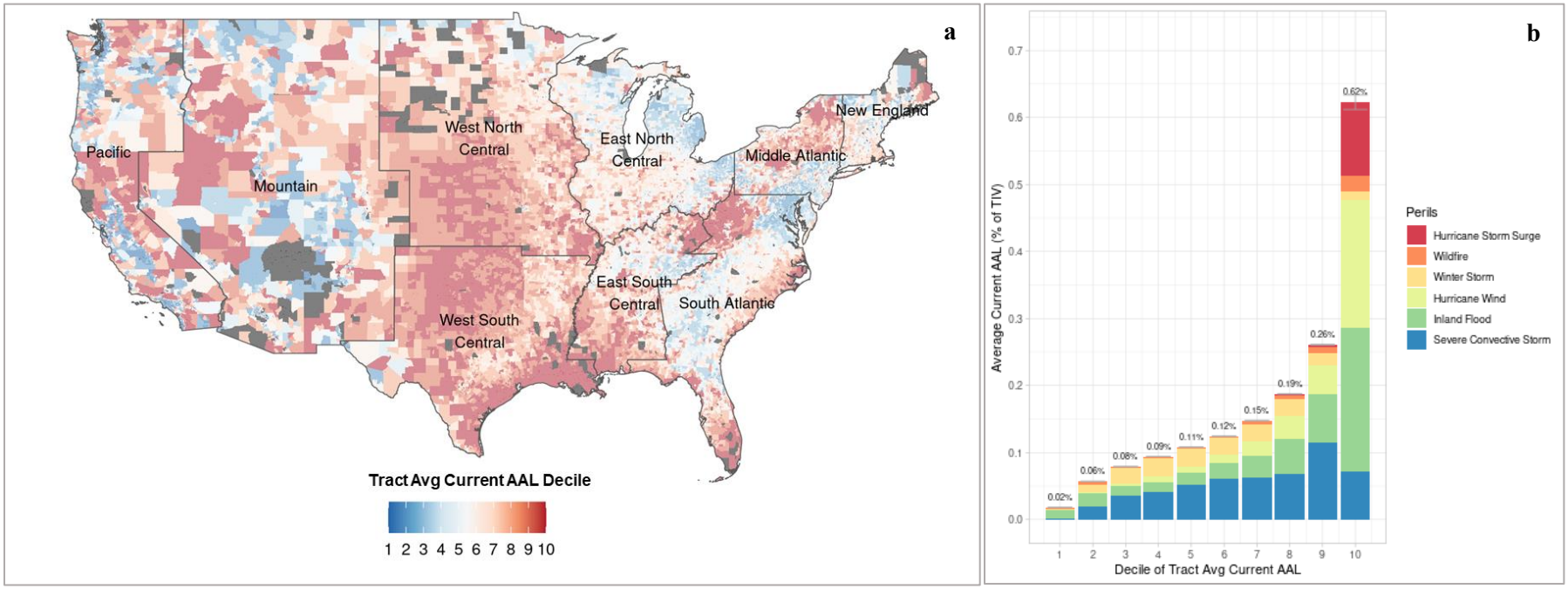
Table 4. Change in Average Annual Loss (AAL) from Current to 2050 Under RCP 4.5 and RCP 8.5, by Peril

	AAL as % of TIV			*AAL in Dollars*		
Peril	**Current Avg AAL (% of TIV)**	**% Change in Avg AAL by 2050 Under RCP 4.5**	**% Change in Avg AAL by 2050 Under RCP 8.5**	**Current Total AAL ($B)**	**% Change in Total AAL by 2050 Under RCP 4.5**	**% Change in Total AAL by 2050 Under RCP 8.5**
Severe Convective Storm	0.06%	35%	46%	12	35%	45%
Inland Flood	0.05%	4.4%	4.7%	10	4.9%	4.4%
Hurricane Wind	0.03%	21%	42%	7.9	22%	44%
Winter Storm	0.02%	1.3%	5.7%	4.0	1.3%	5.7%
Hurricane Storm Surge	0.01%	76%	116%	2.9	73%	112%
Wildfire	0.01%	34%	45%	2.4	35%	45%
All	0.17%	22%	33%	39	24%	36%

Note: By-peril percentage change in AAL from current to 2050 under RCP 4.5 and RCP 8.5. Results displayed for AAL measured as share of insurable value (TIV) as well as AAL estimated in 2021 dollars. RCP = Representative Concentration Pathway.

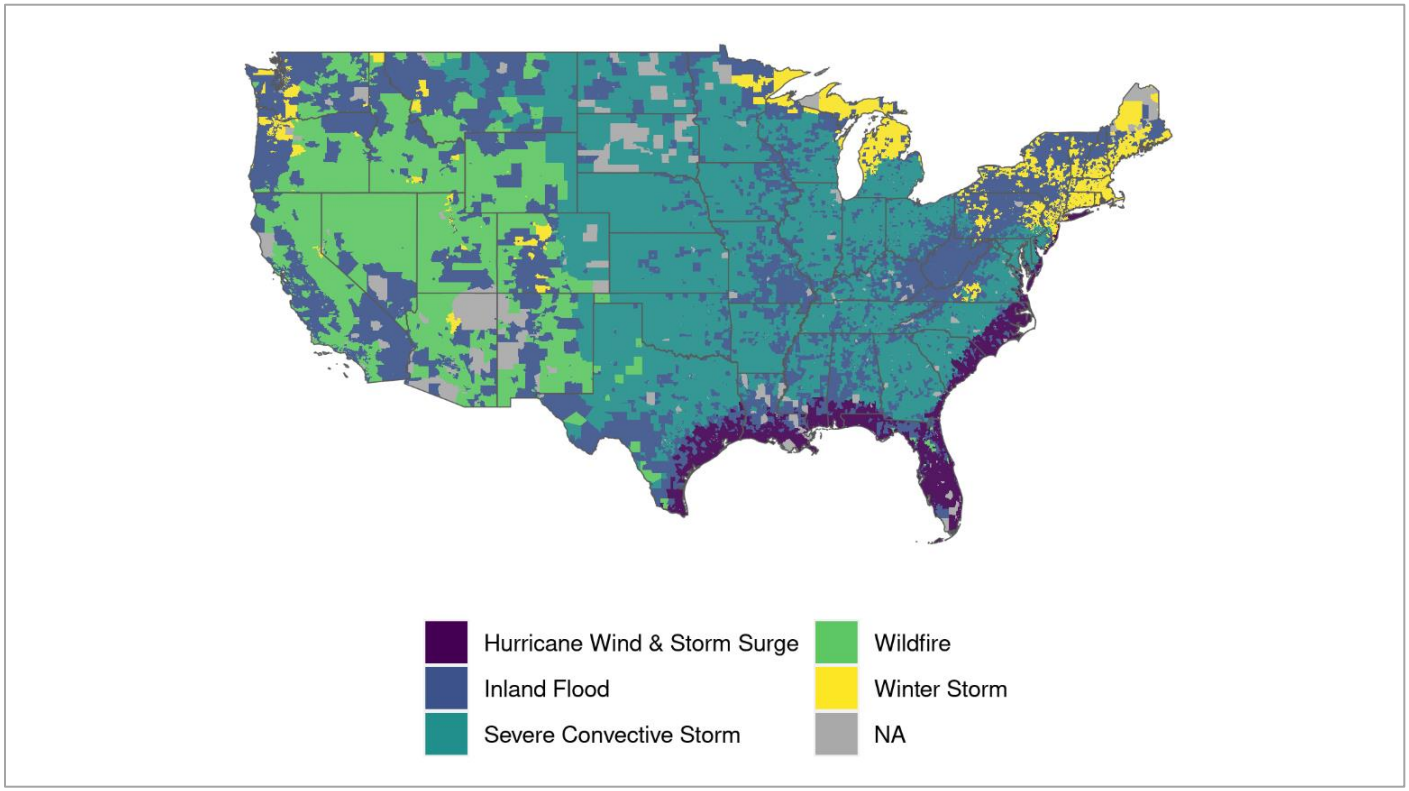
Figures

Fig 1. Deciles of Tract Average Current AAL for SFRs and By-Peril Contribution Within Each Decile



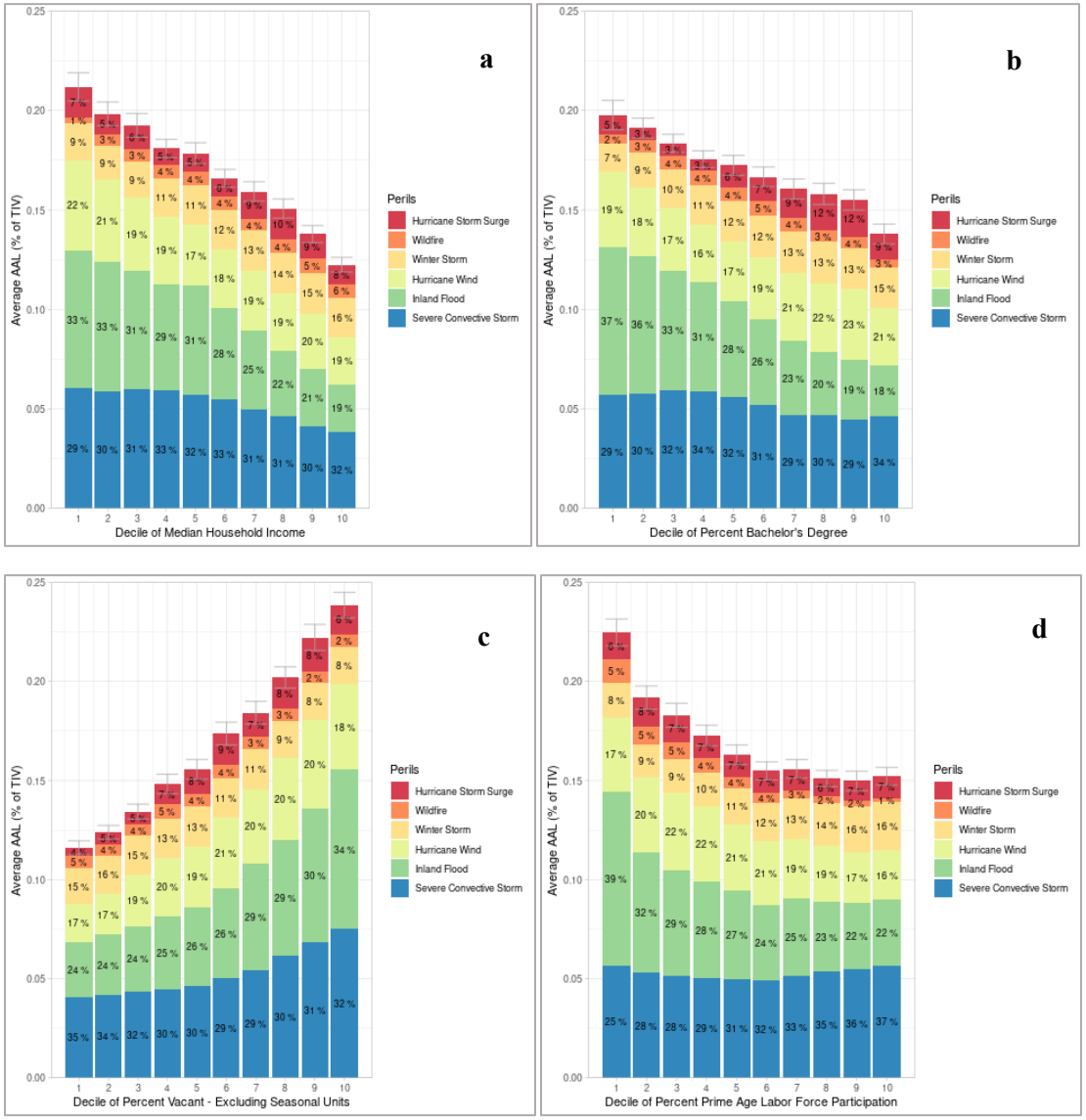
(a) Tract-level average current composite AAL. Tracts without sufficient data to calculate an average current AAL are shown in dark gray. (b) By-peril contribution of average current AAL in each decile of tract average current AAL. Ninety-five percent confidence intervals for decile average current AALs appear in gray. The confidence intervals characterize the cross-sectional variation in tract-level average current AALs and do not account for model uncertainty because CoreLogic does not provide sufficient information for us to account for such uncertainty; TIV = total insurable value.

Figure 2. Predominant Peril by Tract



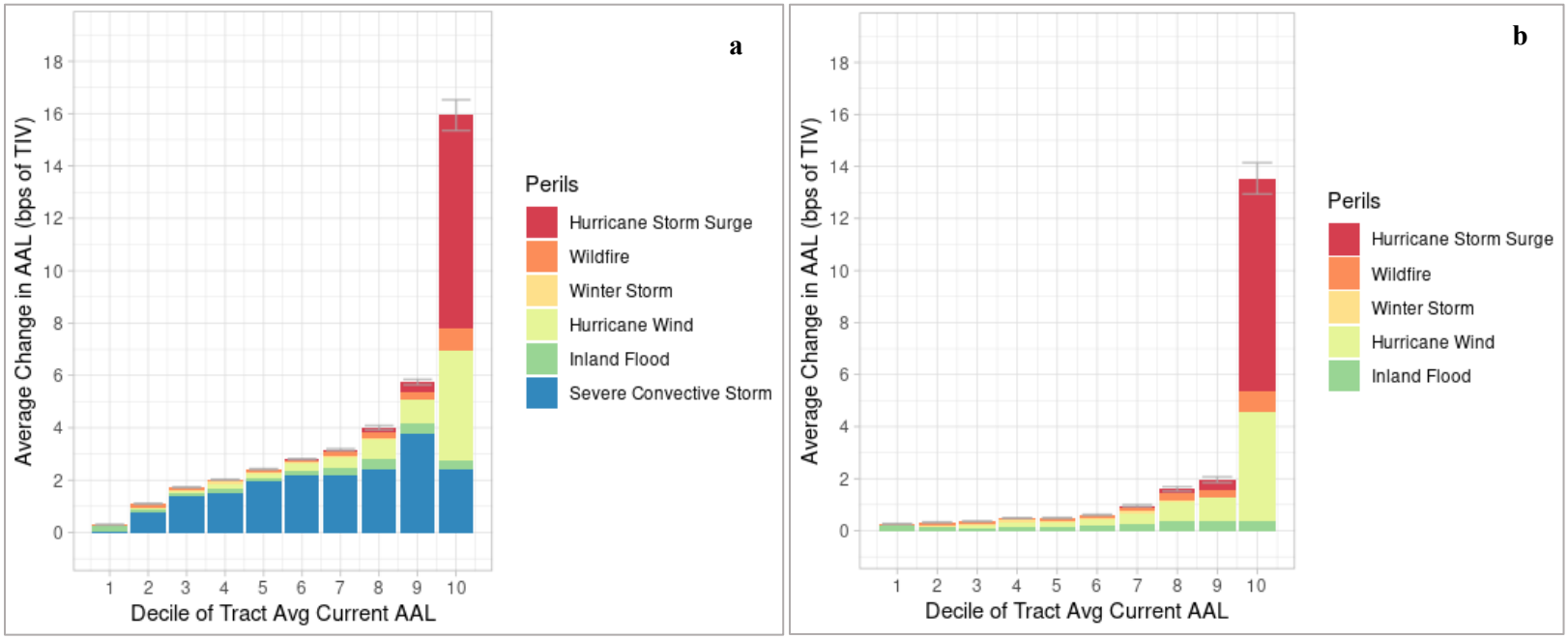
Tract colored according to the peril or set of perils that make largest contribution to the tract average all-peril current AAL. AAL measured as share of total insurable value.

Fig 3. By-Peril Average Current AAL by Deciles of Median Household Income, Bachelor's Degree or Higher Share, Vacancy Rate, and Prime Age Labor Force Participation Rate.



By-peril average contribution to tract-level average current AAL sorted by (a) 2019 median household income; (b) average 2019 share of adults with bachelor's degree or higher decile; (c) 2019 percent vacant home (excluding seasonal units) decile; (d) average 2019 prime age labor force participation decile. Ninety-five percent confidence intervals for decile average current AALs appear in gray. The intervals characterize the cross-sectional variation in tract-level average current AALs and do not account for model uncertainty because CoreLogic does not provide sufficient information for us to account for such uncertainty.

Fig 4. Average Change in AAL from Current to 2050, by Tract Average Current AAL Decile.



(a) Average change in AAL between circa 2021 and 2050 sorted by current average tract AAL decile. (b) Average change in AAL between circa 2021 and 2050 assuming severe convective storm does not change, sorted by current average tract AAL decile. Ninety-five percent confidence intervals for decile average AALs appear in gray. The confidence intervals characterize the cross-sectional variation in tract-level average AALs and do not account for model uncertainty because CoreLogic does not provide sufficient information for us to account for such uncertainty.

Supplementary Tables

Supplementary Table 1. Current Average Annual Loss (AAL) for SFRs, by Census Region Division and Peril

	Percent of Census Region Division's Average Current AAL									
	East North Central	**East South Central**	**Middle Atlantic**	**Mountain**	**New England**	**Pacific**	**South Atlantic**	**West North Central**	**West South Central**	**U.S.**
Severe Convective Storm	53%	36%	19%	24%	13%	2%	23%	56%	40%	**33%**
Inland Flood	26%	40%	35%	39%	19%	52%	19%	33%	25%	**28%**
Hurricane Wind	0%	16%	10%	0%	17%	0%	39%	0%	24%	**19%**
Winter Storm	21%	5%	28%	7%	46%	6%	7%	11%	3%	**11%**
Hurricane Storm Surge	0%	3%	8%	0%	5%	0%	11%	0%	7%	**6%**
Wildfire	0%	0%	0%	30%	0%	40%	1%	0%	2%	**4%**
Avg AAL (% of TIV)	0.12%	0.21%	0.14%	0.11%	0.15%	0.07%	0.19%	0.21%	0.32%	**0.17%**
	Property Exposure									
Count SFRs (millions)	14.2	7.3	10.0	7.6	3.7	11.8	21.9	7.1	12.9	**96.5**
Avg Structure Value ($)	172,861	188,445	252,229	365,063	269,502	413,085	257,413	193,591	211,948	**256,423**
	Expected Loss in Dollars									
Avg AAL ($)	192	342	350	385	411	267	513	392	649	**401**
Total AAL ($ Billions)	2.7	2.5	3.5	2.9	1.5	3.2	11.2	2.8	8.4	**39**

Note: By-peril contribution to average current AAL, measured as share of total insurable value (TIV). Structure value does not include land value. Dollar values are shown in 2021 dollars.

Supplementary Table 2. By-Peril, By-State, and By-MSA Summary of Tracts in Top 1% of Tract AAL

By-Peril		*By-State*		*By-MSA*	
Peril	**Percent of AAL**	**State**	**Percent of Tracts**	**MSA**	**Percent of Tracts**
Hurricane Storm Surge	42%	LA	30%	New Orleans-Metairie, LA	28%
Inland Flood	28%	FL	26%	Miami-Fort Lauderdale-Pompano Beach, FL	12%
Hurricane Wind	25%	TX	12%	Gulfport-Biloxi, MS	7%
Severe Convective Storm	3%	MS	8%	Houston-The Woodlands-Sugar Land, TX	6%
Wildfire	1%	WV	5%	Tampa-St. Petersburg-Clearwater, FL	5%
Winter Storm	0.4%	NY	5%	New York-Newark-Jersey City, NY-NJ-PA	4%
		KY	2%	Key West, FL	3%
		CA	2%	Beaumont-Port Arthur, TX	3%
		AL	1%	Charleston, WV	2%
		NJ	1%	Sebastian-Vero Beach, FL	2%

Note: By-peril contribution and top geographic locations of the top one percent of riskiest tracts in the U.S. based on AALs measured as share of total insurable value.

Supplementary Table 3. Urban Core 2019 Census Tract Characteristics by Tract Average Current AAL Decile

	Mean (Standard Error)									
	Decile of Tract Average Current AAL (% of TIV)									
Description	**1**	**2**	**3**	**4**	**5**	**6**	**7**	**8**	**9**	**10**
Percent White	43.7	51.1	57.4	55.7	57.4	59.8	58.2	55.4	51.4	49.7
	(0.4)	(0.4)	(0.4)	(0.4)	(0.4)	(0.4)	(0.5)	(0.5)	(0.5)	(0.5)
Percent with Bachelor's Degree or Higher	35.1	34.5	33.4	34.8	35.6	35.9	35.4	32.3	30.6	31.0
	(0.3)	(0.3)	(0.3)	(0.3)	(0.3)	(0.3)	(0.3)	(0.3)	(0.3)	(0.3)
Median Household Income	85,026	78,720	73,430	75,757	75,287	74,487	73,645	70,334	66,651	63,905
	(505)	(573)	(556)	(543)	(547)	(552)	(591)	(593)	(571)	(523)
Home Value	866,904	506,944	371,729	431,469	399,194	386,362	419,675	384,883	330,175	424,745
	(7,457)	(5,661)	(3,813)	(4,193)	(3,985)	(3,669)	(4,948)	(4,612)	(3,750)	(6,042)
Percent Prime Age Labor Force Participation	83.0	82.7	82.9	83.3	83.8	83.9	83.6	82.9	82.0	81.5
	(0.1)	(0.1)	(0.1)	(0.1)	(0.1)	(0.1)	(0.1)	(0.1)	(0.1)	(0.1)
Percent Vacant (Excluding Seasonal Units)	4.9	7.8	8.4	7.7	8.1	7.7	8.0	8.2	9.0	10.0
	(0.05)	(0.11)	(0.10)	(0.09)	(0.10)	(0.10)	(0.10)	(0.10)	(0.10)	(0.11)
Number of Urban Core Tracts	6,084	5,166	4,689	4,628	4,352	4,016	3,655	3,325	3,378	3,437

Note: Urban core census tract average characteristics by tract-level average current AAL decile. Home Values are as of 2021. Dollar values are in 2021 dollars.

Supplementary Table 4. 2019 Census Tract Characteristics by Current Tract AAL Decile Sorted Within MSA

	Mean (Standard Error)									
	Decile of Tract Average Current AAL (% of TIV) within MSA									
Description	**1**	**2**	**3**	**4**	**5**	**6**	**7**	**8**	**9**	**10**
Percent White	59.2	56.8	57.1	56.9	56.4	57.7	59.0	61.2	63.2	64.6
	(0.4)	(0.4)	(0.4)	(0.4)	(0.4)	(0.4)	(0.4)	(0.4)	(0.4)	(0.4)
Percent with Bachelor's Degree or Higher	33.8	33.1	33.2	32.7	32.7	32.2	32.2	32.3	31.8	30.7
	(0.3)	(0.3)	(0.3)	(0.3)	(0.3)	(0.3)	(0.3)	(0.3)	(0.3)	(0.3)
Median Household Income	75,302	74,338	74,052	74,013	73,898	74,558	75,300	76,488	76,259	73,852
	(474)	(468)	(466)	(465)	(475)	(475)	(480)	(486)	(488)	(482)
Home Value	439,936	435,164	443,989	436,560	440,513	436,495	448,987	448,828	454,085	473,207
	(4,450)	(4,336)	(4,605)	(4,567)	(4,716)	(4,575)	(5,032)	(4,853)	(5,120)	(5,823)
Percent Prime Age Labor Force Participation	83.1	82.9	82.8	82.8	83	82.8	82.6	82.6	82.5	81.4
	(0.1)	(0.1)	(0.1)	(0.1)	(0.1)	(0.1)	(0.1)	(0.1)	(0.1)	(0.1)
Percent Vacant (Excluding Seasonal)	7.4	7.8	7.7	7.8	7.8	7.7	7.7	7.6	7.9	8.6
	(0.1)	(0.1)	(0.1)	(0.1)	(0.1)	(0.1)	(0.1)	(0.1)	(0.1)	(0.1)

Note: Census tract average characteristics by within-MSA tract-level average current AAL decile. Home Values are as of 2021. Dollar values are in 2021 dollars.

Supplementary Table 5. Net Migration (2010–2019) by Tract Average Current AAL Decile

Panel A: Mean Tract Net Migration (2010-2019) as % of 2010 Population

	Decile of Tract Average Current AAL of Each Peril or Peril Group									
	1	**2**	**3**	**4**	**5**	**6**	**7**	**8**	**9**	**10**
All Perils	**-1.7**	**-1.0**	**-1.3**	**-1.8**	**-0.9**	**0.1**	**0.3**	**0.8**	**1.0**	**0.6**
	(0.2)	**(0.2)**	**(0.2)**	**(0.2)**	**(0.2)**	**(0.2)**	**(0.2)**	**(0.2)**	**(0.2)**	**(0.2)**
Severe Convective Storm	-1.5	2.7	1.8	-2.2	-3.2	-1.7	0.5	0.7	-1.2	0.4
	(0.2)	(0.3)	(0.3)	(0.2)	(0.2)	(0.2)	(0.2)	(0.2)	(0.2)	(0.3)
Inland Flood	-2.7	-1.3	-0.2	-0.1	0.4	0.2	0.1	0.9	0.3	-1.4
	(0.2)	(0.2)	(0.2)	(0.2)	(0.2)	(0.2)	(0.2)	(0.2)	(0.2)	(0.2)
Hurricane Wind	-2.7	-0.7	0.3	0.4	0.1	-3.2	-2.5	0.2	6.3	2.9
	(0.2)	(0.3)	(0.4)	(0.4)	(0.3)	(0.3)	(0.3)	(0.4)	(0.5)	(0.4)
Winter Storm	-3.4	7.1	3.6	2.8	-0.4	0.0	-1.7	-3.3	-3.7	-4.1
	(0.2)	(0.3)	(0.3)	(0.3)	(0.2)	(0.2)	(0.2)	(0.2)	(0.2)	(0.2)
Hurricane Storm Surge	2.4	1.2	-4.4	-6.9	0.5	-2.0	1.8	1.9	1.1	5.9
	(0.4)	(0.3)	(0.2)	(0.2)	(0.3)	(0.2)	(0.5)	(0.4)	(0.4)	(0.4)
Wildfire	3.4	-0.8	1.8	4.8	0.2	-0.5	2.0	5.7	6.3	4.6
	(0.5)	(0.5)	(0.5)	(0.6)	(0.5)	(0.5)	(0.5)	(0.5)	(0.5)	(0.4)

Panel B: Mean Tract Net Migration (2010-2019) as % of 2010 Population Within MSA

	Decile of Tract Average Current AAL Within MSA									
	1	**2**	**3**	**4**	**5**	**6**	**7**	**8**	**9**	**10**
All Perils	-0.8	-1.3	-0.4	-0.4	-0.7	-0.7	-0.2	0.6	0.4	-0.3
	(0.2)	(0.2)	(0.2)	(0.2)	(0.2)	(0.2)	(0.2)	(0.2)	(0.2)	(0.2)

Panel A: Average tract net in-migration during 2010–2019 by decile of tract composite average current AAL and decile of tract sub-peril average AAL. Perils with non-modeled areas (Wildfire, Hurricane Storm Surge, and Hurricane Wind) exclude tracts outside the modeled area. For example, Hurricane Wind only includes tracts in states on the Gulf and Atlantic coasts. Panel B: Average tract net in-migration during 2010–2019 among the set of movers who moved within the same MSA by decile of tract composite average current AAL sorted within MSA. Standard errors in parentheses.

Supplementary Table 6. Climate Change Beliefs by County Average Current AAL Decile

	Mean (Standard Error)									
	Decile of County Average Current AAL									
Description	**1**	**2**	**3**	**4**	**5**	**6**	**7**	**8**	**9**	**10**
Percent Believe Global Warming is Happening	69.9	66.6	66.4	65.2	64.8	64.9	63.9	64.3	62.7	63.1
	(0.4)	(0.4)	(0.4)	(0.4)	(0.3)	(0.3)	(0.3)	(0.3)	(0.3)	(0.3)
Percent Said Personally Affected by Global Warming	44.4	42.0	41.5	40.5	40.7	41.0	40.4	40.8	39.8	40.5
	(0.3)	(0.3)	(0.3)	(0.3)	(0.3)	(0.3)	(0.2)	(0.3)	(0.3)	(0.3)

Note: Average county climate change beliefs survey response by tract average current AAL decile. AALs measured as share of total insurable value.

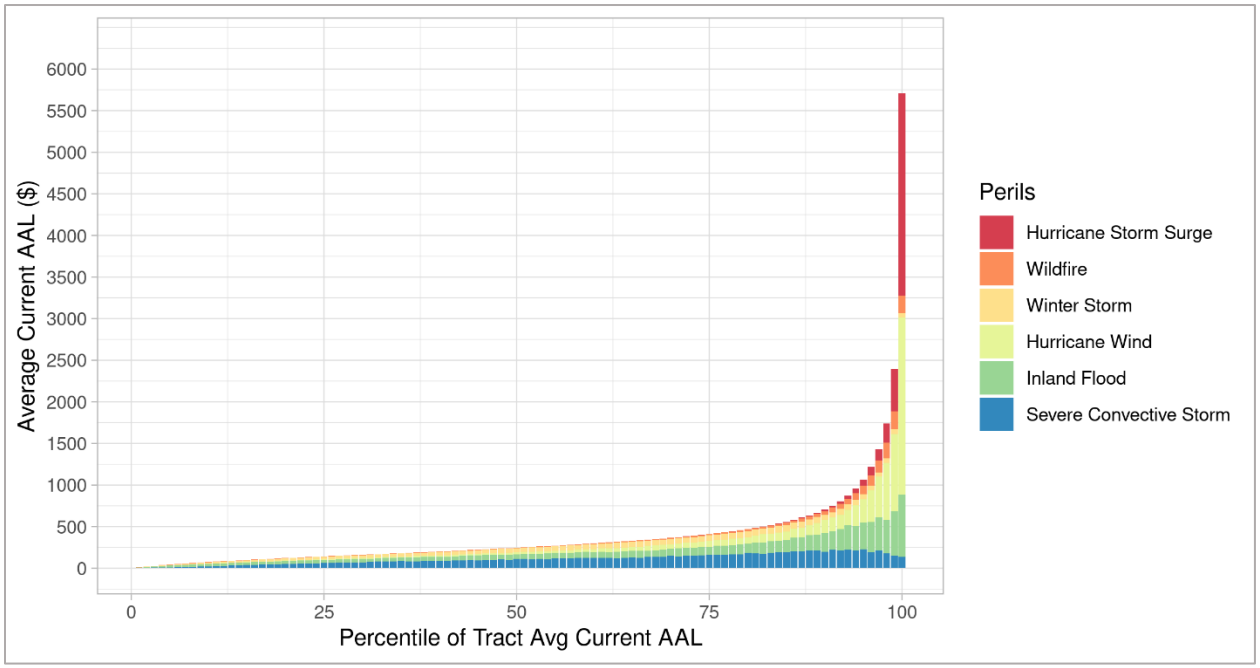
Supplementary Table 7. Current Average Annual Loss (AAL) Measured in Dollars for SFRs, by Census Region Division and Peril

	Percent of Census Region's Expected Losses (in terms of dollars)									
	East North Central	**East South Central**	**Middle Atlantic**	**Mountain**	**New England**	**Pacific**	**South Atlantic**	**West North Central**	**West South Central**	**U.S.**
Severe Convective Storm	55%	42%	18%	24%	13%	1%	21%	58%	43%	**30%**
Inland Flood	23%	32%	28%	36%	17%	52%	14%	32%	23%	**25%**
Hurricane Wind	0%	15%	14%	0%	18%	0%	43%	0%	23%	**20%**
Winter Storm	22%	6%	28%	8%	46%	6%	6%	11%	3%	**10%**
Hurricane Storm Surge	0%	4%	13%	0%	5%	0%	15%	0%	7%	**8%**
Wildfire	0%	0%	0%	31%	0%	41%	1%	0%	1%	**6%**
Avg AAL ($)	192	342	350	385	411	267	513	392	649	**401**
Total AAL ($ Billions)	2.7	2.5	3.5	2.9	1.5	3.2	11.2	2.8	8.4	**39**

Note: By-peril contribution to average current AAL in dollars. Dollar values are shown in 2021 dollars.

Supplementary Figures

Supplementary Fig. 1. By-Peril Contribution to Tract Average Current AAL in Dollars by Percentile of Tract Average Current AAL in Dollars.



Supplementary Section A: Comparing Expected Dollar Losses with Realized Historical Losses in SHELDUS

One way to assess the reasonableness of our estimates of expected losses in the aggregate is to compare them with historical losses. In this supplemental section, we compare realized loss totals and by-peril realized loss shares to our estimate of total expected losses and by-peril expected loss shares.

We rely on the Spatial Hazard Events and Losses Database for the United States (SHELDUS) for data on historical losses. SHELDUS is a public database of historical direct losses caused by natural disasters in the U.S. The database contains county-level information on property and crop losses as well as injuries and fatalities from 1960 to the present for a wide selection of hazards. The data are primarily sourced from the National Centers for Environmental Information (NCEI) Storm Data publication, which catalogs information on "storm paths, deaths, injuries, and property damage" [37]. SHELDUS is updated regularly with data additions and corrections. The subsequent analysis is based on SHELDUS v22.

We expect SHELDUS to systemically underreport losses because, when the original data source reports a loss estimate as a range, SHELDUS uses the lower bound of that estimate. In fact, prior to 1994, all NCEI Storm Data estimates were reported as logarithmic ranges (<$50, $50-500, $500-5,000, $5,000-50,000, $50,000-500,000, $500,000-5 million, $5 million-50 million, $50 million-500 million, $500 million-5 billion) [38].

There are several additional considerations when trying to compare our expected losses for today with historical losses in SHELDUS. The main ones are hazard types, property types, and time frame. Regarding hazard types, SHELDUS classifications allow us to construct a collection of hazards that are comparable in the aggregate with the set of hazards included in our expected loss estimates. We exclude losses from the following SHELDUS hazard types:

heat, tsunamis/seiches, earthquakes, volcanoes, avalanches, fog, droughts, and landslides.

Regarding property types, our estimate of expected losses is for SFRs only. SHELDUS property losses include damages to all property types as well as damage to vehicles and infrastructure like roads and power lines [38]. We cannot isolate types of property losses in SHELDUS and so this feature will be a countervailing force against the underestimation stemming from SHELDUS using lower bound estimates.

The trickiest consideration is time frame. CoreLogic AALs are based on many simulations of a given year and therefore represent a large-sample average for a given point in time. The same quantitative exercise cannot be applied to the SHELDUS data. If conditions were held constant, we could "observe" annual expected loss by averaging across a very long period of historical losses. However, conditions are not held constant, which leaves a fundamental trade-off between getting a historical average that is "longer-run" and one that better reflects current conditions. Thus, on one hand, we would like to go as far back in time as possible to avoid being misled by "lucky" or "unlucky" periods. On the other hand, environmental conditions and property exposure are not held constant over time, so the underlying risk may be less reflective of current conditions as one looks further into the past.

To address this issue, we examine multiple time frames and explicitly adjust for changes in exposure. The exposure adjustment accounts for the fact that the housing value that is exposed to losses from hazards has increased over time. If we are trying to make a comparison between SHELDUS losses and expected losses today, we want SHELDUS losses to be scaled to current exposure. Consequently, we perform an exposure adjustment similar to the one performed in Wiese (2020) [39]. We scale nominal property damages observed in SHELDUS for county, c, state, s, hazard, h, and year, t, by the growth in total housing units and growth in house prices as shown in Equation 1. We use county-level total housing unit counts for decennial census years 1970, 1980, 1990, 2000, 2010, and 2020. We linearly interpolate the intervening years and pull

back the 1970 value for 1960-1969. We also assume housing counts in 2021 and 2022 are the same as in 2020. For house prices, we use the state-level Federal Housing Finance Agency (FHFA) All-Transactions House Price Index for the period from 1970 to 2022. For 1960-1969, we use the 1970 value.

$$ExposureAdjDmg_{csht} = Dmg_{csht} * \frac{TotHousingUnits_{cs,2021}}{TotHousingUnits_{cst}} * \frac{HPI_{s,2021}}{HPI_{st}} \quad (1)$$

The full history of exposure-adjusted losses compared are presented in Supplementary Fig. A1. The figure highlights the importance of the exposure adjustment when examining historical damages. Total exposure-adjusted damages are 70% larger over the entire SHELDUS history compared to damages only adjusted for inflation. We use the GDP Price Deflator for the inflation adjustment.

The exposure-adjusted property damages for the entire history of SHELDUS (1960–2022) and for the post-2000 period are shown in Supplementary Table A1. The average annual damage recorded in SHELDUS for 1960–2022 and for 2000–2022 are $22 billion and $30 billion, respectively, when adjusted for exposure. Given worsening environmental conditions and the underestimation built into SHELDUS estimates, it is not surprising our current expected damage estimate of $39 billion for SFRs is larger than the SHLEDUS annual averages but is closer to the 2000-2022 annual average than the 1960-2022 annual average. Overall, we assess our current expected damage estimate of $39 billion to be in a reasonable range of exposure-adjusted average historical losses.

In addition to assessing the aggregate damage estimate, we can also compare the breakdown of historical losses among hazards with the breakdown of our estimated expected losses by hazard. In this case, the best comparison is with the peril shares provided in Supplementary Table 7 because the shares in that table were determined using dollar-value AALs instead of AALs as a share of TIV. The crosswalk between SHELDUS hazards and CoreLogic perils is

provided in Supplementary Table A2. In the case of "hurricane/tropical storm", there is no clear 1:1 match to a CoreLogic peril. For example, some non-surge hurricane-related ground flooding is counted as "hurricane/tropical storm" in SHELDUS, while some is counted as "flooding" [39]. Non-surge hurricane-related ground flooding (as well as non-hurricane coastal flooding) is classified as inland flooding in the CoreLogic data. Thus, the hurricane/tropical storm category is somewhat inflated relative to what it would be under CoreLogic classifications. For the same reason, flooding is smaller than what it would be under CoreLogic classifications.

One way to deal with this problem is to combine hurricane and flooding categories. For SHELDUS, this would include hurricane/tropical storm, flooding, and coastal (non-hurricane coastal flooding); for CoreLogic, it would include hurricane wind, hurricane storm surge, and inland flooding. Over the entire SHELDUS history, hurricane and flooding damages have been 63% of damages, while they are 53% of our estimate of 2021 expected losses (see Supplementary Table A3). The difference suggests that we may be modestly understating the influence of hurricanes and flooding. Conversely, the SHELDUS data suggest that we overstate the role of severe convective storms as well as winter storm. The damage share for wildfires lines up exactly. Overall, the by-peril share of expected damage from CoreLogic appears to be qualitatively similar to the realized damage share from SHELDUS.

We posit that there are several factors contributing to the observed differences. First, to the extent that environmental conditions have changed from 1960 to 2022, they may differentially impact the contribution of individual hazards. (Of course, if one thinks that hurricanes and flooding have been most acutely affected by environmental changes over the 1960–2022 period, then this explanation only exacerbates the difference). Similarly, it's possible that hazards have differential impacts on property types that may drive the differences because of the difference in property types included in our expected loss estimate compared with SHELDUS losses. For example, if hurricanes and flooding have a disproportionate impact on public infrastructure, then

that would drive up the SHELDUS share compared with the share we estimate based on SFRs. Third, there is very likely overreporting of flood events in SHELDUS data relative to other hazards due to the collection procedure requirement that a monetary loss amount be provided for all flood events, even if it is a "guesstimate" [40]. For other events, the reporting entity is allowed to provide an unknown amount if they cannot provide a monetary loss estimate based on authoritative data. Fourth, hurricane wind is only modeled by CoreLogic for states on the Gulf and Atlantic coasts. Elsewhere, we assume hurricane wind damage is zero. To the extent that hurricane winds have the potential to reach areas further inland, this assumption would cause us to underestimate the expected losses from hurricane wind.

Supplemental Table A1. Exposure-Adjusted SHELDUS Damages (1960–2022 and 2000–2022)

SHELDUS Hazard	Exposure-Adjusted Damage 1960-2022 (Billions of 2021$)	% of Damage 1960-2022	Exposure-Adjusted Damage 2000-2022 (Billions of 2021$)	% of Damage 2000-2022
Hurricane/Tropical Storm	456	32%	225	32%
Flooding	427	30%	269	38%
Tornado	112	8.0%	51	7.3%
Severe Storm/Thunder Storm	94	6.7%	7	1.1%
Wildfire	85	6.0%	48	6.9%
Hail	83	5.9%	48	6.9%
Wind	81	5.8%	32	4.5%
Winter Weather	55	3.9%	17	2.4%
Lightning	7	0.5%	1	0.2%
Coastal	4	0.3%	0.5	0.1%
Total	**1,403**	**100%**	**700**	**100%**
Annual Average	**22**	**N/A**	**30**	**N/A**

Note: By-hazard exposure-adjusted SHELDUS property losses for 1960-2022 and 2000-2022. “Hurricane/Tropical Storm” category includes some flooding from hurricanes and tropical storms.

Supplemental Table A2. Crosswalk of SHELDUS Hazards and CoreLogic Perils

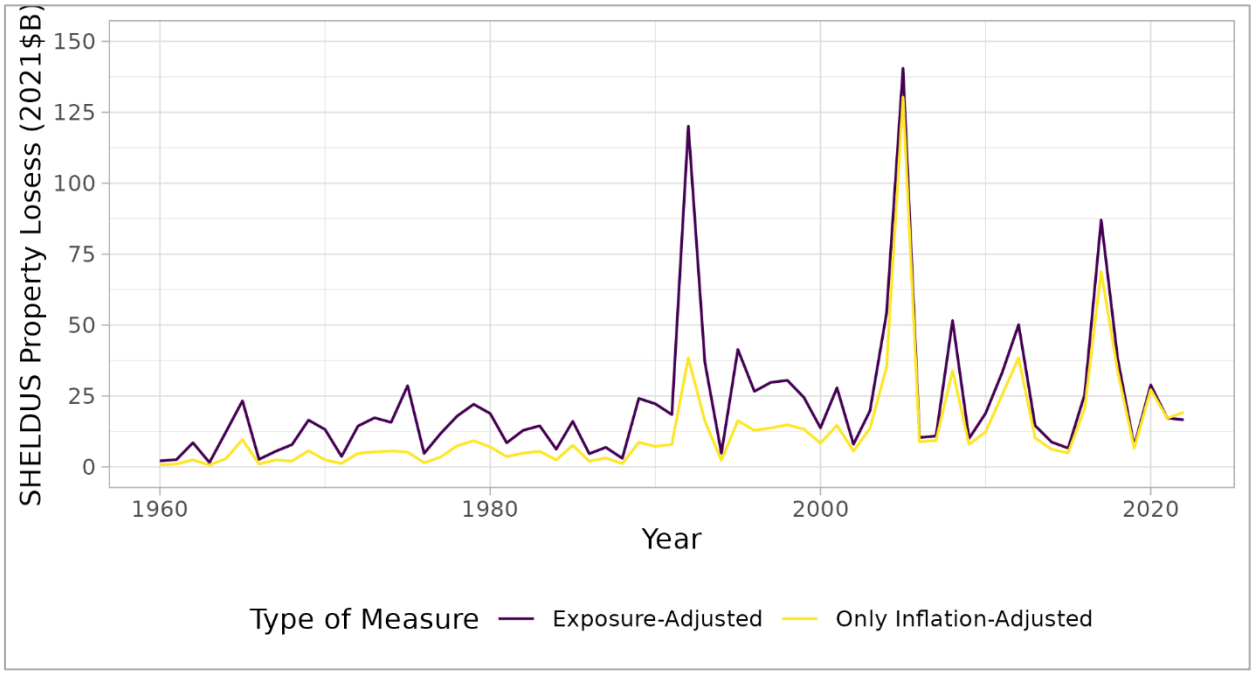
SHELDUS Hazard	CoreLogic Peril
Hurricane/tropical storm	Hurricane wind/inland flooding/hurricane storm surge
Flooding	Inland flooding
Tornado	Severe convective storm
Severe storm/Thunderstorm	Severe convective storm
Hail	Severe convective storm
Wind	Severe convective storm
Wildfire	Wildfire
Winter weather	Winter storm
Lightning	Severe convective storm
Coastal	Inland flooding

Supplemental Table A3. Hazard Shares of SHELDUS Historical Damages and Our Estimate of Current Expected Losses

Hazard Category	SHELDUS Damage Share (1960–2022)	Estimated Current Expected Loss Share Based on CoreLogic AALs
Hurricane and Flooding	63%	53%
Severe Convective Storm	27%	30%
Winter Storm	4%	10%
Wildfire	6%	6%

Note: Current expected loss share is based on estimate of AAL in dollars.

Supplemental Figure A1. SHELDUS Property Losses (1960–2022), Exposure-Adjusted and Not Exposure-Adjusted.



Exposure adjustment accounts for changes in the housing value exposed to damage over time.

Supplementary Section B: Assessing Predictive Power of CoreLogic Risk Estimates Using Recent Realized Disasters

In order to provide additional validation of CoreLogic's climate risk models, we test if CoreLogic's current expected damages, representing 2021, have predictive power over realized disasters in the 2021-2022 time period. To do so, we calculate county-level expected damage per Single Family Residence (SFR) (in $) based on CoreLogic current AAL estimates and merge it with disaster-caused property damage per housing unit in 2021-2022 from SHELDUS (See Materials and Methods for description of estimating expected losses in dollars from CoreLogic AAL estimates).

If CoreLogic models are informative about future climate risk, we should find a positive association between expected damage from climate-related disasters and realized damage in the post-period (2021-2022). In addition, we test if CoreLogic models provide additional information on future realized climate risk on top of past realizations by controlling for exposure-adjusted realized property damage from SHELDUS in past periods (2001-2020 and 1960-2020). (See Supplementary Information Section A for details on exposure adjustment to property damage recorded in SHELDUS.)

Supplementary Table B1 shows a positive association between expected losses based on CoreLogic modeling and realized losses in the out-of-sample period. In particular, at the county-level, an increase in CoreLogic expected damage per SFR of $1.00 is related to $1.19 increase in property damage per unit in the post period. A coefficient above 1 is reasonable as SHELDUS damage measures can include damage to non-residential property, while CoreLogic only models damage to the primary structure of residential properties. Columns (2) and (3) show that CoreLogic's model has predictive power of future climate-related damages even after controlling for past exposure-adjusted damage from SHELDUS, making it clear that CoreLogic's

model is not simply based on past realizations.

It is notable that the 2021 CoreLogic climate model has predictive power over future realized property damages as there are multiple factors working against finding a positive association. First, the out-of-sample period is extremely short (2 years), and CoreLogic's annual expected loss estimates are meant to represent the long-run average of losses for a given set of environmental conditions. The low-frequency, high-cost nature of climate-related disasters means that climate events are difficult to predict over short time periods and require many years to converge to long-run averages. Second, the CoreLogic expected loss estimates incorporates damages to the primary structure of SFR parcels. This is only a subset of property damages reported by SHELDUS (e.g. damage to public infrastructure), which should attenuate the estimated coefficients. Lastly, when comparing CoreLogic models to past realizations, reported SHELDUS damages may be similarly biased across time periods in a way that advantages their predictive power. For example, when a disaster hits multiple counties, SHELDUS typically splits damages across the impacted counties equally [38]. If similar groups of neighboring counties are hit in 2000-2020 as in 2021-2022, the weighting scheme employed by SHELDUS could bias upward the coefficient on SHELDUS Damage/Unit 2000-2020. Consequently, this would also bias downward the coefficient on CoreLogic Damage/SFR, when controlling for past realized damages.

Supplemental Table B1. Predicting 2021-2022 Realized Property Damage

Dependent Variable: SHELDUS Damage/Unit (2021-2022)			
	(1)	(2)	(3)
CoreLogic Damage/SFR (2021 Model)	1.190***	0.595***	0.649***
	(0.077)	(0.073)	(0.080)
SHELDUS Damage/Unit (2000-2020)		0.461***	
		(0.017)	
SHELDUS Damage/Unit (1960-2020)			0.668***
			(0.039)
Constant	-293.537***	-210.176***	-275.753***
	(38.400)	(34.742)	(36.710)
Observations	3,047	3,047	3,047
R^2	0.073	0.246	0.153
Adjusted R^2	0.073	0.246	0.153

*Note: This table presents coefficients from OLS regressions where the dependent variable is county-level average per unit property damage from SHELDUS during the 2021-2022 out-of-sample period. Independent variables include predicted average damage per single family residence from CoreLogic's model and average historical exposure-adjusted property damage per unit from SHELDUS. *, **, and *** indicate statistical significance at the 10%, 5%, and 1% levels, respectively*

Supplementary Section C: Analyzing CoreLogic Risk Estimates Using Alternative Risk Estimates

Validating the average annual loss (AAL) values from CoreLogic, in the context of using these values for our research, is inherently difficult because the ground truth is unknown. One check of reasonableness is to compare to historical loss data, which we do in Supplementary Information Section A. In that check we focus on the level of aggregate damage and the by-peril contribution to aggregate damage. However, our distributional analysis relies on the risk estimates from CoreLogic being ordinally accurate across geographies. One way to assess that is to examine how well CoreLogic's AAL estimates correlate with estimates from another catastrophic risk modeler. While we take no position on whether estimates from a different modeler are more or less accurate, we think rank-order agreement among the different sets of estimates provides more confidence in our distributional analyses.

We are able to perform this exercise for a subset of perils in our analysis using property-level AAL estimates from First Street Foundation (FSF). FSF is a non-profit organization that models flood, hurricane wind, wildfire, and extreme heat risk for the contiguous U.S. FSF's "flood" peril is equivalent to the combination of CoreLogic's Inland Flooding and Hurricane Storm Surge perils. Detailed methodology for all of First Street Foundation's models can be found on their website [41].

We compare the rank-order of AAL estimates between CoreLogic and FSF for Inland Flooding and Hurricane Storm Surge (together referred to as "Flood"), Hurricane Wind, and Wildfire. We compare tract-level average AALs among SFRs. In order to conduct the comparison, we match the SFRs identified in the CoreLogic data to properties in the FSF data using a nearest-neighbor geospatial match. Like in the main analysis, we limit the comparison to tracts where at least 30 SFRs have a non-missing AAL value reported in the CoreLogic and First Street Foun-

dation data. We normalize the nominal AALs provided by FSF by their estimate of rebuilding cost in order to be consistent with how CoreLogic expresses AAL values. Because nominal AAL values can infrequently exceed FSF's rebuilding cost measure, we top-code AAL values at 1. Note that because we have to normalize FSF's AALs, differences between each entity's AAL estimates could be driven by the underlying the hazard risk estimates, FSF's rebuilding cost estimate, or a combination of both.

There are a few notable differences between the two data sources beyond the inherent differences in their risk modeling approaches. First, the climate modeling data and emissions pathways underlying the risk modeling are of slightly different vintages. The CoreLogic estimates used in this analysis are based on the climate modeling data featured in the Intergovernmental Panel on Climate Change's (IPCC) Fifth Assessment Report (AR5) completed in 2014. Consequently, their baseline estimate is based on Representative Concentration Pathway (RCP) 4.5, which is the "middle-of-the-road" emission pathways featured in AR5. The FSF estimates used in this analysis rely on the latest climate modeling data from the IPCC's Sixth Assessment Report (AR6), which was completed in 2022. Therefore, their baseline estimates are based on Shared Socioeconomic Pathway (SSP) 2-4.5, which is the "middle-of-the-road" emission pathways featured in AR6.

Second, FSF and CoreLogic have different sources of property data that feed into their risk modeling. FSF licenses property data from the company LightBox. CoreLogic uses its own proprietary property data collection.

Third, the modeled areas for some perils differ between CoreLogic and FSF. As noted in the Methods section, CoreLogic only models Wildfire for the western half of the country plus Florida and only models Hurricane Wind risk for states on the Gulf and Atlantic coasts. FSF estimates non-zero Hurricane Wind risk further inland, including properties in states like Tennessee, Arkansas, and Oklahoma. Similarly, FSF models wildfire risk for the entire contiguous

U.S. and finds non-zero wildfire risk for properties outside of the CoreLogic modeled area. According to First Street Foundation's estimates, the areas with the greatest wildfire risk outside of CoreLogic's modeled area are Oklahoma, South Dakota, and parts of West Virginia, Kentucky, North Carolina, and Georgia.

Lastly, FSF does not provide an AAL estimate for wildfire. However, they provide a "destruction probability", which represents the annual likelihood of a structure being destroyed. Given that conditional on a structure combusting, it is very likely to be completely destroyed, the destruction probability can substitute well as an approximation of the AAL (as share of rebuilding cost) [42].

With those caveats in mind, Supplementary Table C1 provides the correlation between the average tract AALs and average tract AAL deciles from CoreLogic and FSF. In constructing the composite AAL (Flood + Hurricane Wind + Wildfire), we assume the expected loss is zero if it is outside the CoreLogic modeled area for Hurricane Wind and Wildfire. The composite AAL deciles correlate moderately well at r = 0.58. The tract average AAL values correlate similarly at r = 0.49. The by-peril correlations suggest that there is greater rank-order agreement for Hurricane Wind damage than for Flood and Wildfire damage.

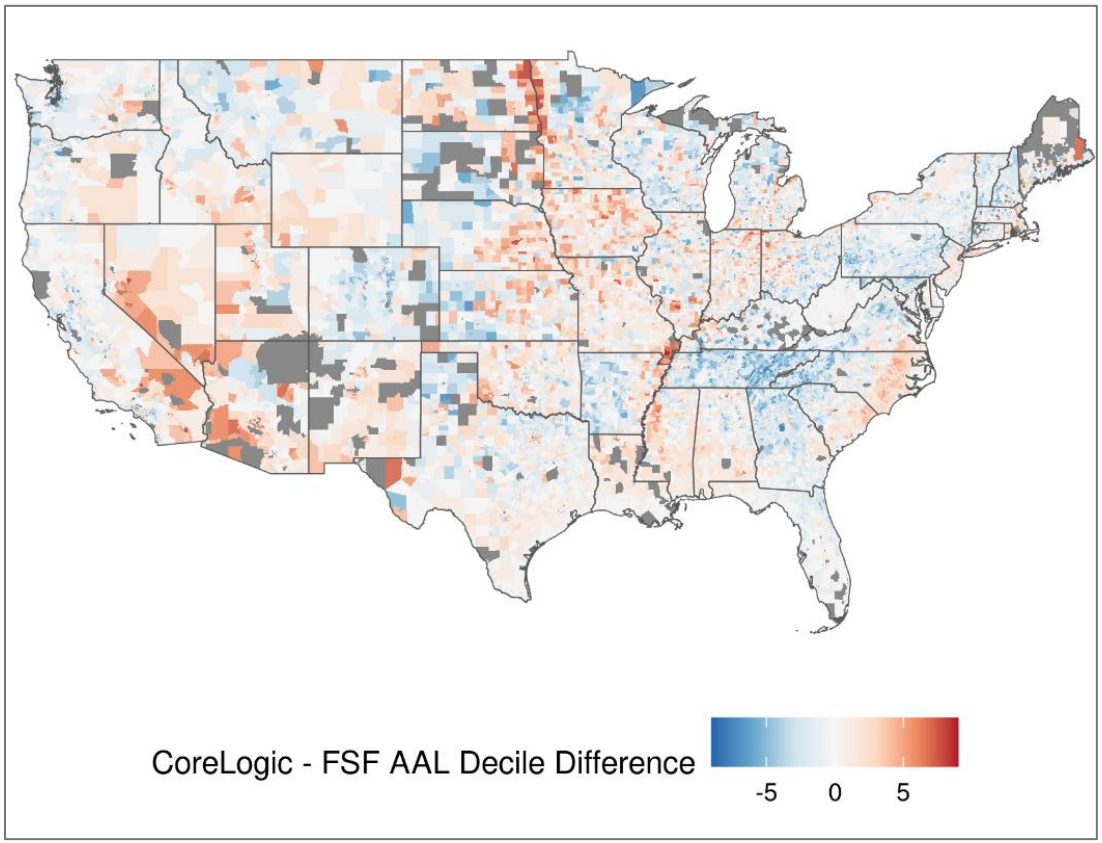
Notably, agreement between the two sets of composite AAL estimates is strongest among the riskiest tracts – 54% of tracts in the 10th decile of AAL according to CoreLogic were also in the 10th decile of AAL according to FSF. Another 21% of CoreLogic's 10th decile tracts were in FSF's 9th decile. This is evident in Supplementary Fig. C1, which maps the difference in tract AAL decile, and shows strong agreement along the Gulf and South Atlantic coasts, where many of the riskiest tracts are located.

Supplemental Table C1. Correlation Between CoreLogic and First Street Foundation Tract Average AALs

Peril	Correlation of Tract Average AAL Decile	Correlation of Tract Average AAL
Flood	0.41	0.37
Hurricane Wind	0.88	0.82
Wildfire	0.56	0.34
Composite (Flood + Hurricane Wind + Wildfire)	**0.58**	**0.49**

Note: In the case of Hurricane Wind and Wildfire, analysis limited to areas modeled by both CoreLogic and First Street Foundation. Tracts outside of peril's modeled area are considered to have no risk for that peril when generating composite AAL.

Supplemental Figure C1. Difference between CoreLogic and First Street Foundation Tract Average Current AAL Decile for Flood, Hurricane Wind, and Wildfire.



Difference between tract average AAL decile using CoreLogic and First Street Foundation data. Positive number (red) indicates the CoreLogic decile is greater than the First Street Foundation decile. The maximum difference in decile placement is nine. Tracts in grey have fewer than 30 single-family residences with AAL estimates in CoreLogic and/or First Street Foundation data.

Supplementary Section D: Validating the CCP Migration Measure Against ACS County-to-County Flows Data

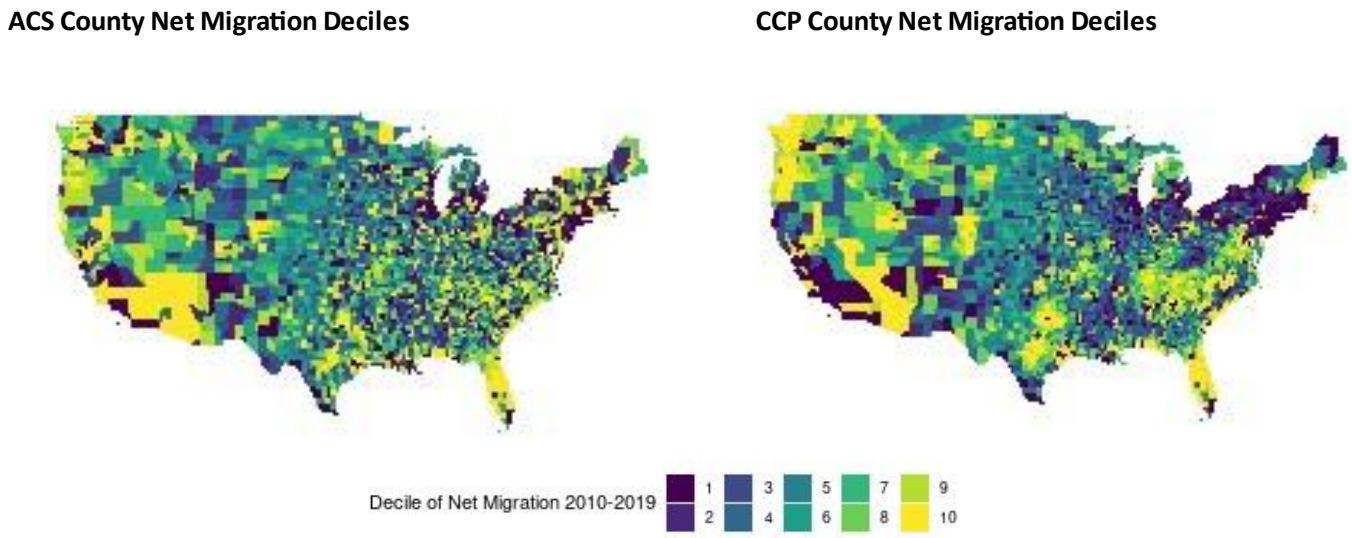
We examine net migration between 2010 and 2019 for areas of different climate risk using the FRB NY/Equifax CCP data (see Supplementary Table 5). One concern with using the CCP data set is its selection criteria of individuals with credit histories, which skews the sample towards older and more financially sophisticated individuals. Thus, CCP-based migration estimates would be biased to the extent that migration patterns systematically differ between those with and without credit histories.

We test the reasonableness of the CCP-based migration measure by comparing its county-level migration estimates with the ACS county-to-county migration flows for 2010–2019. For this comparison, we perform steps (1)-(4) from the approach described in Materials and Methods, except that we aggregate to the county level, which precludes the need to convert to 2010 census tract definitions. For the ACS-based measure, we use the 2010–2014 and 2015–2019 county-to-county flows data and sum the values to generate a total 2010–2019 net migration estimate for each county.

The ACS and the CCP net migration counts correlate relatively strongly (r = 0.84), which lends support to use of the CCP-based net migration estimates at the tract level. This result is consistent with more comprehensive assessments of migration estimates from the CCP using different sources of data, including the ACS data [35].

The deciles of ACS and CCP county net migration counts are shown in Supplementary Fig. D1. The highest decile represents the counties with the most net in-migration. The CCP-based deciles suggest more severe out-migration in the Northeast than the ACS-based deciles, but overall, the deciles are consistent with one another.

Supplemental Figure D1. Comparison of ACS and CCP County-Level Net Migration Estimates, 2010–2019



Deciles of county-level net in-migration during 2010–2019 using ACS (left) and CCP (right) data.

Supplementary Section E: Contribution to Literature

This section presents additional discussions of the marginal contribution that this paper makes to various strands of the climate change and climate risk literature. Special attention is paid to several closely related papers and literatures.

This paper focuses on climate-related physical risk that single family residences in the contiguous United States face now (circa 2021) and in the future (2050). The paper squarely builds on the work by Wing et al. (2022) and Gourevitch et al. (2023) [2, 3], which performs similar exercises for flood risk that properties in the United States face. With respect to these works, the main innovation that the current paper brings is the expected damage data from climate-related perils other than floods (e.g., severe convective storm, hurricane wind, winter storms, and wildfires), which allows us to compute a more comprehensive expected aggregate damage amount and paint a more complete picture of the distribution of expected damages, both geographically and demographically.

There are works that studies the expected economic damage of climate risk and climate-related disasters (Hsiang et al., 2017), which can be seen as a more comprehensive set of channels of damages that encompasses physical risk [13]. The contribution that our paper makes to this line of work is the data, which, if incorporated into projection models, would make the resulting economic damage analysis more complete. For example, the computation presented in Hsiang et al. (2017) only considers physical risk from coastal floods, which implies that the analysis ignores the direct impact of physical damage from other climate-related perils and the interaction between such damages and other economic forces that are embedded in the model. The estimates and data that we bring to the literature, if incorporated into the Hsiang et al. (2017) machinery, would allow researchers to produce a more realistic projection of the economic damage of climate change.

An important point to note is that this paper studies expected physical damages from climate-related perils at different points in time, which is different from studies of realized damages (Emrich and Cutter, 2011; Boustan et al., 2020) [8, 43]. Expected damage is the first moment of the distribution of possible damage values at a certain point in time, while realized damages are draws from the distribution. Although realized damages in the past may be correlated with expected damages in the future, an unbiased estimate of future expected damages is distinctly valuable, especially when we contemplate the evolution of climate change under different emission scenarios. Therefore, relative to work that uses historical damages, our paper's main innovation is the data on expected current and future physical damage.

Our paper shows that current and future composite climate-related physical risk is disproportionately borne by properties located in economically disadvantaged census tracts. With the new data, our contribution to the physical risk literature is to document the inequality of climate-related physical risk when we account for climate-related perils other than flooding. The finding also contributes to the literature on climate change and poverty by suggesting that climate change may exacerbate poverty and inequality through the physical risk channel, which is often understudied due to data limitations (Leichenko and Silva, 2014; Hallegatte and Rozenberg, 2017) [44, 45]. Lastly, although the literature on social vulnerability to natural disasters tells us that certain communities are particularly sensitive and ill-equipped to respond to natural disasters (Cutter and Finch, 2008), it does not inform us about the distribution of current and future climate-related physical risk [46].

Supplementary Section F: CoreLogic Climate Risk Analytics Modeling Documentation

The following documentation was shared with the authors by CoreLogic, who provided written consent for this document to be included as part of supplemental material to this research article.

CoreLogic



Documentation

Climate Risk Analytics

Intellectual Property Notice

© 2024 CoreLogic, Inc. All Rights Reserved.
CoreLogic, the CoreLogic logo, and RQE are trademarks of CoreLogic, Inc. and/or its subisidiaries. All other trademarks are the property of their respective holders.

This manual may not be reproduced or transmitted, in whole or in part, in any form or by any means, electronic, mechanical, photocopying, recording or otherwise, or stored in any retrieval system of any nature, without express written permission of CoreLogic, Inc.

Disclaimer

THIS DOCUMENT WAS PREPARED TO ASSIST USERS OF A DERIVATIVE PRODUCT OF RQE™ (RISK QUANTIFICATION & ENGINEERING), A PRODUCT OF CORELOGIC, INC. INFORMATION IN THIS DOCUMENT IS SUBJECT TO CHANGE WITHOUT NOTICE AND DOES NOT REPRESENT A COMMITMENT ON THE PART OF CORELOGIC, INC. THE MATERIAL CONTAINED HEREIN IS SUPPLIED WITHOUT REPRESENTATION OR WARRANTY OF ANY KIND. CORELOGIC, INC. ASSUMES NO RESPONSIBILITY AND SHALL HAVE NO LIABILITY OF ANY KIND ARISING FROM THE SUPPLY OR USE OF THIS DOCUMENT OR MATERIAL CONTAINED HEREIN.

IN ADDITION, THIS DOCUMENT IS PROVIDED PURSUANT TO A LICENSE AGREEMENT EXECUTED BETWEEN CORELOGIC, INC. AND THE AUTHORIZED USER, AND IS SUBJECT TO THE TERMS, INCLUDING ALL LIMITATIONS ON LIABILITY, CONTAINED THEREIN.

This document describes CoreLogic Climate Risk Analytics (CRA) Models. These Models represent alternative views of risk for future climate scenarios and time horizons. These alternative future climate scenarios are implemented in CoreLogic's Risk Quantification & Engineering catastrophe risk modeling software, RQE. The RQE models are used to assess climate change-related financial risks at the property and portfolio levels.

Contents

Confidentiality Acknowledgement ii

Intellectual Property Notice ii

Disclaimer ii

Contents iii

Table of Figures iv

Introduction. 1

Inland Flood. 1

- Introduction. 1
- Hazard Modeling 2
- Vulnerability Modeling. 2
- Climate Change Background. 3
- Climate Change Modeling 3
- Model Validation 3

Hurricane Wind 8

- Introduction. 8
- Hazard Modeling 8
- Vulnerability Modeling. 8
- Climate Change Background. 9
- Climate Change Modeling 10
- Model Validation 10
- References 12

Hurricane Storm Surge Model 13

- Introduction. 13
- Hazard Modeling 13
- Vulnerability Modeling. 13
- Climate Change Background. 13
- Climate Change Modeling 14
- Model Validation 14
- References. 18

Severe Convective Storm 19

- Introduction. 19
- Hazard Modeling 20
- Vulnerability Modeling. 21
- Climate Change Background. 22
- Climate Change Modeling 22
- Model Validation 23
- References. 24

Winter Storms 25

- Introduction. 25
- Hazard Modeling 25
- Vulnerability Modeling. 25
- Climate Change Background. 26
- Climate Change Modeling 26
- Model Validation 26
- References. 28

Wildfires 29

- Introduction. 29
- Hazard Modeling 29
- Vulnerability Modeling. 29
- Climate Change Background. 29
- Climate Change Modeling 30
- Model Validation 30
- References. 33

Proprietary. This material may not be reproduced in any form without the express written permission of CoreLogic.

Table of Figures

Figure 1: Baseline risk scores for Single-Family Residential (SFR) properties from Inland Flood peril. 4

Figure 2: RCP2.6 risk scores at 2050 for Single-Family Residential (SFR) properties from Inland Flood peril. . . .5

Figure 3: RCP8.5 risk scores at 2050 for Single-Family Residential (SFR) properties from Inland Flood peril. . . 6

Figure 4: Uncertainty considered in vulnerability function. 9

Figure 5: Side-by-side comparison of CoreLogic risk scores from North Atlantic Hurricane Wind peril for base case and RCP8.5 2050 scenarios. 11

Figure 6: Baseline risk scores for Single-Family Residential (SFR) properties from Storm Surge peril. 15

Figure 7: RCP2.6 risk scores at 2050 for Single-Family Residential (SFR) properties from Storm Surge peril. . .16

Figure 8: RCP8.5 risk scores at 2050 for Single-Family Residential (SFR) properties from Storm Surge peril. . .17

Figure 9: Weather extremes and climate change attribution 22

Figure 10: Comparison of risk scores from SCS peril for base case and RCP8.5 2050 scenarios for single-family residential properties. 23

Figure 11: Comparison of risk scores from Winter Storm peril for base case and RCP8.5 2050 scenarios for single-family residential properties. 27

Figure 12: Baseline risk scores for Single-Family Residential (SFR) properties from Wildfire peril. 31

Figure 13: RCP8.5 risk scores at 2050 for Single-Family Residential (SFR) properties from Wildfire peril. . . . 32

Proprietary. This material may not be reproduced in any form without the express written permission of CoreLogic.

Introduction

This document describes CoreLogic® Climate Risk Analytics (CRA) Models. These Models represent alternative views of risk for future climate scenarios and time horizons. These alternative future climate scenarios are implemented in CoreLogic's Risk Quantification & Engineering catastrophe risk modeling software, RQE®. The RQE models are used to assess climate change-related financial risks at the property and portfolio levels.

Inland Flood

Introduction

Flooding occurs when normally dry land is inundated with water and may come about from a variety of causes. Typically, water in an existing waterway, such as a pond, river, or stream, will rise and eventually overtop the normal banks and spread onto adjacent land. Ponding of rainwater in low-lying and poor drainage areas is also a cause of flooding. Coastal flooding can result from unusually high tides, strong onshore winds, and from the storm surge associated with a landfalling tropical cyclone or other strong storm.

Riverine flooding, as the name implies, occurs on existing rivers and waterways and is usually an event lasting a couple of days or even weeks. Riverine flooding can also affect wide expanses of land and extend for hundreds of miles along the length of the waterway. The slow but steady rise in water level can result due to a period of prolonged rainfall over a watershed, a weather pattern that produces successive days of intense rainfall from thunderstorms, or an unusually high spring snow melt.

Flash floods are shorter-term and more localized events that occur within 6 hours of the causative action such as high-intensity rainfall, dam break, levee failure, rapid snowmelt, and ice jams. These floods usually occur on smaller rivers, streams, tributaries, and drainage channels that can fill quickly under intense rainfall. Flash floods can move at incredible speeds and result in destruction of buildings, infrastructure damage to roads and bridges, floating debris such as trees, homes, automobiles, and loss of life. Flash flooding is a leading cause of weather-related deaths in the U.S.

The peril of flood causes significant damage and disruption to the U.S. In its report "Significant Floods in the United States During the 20th Century—United States Geological Survey (USGS) Measures a Century of Floods" (updated in February 2012), the USGS identifies more than 25 floods that have caused $100's of millions of dollars to billions of dollars in damage. Expanding populations and risk concentrations in flood exposed areas are increasing loss potential to citizens and property in the U.S. According to historical storm event data from the National Climatic Data Center (NCDC), 61% of flood events generating flood losses in the U.S. had a flash flooding component, causing extensive property damage and loss of life.

As the #1 natural disaster in the country, flooding represents a huge and largely uninsured risk in the United States. According to a RAND 2006 research report, it is estimated that only 50% of single-family homes within designated Special Flood Hazard Areas (SFHA) carry flood insurance. Outside of the SFHA however, statistics highlight a significant gap in the insurance coverage market, as the residential flood insurance penetration rate drops drastically to approximately 1%—a shocking statistic given that these areas yield one-fifth of all insurance flood claims. One impediment to the development of robust insurance solutions for all properties that are exposed to flood is the availability of accurate and consistent flood catastrophe risk models that enable insurers to assess the full financial risk of a site.

This document describes the methodology used to modify the U.S. Flood model in CoreLogic's RQE (Risk Quantification & Engineering) catastrophe risk modeling software to reflect climate change impacts from the latest nationwide expansion project. The climate-coupled U.S. Flood Model is used to generate the climate change versions of the hazard data sets to assess climate change-related financial risks.

Proprietary. This material may not be reproduced in any form without the express written permission of CoreLogic.

Hazard Modeling

This section describes the hazard component of the U.S. Flood Model, including hydrological and hydraulic modeling of riverine flooding as well as flash flooding. Risk modeling for inland flood risk relies on a robust understanding and modeling of rainfall-runoff and hydraulic processes, how variability in catchment characteristics can influence rates and volumes of runoff, and the relationship between flow and water level at any location. Hydrologic models are designed to estimate the amount of runoff or streamflow generated by individual storm events or by a combination of various storm events. Hydraulic models are then used to compute streamflow characteristics, such as depth and width of water and flow velocity.

The U.S. Flood Model leverages hydraulic models in combination with complex computational hydrological models. The inclusion of both modeling elements is essential to provide a reliable tool to quantify the relationship between water depth and recurrence interval at any location. The model also incorporates flash flooding at a location. A principal component of the model is the adoption of the DFIRM 100-year flood zone boundaries as an input data element. The integration of many other data layers reduces the biases of varying completion dates for the DFIRM maps and comparisons of the CoreLogic flood risk to independent validation sources produces excellent agreement.

For modeling purposes, flash flood is defined as a rapid flooding of geomorphic low-lying areas: washes, rivers, dry lakes, and basins. Flash floods are distinguished from a regular flood by a timescale of hours and may or may not be accompanied by associated riverine flooding. Short-term, high-intensity rainfall that occurs in inland areas with poor drainage often produces urban flash floods. The construction of buildings, highways, driveways, and parking lots increases runoff by reducing the amount of rain absorbed by the ground and densely populated areas have a high risk for flash floods. The risk of flash flooding is incorporated into the analysis to produce a consistent and rational relationship to risk in all areas.

Vulnerability Modeling

The vulnerability module estimates the damaging effects of flooding upon structures, which is used as the basis for a monetary estimate of the reconstruction costs to buildings, contents, and an estimate of the time lost (Additional Living Expense or ALE for personal lines, and Business Interruption or BI for commercial lines).

The critical inputs to the vulnerability model include event information such as water depth and flow velocity. Engineering data that is input by model users includes building age, construction type, occupancy, number of stories, and the presence of a basement. Optional input information that is not typically available to insurers includes the elevation of the first floor, and foundation and utility information that affects the reconstruction costs.

The U.S. Flood Model uses a hierarchical approach to determine the vulnerability of a building. In the first step, the collapse potential of a building is determined using velocity-depth damage curves that are a function of the structure type. These vulnerability curves relate velocity and depth to the collapse potential of buildings. If it is determined that a building would "collapse", the damage ratio is set to 100%. If not, a second set of vulnerability curves is used to ascertain the level of damage to the building.

The second set of vulnerability curves are depth-based and are dependent on the function of the occupancy of the building, the structure type, the number of stories, the presence or absence of a split level, the presence or absence of a basement, and the age of the building.

In general, flood vulnerability is mainly limited to structural finishes, contents, and inventory. However, complete structural failure due to flooding is possible where the flood velocity is significant. Other user- defined parameters involved in the damage calculation include the 1st FE and the SSMs. In this absence of such input, the model uses default values consistent with the building vintage and the flood zone.

Proprietary. This material may not be reproduced in any form without the express written permission of CoreLogic.

Climate Change Background

The average and peak rainfall associated with cyclones, severe convective storms, monsoons, and atmospheric rivers are expected to increase under climate change. With a 1°C increase in air temperature, the capacity of warm air to hold moisture increases by 7% according to Chapter 8 of the IPCC 6th assessment report (Douville et al., 2021). This increase in atmospheric moisture is expected to have measurable impacts on precipitation, with projected increases for many regions of the globe. The higher latitudes and monsoon regions are expected to see an increase in heavy precipitation, while parts of subtropics and tropics are expected to see declines in precipitation. Under climate change, the frequency and severity of severe tropical cyclones (category IV and V) are also expected to increase according to the IPCC Ar6 report, chapter 11 (Seneviratne et al., 2021). Such increases in extreme precipitation and severe storm events will coincide with an increase in extreme runoff, contributing to various types of flood events. However, widespread drought may cause streamflow to decline in many regions, with minor riverine flooding events limited by declines in mean water levels in U.S. rivers and streams. Whereas streams that become seasonally dry in the U.S. West may become more prone to flash-flood events.

Climate Change Modeling

The climate change versions of the CoreLogic inland flood model incorporate the effects of expected changes in extreme surface runoff and the potential changes in characteristic streamflow conditions due to climatological shifts in baseflow runoff. The hydrologic projections for the future Representative Concentration Pathways (RCPs) used in this model are based on the high-resolution models' outputs. Thirty-one general circulation models (GCMs) were downscaled to the Contiguous United States by the hydrological model. The hydrological variables used to assess the impact of future changes in inland flooding are computed by the Variable Infiltration Capacity (VIC) hydrologic model (Hamman et al., 2018). VIC was driven by daily meteorological variables from the 31 GCMs.

Based on hydrological and statistical analysis GCMs were selected for inclusion into a model ensemble that weighted GCMs based on their performance capturing spatial patterns in historical streamflow trends at USGS gage locations, as well as their ability to replicate the daily runoff from VIC when driven by meteorological variables derived from a climatological reanalysis (Livneh et al., 2013). A GCM's ability to provide novel information relative to other ensemble members was also considered in the final weighting, to better capture the range of potential future outcomes related to extreme runoff. This selection process for the weighted ensemble was applied regionally across the U.S. to best capture observed trends for both wetter and drier climate regions.

Furthermore, in coastal areas, inland severe flood events could be induced by hurricanes. The analytic linkage between inland flood events and hurricane events were established in RQE. As a result, related climate changes (such as frequency changes) on hurricanes can trigger additional changes on inland flood losses, so that correlated influences on inland floods from hurricanes are considered during flood loss computation.

Model Validation

Percent changes in runoff from hydrological downscaling were evaluated on their performance and correlations against USGS gauge data over 4,000 stations from 1991 to 2021. Our investigation found that GCMs could have vastly different performances in different climate regions, with some better suited to wetter or drier regions. GCMs with poor performance were excluded from the analysis to ensure the accuracy and reliability of inland flood projections. Additional data from USGS gages were withheld for independent validation of the findings. The inclusion of these additional gage stations and years prior to 1991 led to similar performance metrics, indicating the robustness of the model ranking over multiple decades of observations.

Proprietary. This material may not be reproduced in any form without the express written permission of CoreLogic.

A sufficient uncertainty control strategy was facilitated based on a comprehensive sensitivity analysis on runoff outputs to ensure that small catchments did not deviate strongly from others in proximity, especially those that experience seasonal variability or low streamflow, which would make them sensitive to the timing of runoff inputs or even small variations in the quantity of runoff. In our AR5 solution inland flood climate risk projections, there is spatial heterogeneity in the direction of percent changes in runoff. Our assessment also includes flood loss validations on multiple scenarios and time horizons by using large national portfolios. Further, the AR5 portfolio-wide percent losses in AALs span a wide range across the various RCPs and time horizons. Figure 1-3 show the inland flood risk score maps for baseline, RCP2.6 2050 and RCP8.5 2050.

FLXX–SFR–base

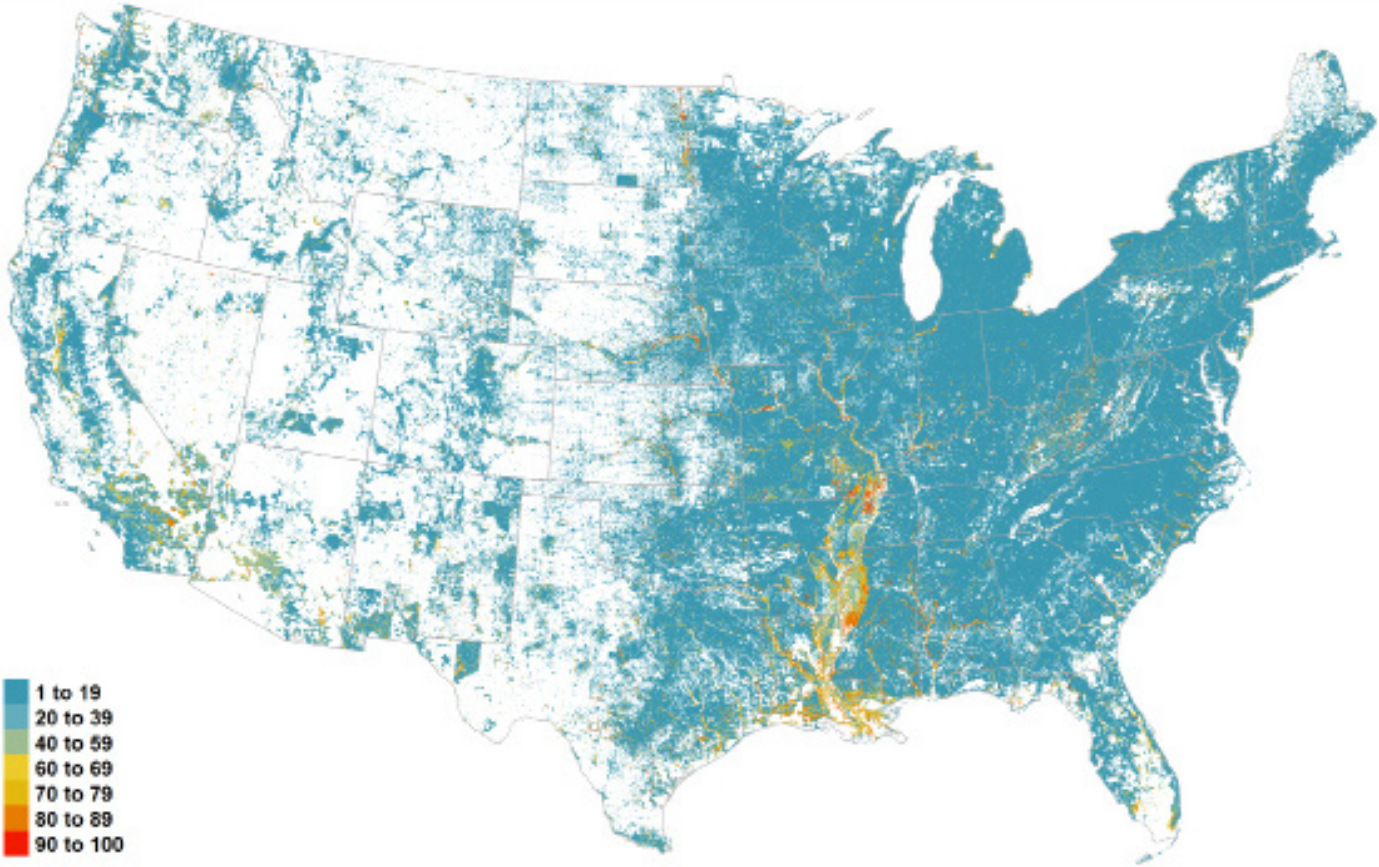


Figure 1: Baseline risk scores for Single-Family Residential (SFR) properties from Inland Flood peril.

Proprietary. This material may not be reproduced in any form without the express written permission of CoreLogic.

FLXX–SFR–rcp26_2050

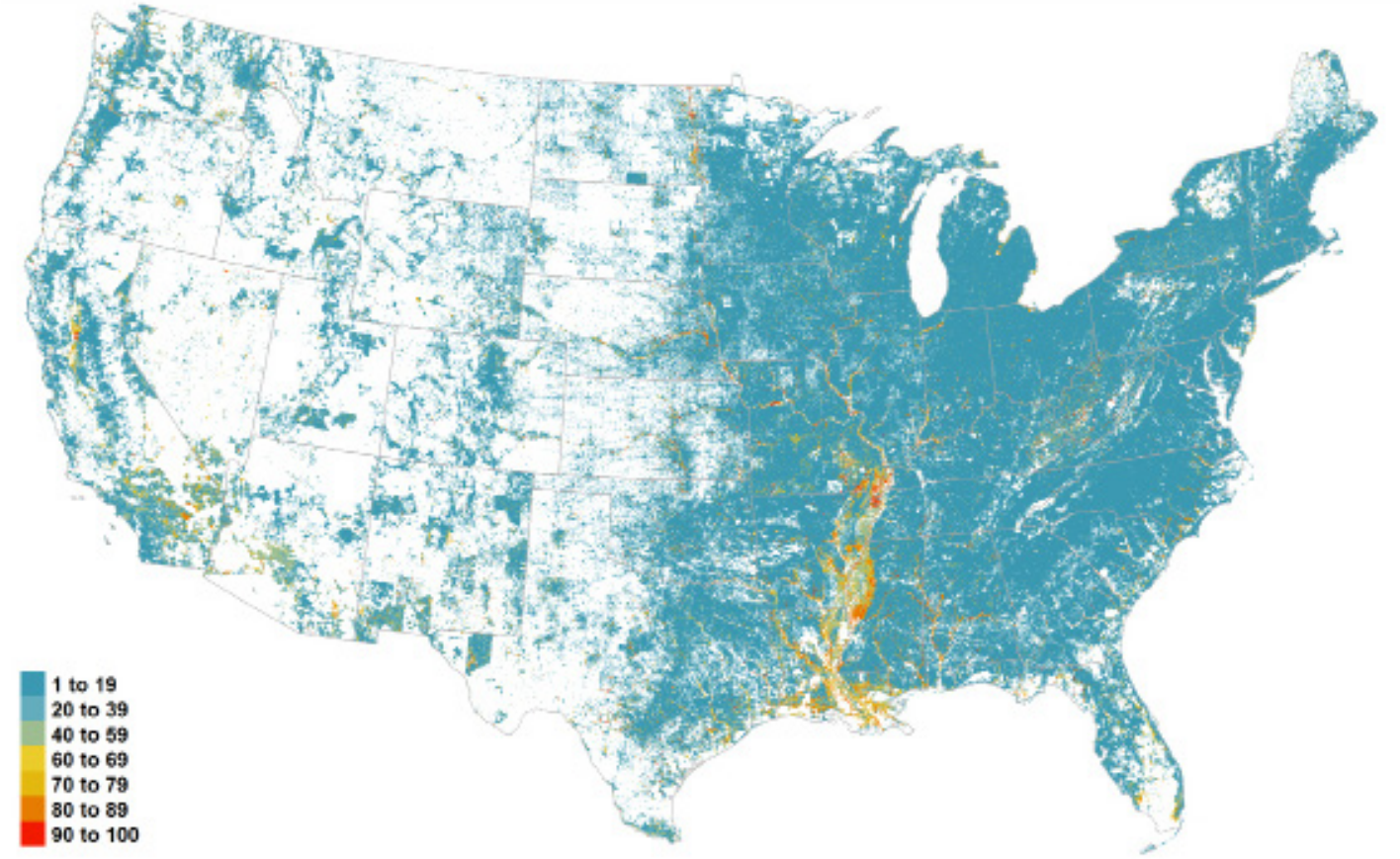


Figure 2: RCP2.6 risk scores at 2050 for Single-Family Residential (SFR) properties from Inland Flood peril.

Proprietary. This material may not be reproduced in any form without the express written permission of CoreLogic.

FLXX–SFR–rcp85_2050

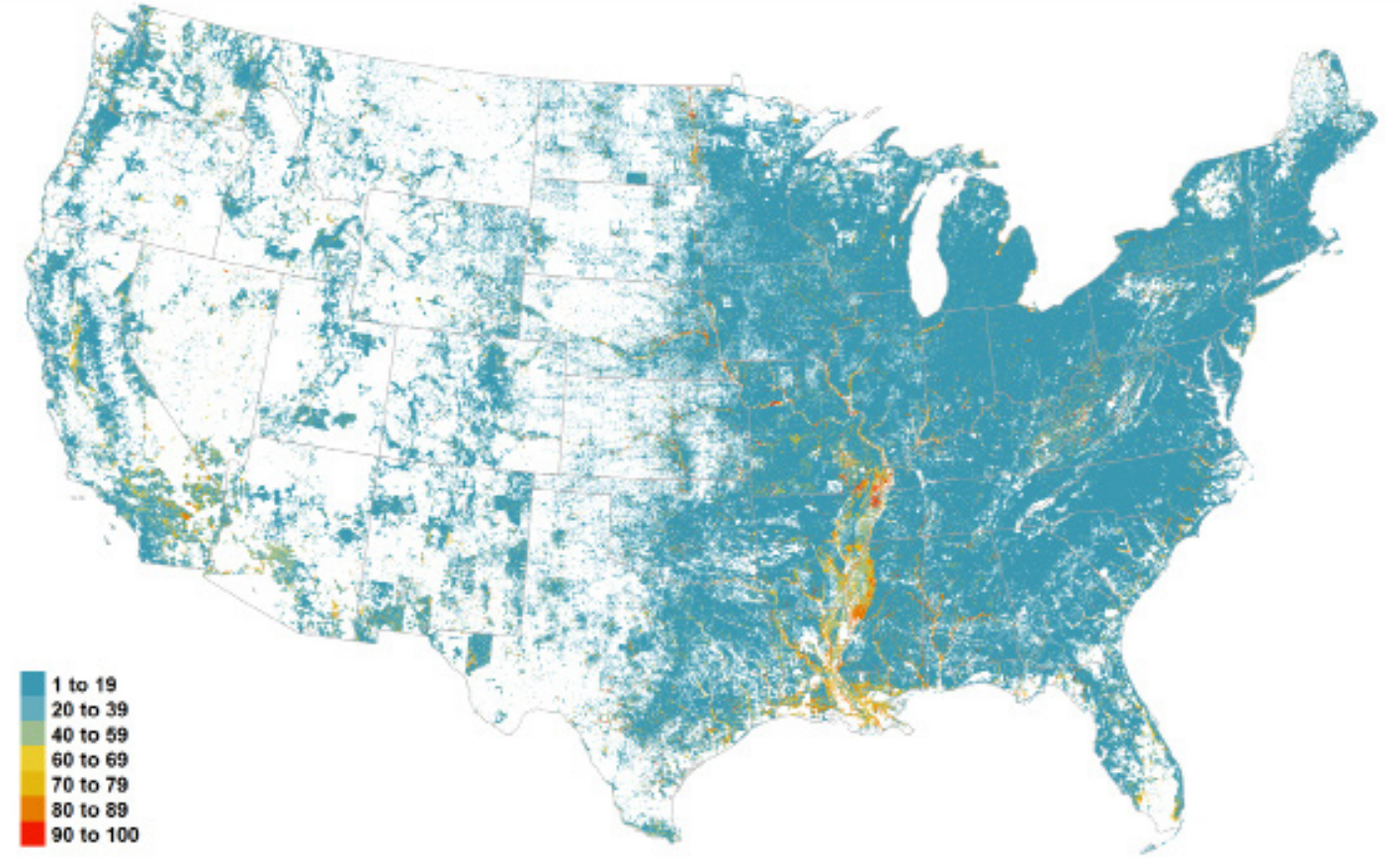


Figure 3: RCP8.5 risk scores at 2050 for Single-Family Residential (SFR) properties from Inland Flood peril.

Proprietary. This material may not be reproduced in any form without the express written permission of CoreLogic.

References

Douville, H., K. Raghavan, J. Renwick, R.P. Allan, P.A. Arias, M. Barlow, ...& O. Zolina (2021). Water Cycle Changes. In Climate Change 2021: The Physical Science Basis. Contribution of Working Group I to the Sixth Assessment Report of the Intergovernmental Panel on Climate Change [Masson-Delmotte, V., P. Zhai, A. Pirani, S.L. Connors, C. Péan, S. Berger, N. Caud, Y. Chen, L. Goldfarb, M.I. Gomis, M. Huang, K. Leitzell, E. Lonnoy, J.B.R. Matthews, T.K. Maycock, T. Waterfield, O. Yelekçi, R. Yu, and B. Zhou (eds.)]. Cambridge University Press, Cambridge, United Kingdom and New York, NY, USA, pp. 1055–1210. doi:10.1017/9781009157896.010

Hamman, J. J., Nijssen, B., Bohn, T. J., Gergel, D. R., & Mao, Y. (2018). The Variable Infiltration Capacity model version 5 (VIC-5): Infrastructure improvements for new applications and reproducibility. Geoscientific Model Development, 11(8), 3481–3496.

Livneh, B., Rosenberg, E. A., Lin, C., Nijssen, B., Mishra, V., Andreadis, K. M., ... & Lettenmaier, D. P. (2013). A long-term hydrologically based dataset of land surface fluxes and states for the conterminous United States: Update and extensions. Journal of Climate, 26(23), 9384–9392.

Merrifield, A., Brunner, L., Lorenz, R., & Knutti, R. (2020, May). A weighting scheme to incorporate large ensembles in multi-model ensemble projections. In EGU General Assembly Conference Abstracts (p. 4524).

Pierce, D.W., D.R. Cayan and B.L. Thrasher, (2014). Statistical Downscaling Using Localized Constructed Analogs (LOCA). Journal of Hydrometeorology, 15,2558–2585. doi:10.1175/JHM-D-14-0082.1

Seneviratne, S.I., X. Zhang, M. Adnan, W. Badi, C. Dereczynski, A. Di Luca, ... & B. Zhou, 2021: Weather and Climate Extreme Events in a Changing Climate. In Climate Change 2021: The Physical Science Basis. Contribution of Working Group I to the Sixth Assessment Report of the Intergovernmental Panel on Climate Change [Masson-Delmotte, V., P. Zhai, A. Pirani, S.L. Connors, C. Péan, S. Berger, N. Caud, Y. Chen, L. Goldfarb, M.I. Gomis, M. Huang, K. Leitzell, E. Lonnoy, J.B.R. Matthews, T.K. Maycock, T. Waterfield, O. Yelekçi, R. Yu, and B. Zhou (eds.)]. Cambridge University Press, Cambridge, United Kingdom and New York, NY, USA, pp. 1513–1766, doi:10.1017/9781009157896.013.

Proprietary. This material may not be reproduced in any form without the express written permission of CoreLogic.

Hurricane Wind

Introduction

Hurricanes, like tornadoes, move in a circular motion: anticlockwise in Northern Hemisphere and clockwise in Southern Hemisphere. A storm gains energy from warm ocean water, and as it becomes stronger (>74mph) develops as a hurricane (https://oceanservice.noaa.gov/). Hurricanes can create destructive weather resulting in catastrophic economic and human loss. Because warm air can hold more moisture, hurricanes developing over a warm ocean can bring large volume of water, causing flash flooding at the site of landfall, whether coastal or inland. Hurricanes also cause damage due to their destructive winds, but loss from flooding is more significant in comparison. Hurricanes can cause storm surge, that is push more water towards shore due to the strong winds, which increases sea level and resulting in coastal flash flooding. For these reasons, it is imperative to study and model hurricane hazards and their associated financial losses to make our economies and society more resilient.

This document describes the methodology used to modify the North Atlantic Hurricane model in CoreLogic's RQE (Risk Quantification & Engineering) catastrophe risk modeling software to reflect nationwide climate change impacts. The climate-coupled North Atlantic Hurricane model is used to assess climate change-related financial risks, by generating the hazard data sets for various future climate change scenarios.

Hazard Modeling

The CoreLogic's North Atlantic Hurricane Model is a probabilistic model that uses the National Hurricane Center's HURDAT2 data set. Its robust probabilistic set includes approximately 110,000 events. All stochastic events have a maximum landfall intensity of at least hurricane intensity (1-minute maximum sustained wind speed of at least 74 mph). Storms in the event table are categorized at landfall.

Each event in the set is assigned the annual probability of occurrence ("frequency"), one based on the near-term view of risk and the other on the long-term view of risk. The simulation process selects (samples) an event from the probabilistic event set, and calculates losses associated with that event. This is repeated 300,000 times. The event frequencies are expressed on an annual basis equivalent to 300,000 "simulation years". After an event is used for the simulation, it is returned to the set of possible events from which the next sampling is randomly selected. In addition, 300,000 simulation years covers gaps in the historical data set to provide a consistent, credible, and realistic view of hurricane risk, particularly for low-probability, high-consequence events. The model also accounts for temporal clustering of hurricane events. The probabilistic set is evaluated against the historical data set for completeness and validation. Hurricane landfall intensity and locations vary by region and are based on climatology and seasonality. The event set is optimized to be sufficiently comprehensive to capture the full range of possibilities and to facilitate model analysis speed. The model includes 109,288 events impacting the basin, of which about 33,082 events impact the U.S. mainland.

The hazard model calculates the peak gust wind speeds at any location by producing a probabilistic distribution of wind speed for each event in the stochastic event set covering the geographic region included in the model. The hazard model includes creation of the storm events database used for simulation and the high-resolution time-stepping wind field model calculates the peak gust, which is the quantified output of the hazard model used to estimate damage.

Vulnerability Modeling

The vulnerability module estimates the damage ratio, given the peak gust, flood depth and velocity, structure type, occupancy type and total value of the exposure. The quantified output of the vulnerability module is ground-up damage for each exposed asset or coverage type. The financial loss module calculates the losses, given the damage output and the policy term or treaty structure and conditions of the insurance contracts.

Proprietary. This material may not be reproduced in any form without the express written permission of CoreLogic.

The output of the vulnerability module is damage, typically expressed as a ratio, or percent, of the full replacement value. Damage is also known as "ground-up loss," or "ground-up damage" because it represents losses before applying insurance policy structures, terms, and conditions.

The vulnerability module significantly influences model results. These results will be most reliable when the input data most closely matches actual exposures. Vulnerability calculations are particularly sensitive to the classification of structure type, occupancy, height, age, cladding, and secondary structural modifiers (SSMs). Next, the vulnerability calculations are sensitive to the total insured value because it is the denominator for the calculation of damage as a ratio.

A building vulnerability (or damage) function correlates the damage sustained by a building of specific characteristics to a hazard parameter defining the intensity of the peril, in this case wind or flood, at the site. In the North Atlantic Hurricane Model, wind damage is a function of wind speed, whereas flood damage is a function of water depth. In addition to the building vulnerability function, a corresponding contents vulnerability function and a time element vulnerability function are used to estimate the total ground-up loss at a site.

Buildings of similar construction and vintage located in the same vicinity will sustain varying levels of damage despite the similar wind field they are subjected to. This is illustrated in Figure 4, which depicts a vulnerability function, the distribution around the wind speed, W, representing its uncertainty at the site, and the corresponding conditional damage distribution at that same wind speed, W. The damage at the site is represented by the probability density function along the vertical axis.

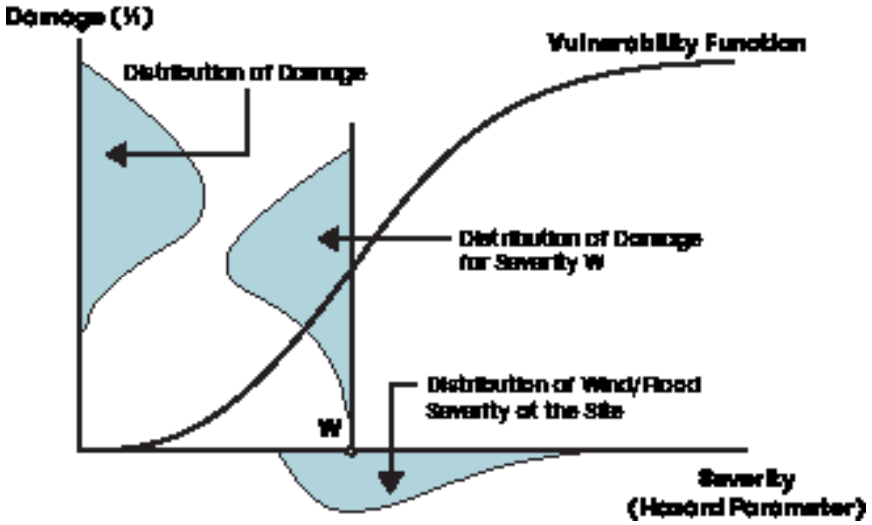


Figure 4: Uncertainty considered in vulnerability function

Climate Change Background

With climate change, there is high confidence that the frequency of severe hurricanes will increase, per the IPCC AR6 report Ch. 11 (Seneviratne et al., 2021). It is likely these events will bring more rain under a warmer future as warm air can hold more moisture (Douville et al., 2021). These frequency and atmospheric moisture increase have implications for coastal and inland flooding and increase the height and frequency of damaging storm surge. Studies have found a global reduction in translation speed and increase in the landfalling duration of the hurricanes (Kossin 2018; Kopp et al., 2021), meaning these severe events can stay for a longer period, increasing the risks to properties from flooding and wind damage.

Proprietary. This material may not be reproduced in any form without the express written permission of CoreLogic.

Climate Change Modeling

To elucidate the catastrophic effects of North Atlantic Hurricanes under climate change, CoreLogic has quantified the climate change impact on North Atlantic Hurricanes by estimating the hurricane frequency changes as a function of severity class. Our current modeling of climate change impact on hurricanes includes notable improvements from our previous methods. Some of the updates include: 1) the use of the projected hurricane frequency data from dynamical, statistical-dynamical and statistically downscaled models, 2) the estimation of regional changes in hurricane landfall frequency as a function of severity class regionally along the U.S. coast from the Gulf of Mexico to New England, thus highlighting the spatial heterogeneity of future projections, and 3) deriving the severity of hurricane frequency changes for three time horizons for each of the three different emission scenarios in the 21st century.

We modeled our projections based on landfall frequency rather than formation frequency in the North Atlantic basin, providing a more accurate estimation of changes in future hurricane frequency. The frequency changes for 2030-, 2040- and 2050-time horizons are systematically estimated to better represent the RCP GHG emission trajectories.

Model Validation

CoreLogic modeled regional frequencies of hurricanes by severity for different RCP scenarios and future time horizons. Our modeled projections align with the projections of the global scientific community. Our current scientific understanding states that hurricane severity will increase in a warming climate, thus shifting the distribution of hurricane frequency towards the higher end of the severity spectrum. These changes in hurricane frequency further vary spatially from basin to basin and locally from coastal region to region. Our modeled projections were able capture this spatial heterogeneity in the hurricane frequency and severity along the U.S Gulf Coast and East Coast. For example, in the Gulf it is projected that SSI3-5 would increase at all future horizons with a 91% increase in SSI5 frequencies in 2050 under RCP8.5.

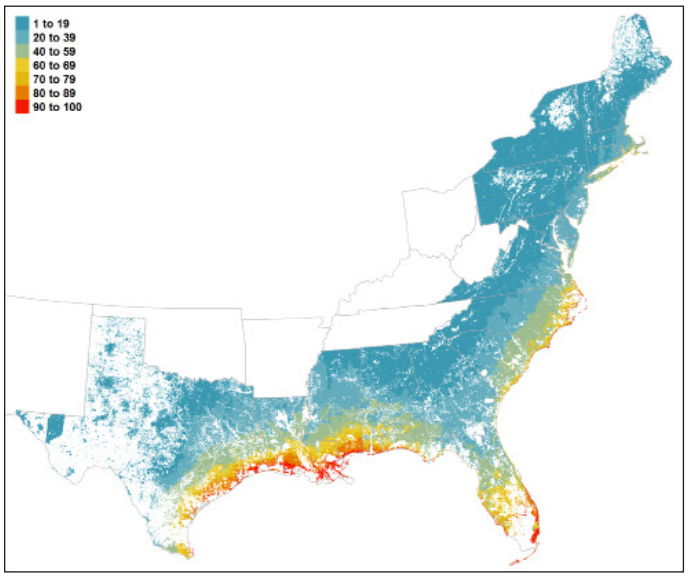
This increase in SSI3-5 in Gulf Coast can be attributed to the rapid intensification of hurricanes as they move into the Gulf of Mexico region, with a warm pool of waters closer to the coast. On the other hand, the Southeast (FL keys-VA) and Northeast (VA-ME) region are expected to see an increase in all SSI hurricanes, with the Southeast seeing more increase in SSI3-5 compared to SSI1-2. The slow movement along the East Coast allows for the intensification of hurricanes, increasing the risk for the Southeastern states, with the Northeast seeing an increase in SSI1-4. The Northeast is projected to have the highest increase in the SSI3 and 4 compared to the Gulf and Southeast by 2050 under RCP8.5. The penetration of tropical warm water to higher latitudes would lead to the development of hurricanes at higher latitudes, also known as sub-tropical cyclones, which increases risk for the Northeastern states like New York and Maine and even Canada, as these hurricanes interact with mid-latitude systems. Our hurricane climate change results have been thoroughly tested and meticulously validated against different peer-reviewed hurricane modeling studies and regional climate assessment reports, increasing our confidence in the spatial heterogeneity of risk captured in our modeling.

Further, our model testing includes the hurricane wind loss analysis for various portfolios. The use of regional changes in hurricane landfalls results in a more accurate and increased change in hurricane wind related losses, with a maximum of 55–60% increase in AAL in Florida at 2050 under RCP8.5. Furthermore, the non-linear variation in the projected losses across the States highlights the varying impacts of hurricane landfalls. It is noted that the losses incurred in the Northeast states will increase significantly in the future; this increase in wind losses in the Northeast can be attributed to the poleward migration of hurricanes and the expansion of warm tropical waters.

Proprietary. This material may not be reproduced in any form without the express written permission of CoreLogic.

Figure 5 below shows the comparisons of CoreLogic modeled hurricane wind risk scores at property level for base climate and different RCP8.5 scenario in 2050. The risk scores range from 1 to 100 with 100 being the highest risk. We can see that as we move towards worse RCP scenario like RCP8.5 into the future, the number of locations at higher risk from hurricane wind increases. Increasingly, inland locations will be affected with an increased risk. The increase of risk along the Southeast and Northeast is also observed in Figures 5. These hurricane wind related risks combined with hurricane induced storm surge and floods would exacerbate the loss of life and property in the U.S in the future.

TCWI–SFR–base



TCWI–SFR–rcp85_2050

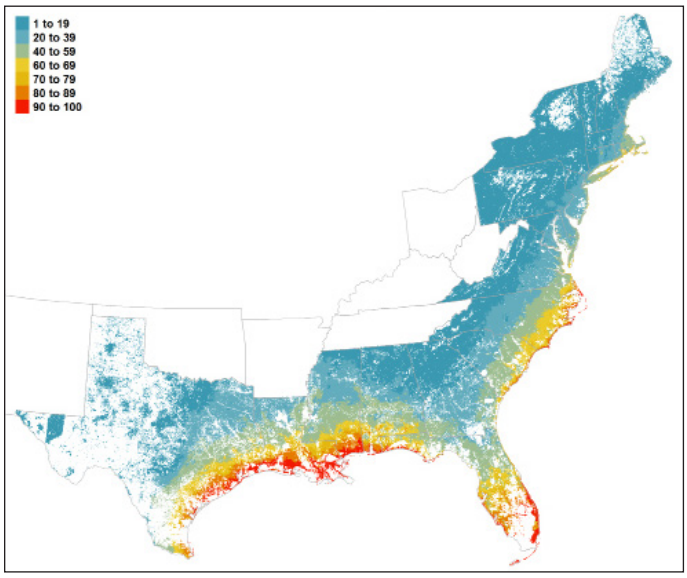


Figure 5: Side-by-side comparison of CoreLogic risk scores from North Atlantic Hurricane Wind peril for base case and RCP8.5 2050 scenarios.

Proprietary. This material may not be reproduced in any form without the express written permission of CoreLogic.

References

Emanuel, K. (2006). Climate and tropical cyclone activity: A new model downscaling approach. *Journal of Climate*, 19(19), 4797–4802.

Emanuel, K. (2021). Response of global tropical cyclone activity to increasing CO 2: results from downscaling CMIP6 models. *Journal of Climate*, 34(1), 57–70.

Hallegatte, S. (2007). The use of synthetic hurricane tracks in risk analysis and climate change damage assessment. *Journal of applied meteorology and climatology*, 46(11), 1956–1966.

IPCC, 2021: Summary for Policymakers. In: Climate Change 2021: The Physical Science Basis. Contribution of Working Group I to the Sixth Assessment Report of the Intergovernmental Panel on Climate Change.

Jing, R., Lin, N., Emanuel, K., Vecchi, G., & Knutson, T. R. (2021). A Comparison of Tropical Cyclone Projections in a High-Resolution Global Climate Model and from Downscaling by Statistical and Statistical-Deterministic Methods. *Journal of Climate*, 34(23), 9349–9364.

Knutson et al., (2020). Tropical cyclones and climate change assessment: Part II: Projected response to anthropogenic warming. *Bulletin of the American Meteorological Society*, 101(3), E303–E322.

Proprietary. This material may not be reproduced in any form without the express written permission of CoreLogic.

Hurricane Storm Surge Model

Introduction

Storm surge is an abnormal rise of water generated by a storm, over and above the predicted astronomical tides. In the case of hurricanes, storm surge is primarily the result of extreme winds pushing the shallow coastal waters in such a way that causes the sea level to rise. The rise in water level can cause extreme flooding in coastal areas, particularly when storm surge coincides with normal high tide. Powerful storms can cause up to 30 feet of storm surge.

Hazard Modeling

CoreLogic possesses a stochastic event set of 110,000 storm events based on perturbed historical hurricanes. For each event, the CoreLogic storm surge model computes storm surge heights along the U.S. coast based on a numerical model that solves the equations of motion for seawater, with hurricane wind stress as a boundary condition. The model considers variations in astronomical tides, flood defense systems, and first floor elevation of buildings when determining structure damage.

Vulnerability Modeling

The vulnerability module estimates the damage ratio given the storm surge flood depth and velocity, structure type, occupancy type and total value of the exposure. As with the hurricane wind component, the quantified output of the vulnerability module is ground-up damage for each exposed asset or coverage type, typically expressed as a ratio, or percent, of the full replacement value.

The vulnerability module significantly influences model results. These results will be most reliable when the input data most closely matches actual exposures. Vulnerability calculations are particularly sensitive to the classification of structure type, occupancy, first-floor height, age, cladding, and secondary structural modifiers (SSMs). The vulnerability calculations are also sensitive to the total insured value because it is the denominator for the calculation of damage as a ratio.

A building vulnerability (or damage) function correlates the damage sustained by a building of specific characteristics to a hazard parameter defining the intensity of the flooding at the site, with flood damage being a function of storm surge water depth. In addition to the building vulnerability function, a corresponding contents vulnerability function and a time element vulnerability function are used to estimate the total ground-up loss at a site.

Climate Change Background

Sea level rise increases the still water height of the ocean relative to the land, raising the height of tides and allowing a storm surge of equivalent magnitude today to penetrate farther inland. Since 1950, U.S. coastlines that are at risk of hurricane landfall have experienced between 7–20 inches of sea level rise, with more than half of that rise since the year 2000. Sea level rise will accelerate under future climate change as increasing temperatures melt ice sheets and warm the oceans, causing thermal expansion. Changes in ocean circulation due to the input of freshwater and heat will cause the migration of ocean currents, such as the Gulf Stream, contributing to regional sea level rise. Additionally, natural land sinking, mass loading from human development, and extraction of groundwater has led to subsidence of many coastal areas.

The frequency of severe hurricanes (category IV and V) will also likely increase under climate change, and there is high-confidence in this outcome per the IPCC AR6 report Ch. 11 (Seneviratne et al., 2021). Excluding the impacts of local bathymetry, storm surge heights correspond with the strength of hurricane winds, so it is anticipated that more severe hurricanes will lead to increased storm surge flooding.

Proprietary. This material may not be reproduced in any form without the express written permission of CoreLogic.

Climate Change Modeling

The climate change versions of the CoreLogic storm surge model incorporate the effects of expected increases in the frequency of hurricanes as a function of severity, and the effects of sea level rise, in response to future global warming. Frequencies by hurricane severity class are derived from the downscaling of hurricane storm tracks using the high-resolution dynamical model, a regional dynamical downscaling approach. Sea level rise projections are obtained from the US Interagency Sea Level Rise Task Force, a joint task force of the National Ocean Council (NOC) and the US Global Change Research Program (USGCRP), which provides a comprehensive assessment of future sea level rise scenarios for the US under various future emission pathways. The raw data adopted in CoreLogic's analytics to assess the impact of sea level rise along the Texas to Maine coastline and the technical documentation on the different sea level rise scenarios come from a 2022 update of the projections given by the Fourth National Climate Assessment.

Based on the findings documented in NOAA's most recent technical assessment (Sweet et al., 2022), CoreLogic adopted different sea level rise scenarios to correspond with the various future emissions pathways outlined by the IPCC. These chosen scenarios represent several possibilities bounded by observation-based projections and supported by expert judgements of risks associated with ice shelf destabilization in Antarctica over the next several decades. Each sea level rise scenario was regionalized to CoreLogic's storm surge model grid, with the added sea level being incorporated into the model's stillwater height. Site specific vertical land motion was calculated by considering long term measurements from tide-gauges (Kopp et al., 2014) and available GPS networks (Hammond et al., 2021). These estimates of local subsidence were also incorporated into the storm surge model's coastal grid, as they affect the ocean's elevation relative to the land.

Model Validation

Regional sea level rise scenarios from NOAA (National Oceanic Atmospheric Association) were validated against trajectories based on historical tide-gauge data, as well as rates of historical coastal sea level rise from NASA's Estimating the Circulation and Climate of the Ocean (ECCO) re-analysis model (Wang et al., 2017), confirming the ability of the product to reconstruct observations. This should not be surprising, as overall, there is medium to high confidence in many of the underlying physical drivers of sea level rise (Fox-Kemper et al., 2021). One of the largest contributing factors to local variations in the rate of sea level rise is vertical land motion, which is not modeled by climate models. Estimates of vertical land motion from GPS (Hammond et al., 2021) and tide-gauges (Kopp et al., 2014) have been broadly similar for the U.S. where coverage is of good quality. However, there remains large uncertainty around the impact of future human development on rates of coastal subsidence.

Tests on several national property portfolios were conducted to ensure that these sea level rise scenarios, in conjunction with changes in hurricane storm frequency and severity, contributed realistic patterns to property losses. State-by-state and county assessments for the Gulf Coast and East Coast found that most of the increased loss occurred for properties that already experienced large losses under present conditions. However, properties that once experienced small losses saw the largest percentage increases in losses, as storm surge affected more properties further away from the coast. Nationwide, over 19 thousand more properties were affected by storm surge under RCP2.6 in the year 2040 than at the present, indicating that properties not currently under risk may soon be in the future.

Proprietary. This material may not be reproduced in any form without the express written permission of CoreLogic.

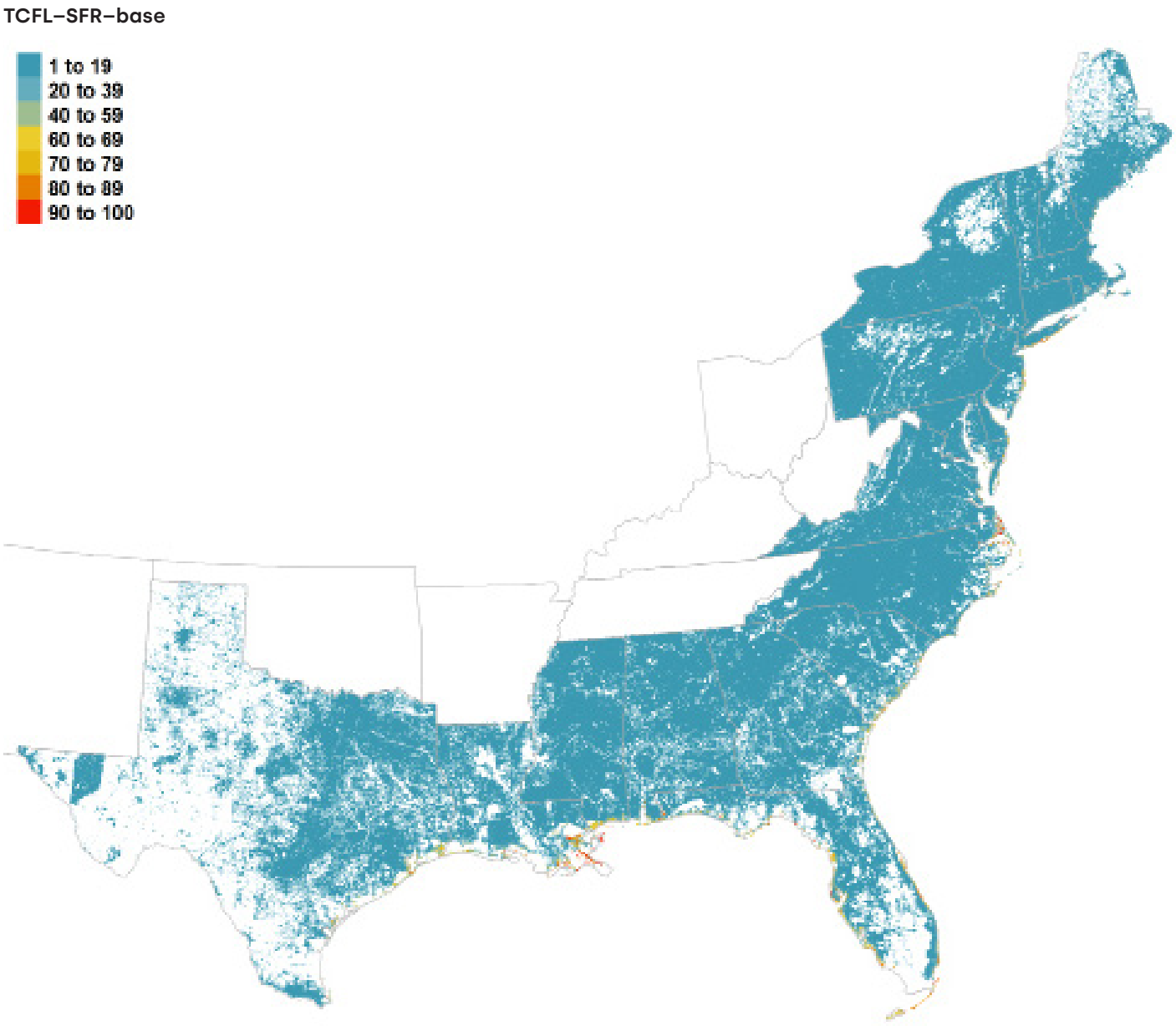


Figure 6: Baseline risk scores for Single-Family Residential (SFR) properties from Storm Surge peril.

Proprietary. This material may not be reproduced in any form without the express written permission of CoreLogic.

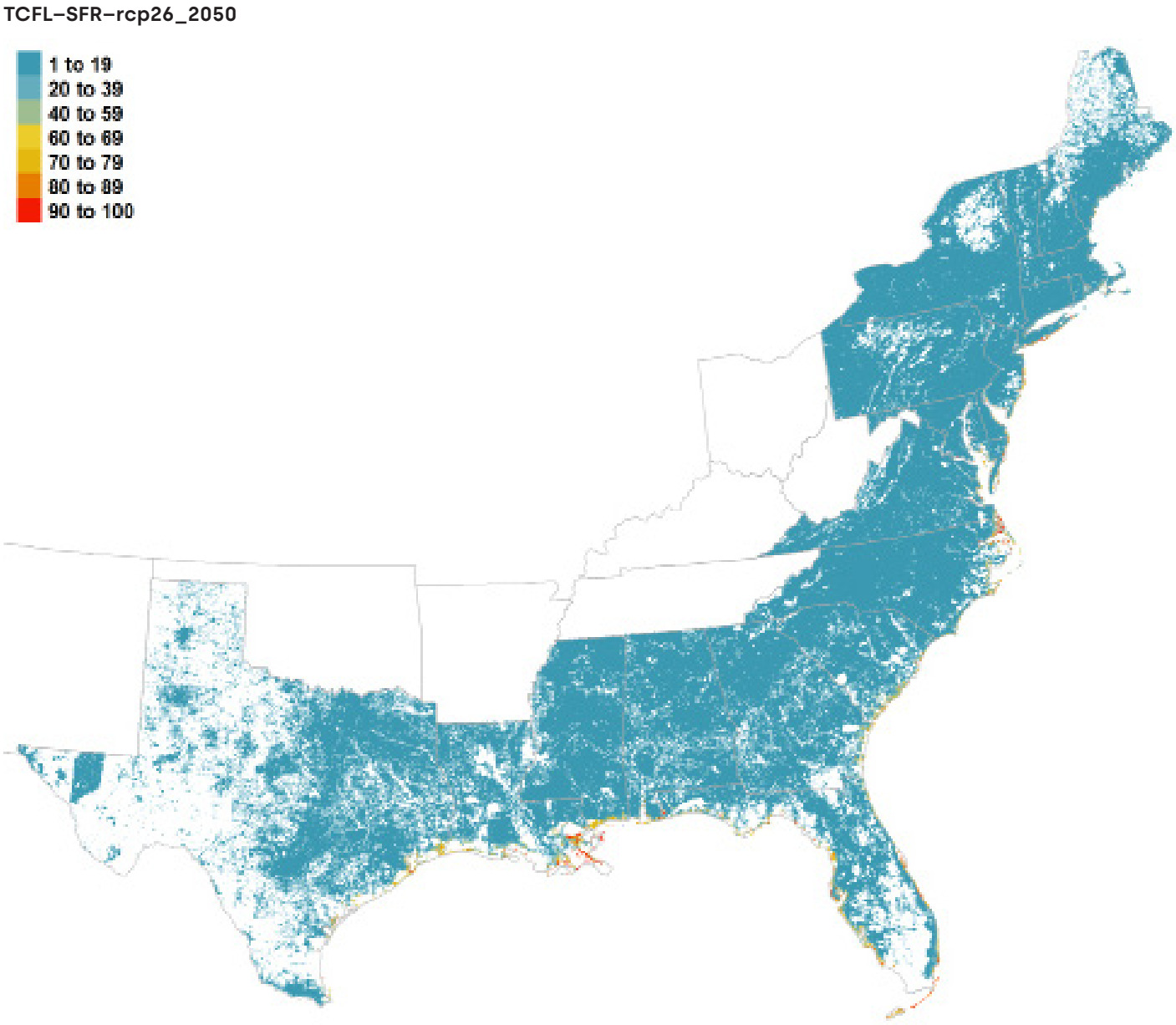


Figure 7: RCP2.6 risk scores at 2050 for Single-Family Residential (SFR) properties from Storm Surge peril.

Proprietary. This material may not be reproduced in any form without the express written permission of CoreLogic.

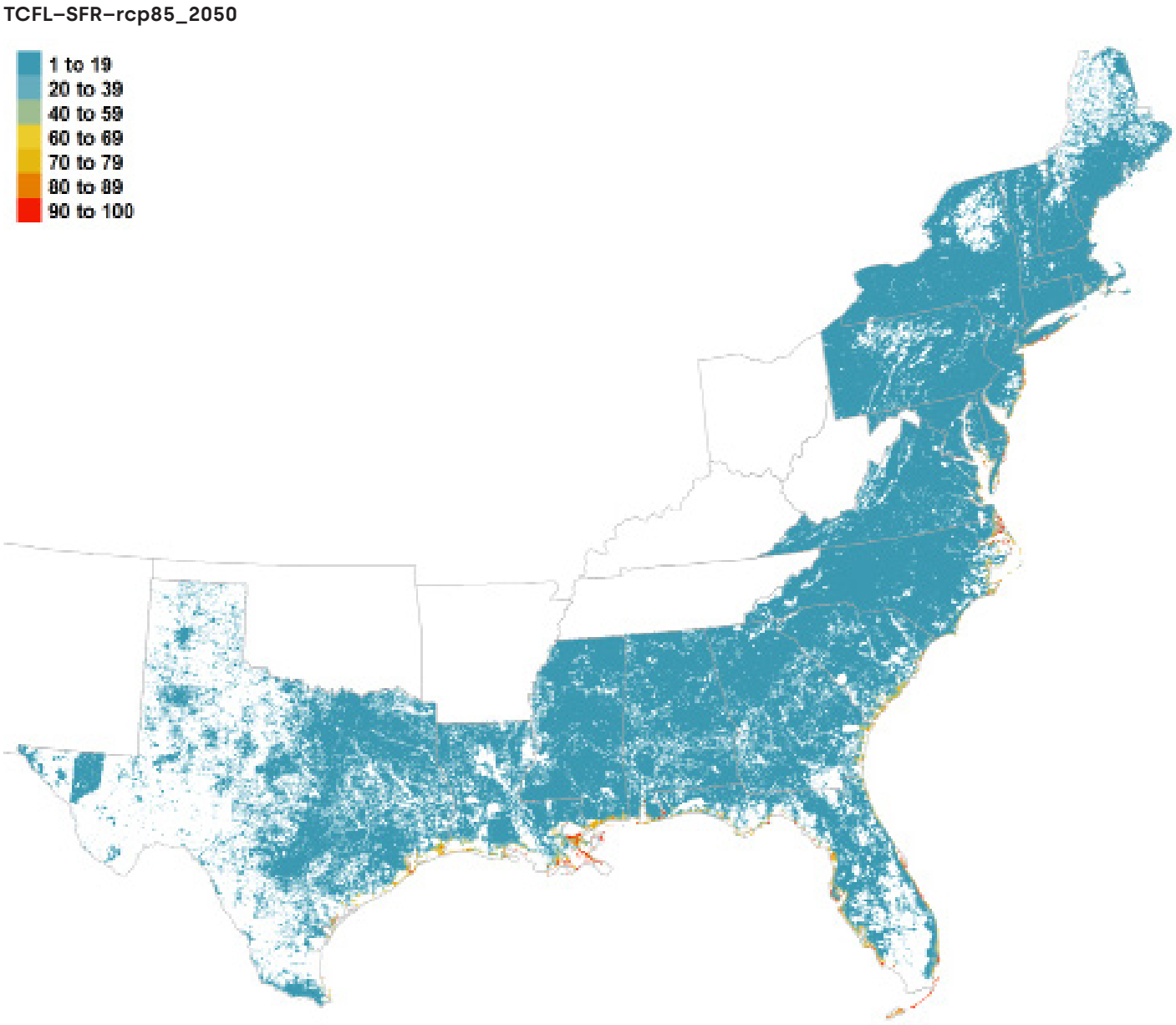


Figure 8: RCP8.5 risk scores at 2050 for Single-Family Residential (SFR) properties from Storm Surge peril.

Proprietary. This material may not be reproduced in any form without the express written permission of CoreLogic.

References

Fox-Kemper, B., H.T. Hewitt, C. Xiao, G. Aðalgeirsdóttir, S.S. Drijfhout, T.L. Edwards, ... & Y. Yu, 2021: Ocean,Cryosphere and Sea Level Change. In Climate Change 2021: The Physical Science Basis. Contribution of Working Group I to the Sixth Assessment Report of the Intergovernmental Panel on Climate Change [Masson-Delmotte, V., P. Zhai, A. Pirani, S.L. Connors, C. Péan, S. Berger, N. Caud, Y. Chen, L. Goldfarb, M.I. Gomis, M. Huang, K. Leitzell, E. Lonnoy, J.B.R. Matthews, T.K. Maycock, T. Waterfield, O. Yelekçi, R. Yu, and B. Zhou (eds.)]. Cambridge University Press, Cambridge, United Kingdom and New York, NY, USA, pp. 1211–1362, doi:10.1017/9781009157896.011

Kopp, R. E., Horton, R. M., Little, C. M., Mitrovica, J. X., Oppenheimer, M., Rasmussen, D. J., ... & Tebaldi, C. (2014). Probabilistic 21st and 22nd century sea-level projections at a global network of tide-gauge sites. Earth's future, 2(8), 383–406. doi:10.1002/2014EF000239

Hammond, W. C., Blewitt, G., Kreemer, C., & Nerem, R. S. (2021). GPS imaging of global vertical land motion for studies of sea level rise. Journal of Geophysical Research: Solid Earth, 126(7), e2021JB022355. doi:10.1029/2021JB022355

Murakami, H., Vecchi, G. A., Underwood, S., Delworth, T. L., Wittenberg, A. T., Anderson, W. G., ... & Zeng, F. (2015). Simulation and prediction of category 4 and 5 hurricanes in the high-resolution GFDL HiFLOR coupled climate model. Journal of Climate, 28(23), 9058–9079. doi:10.1175/JCLI-D-15-0216.1

Seneviratne, S.I., X. Zhang, M. Adnan, W. Badi, C. Dereczynski, A. Di Luca, ... & B. Zhou, 2021: Weather and Climate Extreme Events in a Changing Climate. In Climate Change 2021: The Physical Science Basis. Contribution of Working Group I to the Sixth Assessment Report of the Intergovernmental Panel on Climate Change [Masson-Delmotte, V., P. Zhai, A. Pirani, S.L. Connors, C. Péan, S. Berger, N. Caud, Y. Chen, L. Goldfarb, M.I. Gomis, M. Huang, K. Leitzell, E. Lonnoy, J.B.R. Matthews, T.K. Maycock, T. Waterfield, O. Yelekçi, R. Yu, and B. Zhou (eds.)]. Cambridge University Press, Cambridge, United Kingdom and New York, NY, USA, pp. 1513–1766, doi:10.1017/9781009157896.013.

Sweet, W.V., B.D. Hamlington, R.E. Kopp, C.P. Weaver, P.L. Barnard, D. Bekaert, ... & C. Zuzak, 2022: Global and Regional Sea Level Rise Scenarios for the United States: Updated Mean Projections and Extreme Water Level Probabilities Along U.S. Coastlines. NOAATechnical Report NOS 01. National Oceanic and Atmospheric Administration, National Ocean Service, Silver Spring, MD, 111 pp. https://oceanservice.noaa.gov/hazards/sealevelrise/noaa-nostechrpt01-global-regional-SLR-scenarios-US.pdf

Wang, O., Fukumori, I., & Fenty, I. (2017). An Overview of ECCO Version 4 Release 3's ftp Site ftp://ecco. jpl. nasa. gov/Version4/Release3. https://web.corral.tacc.utexas.edu/OceanProjects/ECCO/doc/v4r3_overview.pdf

Proprietary. This material may not be reproduced in any form without the express written permission of CoreLogic.

Severe Convective Storm

Introduction

A Severe Convective Storm (SCS) event is a weather phenomenon that occurs due to land surface heating, causing warm moist air to rise into the atmosphere. The three types of SCSs, Tornado, Hailstorm and Straight-line winds, are discussed below.

Tornado: Tornadoes are one of the most devastating natural hazards worldwide. Tornados are violently rotating columns of air, pendant from a cumuliform cloud or underneath a cumuliform cloud, and often (but not always) visible as a funnel cloud. Tornadoes tend to form with severe thunderstorms and most destructive and deadly tornadoes are often spawned by supercells. Tornadoes can last from several seconds to more than an hour, though most last less than 10 minutes.

Supercells are rotating thunderstorms with a well-defined radar circulation called a mesocyclone. They can also produce damaging hail, severe non-tornadic winds, unusually frequent lightning, and flash floods. Typically, the area of rotation in a supercell occurs in the south side of the storm and a low-hanging cloud base with rotation is often seen. This area may not always be visible since rain sometimes wraps around the area of circulation. Some tornadoes appear as a visible funnel extending only partially to the ground.

Hail: The strong convective updrafts in a developing thunderstorm or supercell can reach 100 mph, bringing substantial amounts of moisture and debris into the storm. The debris (aerosols, dust, dirt, insects) act as nuclei for the water to collect on, creating a tiny raindrop. As the new raindrop travels upward in the updraft, it collects more water droplets—a process called coalescence. Above the freezing point, which occurs mostly above 2 to 3 miles, solid particles (ice crystals, graupel) or supercooled water droplets collect on each other to become larger in size. At some point, the mass of the ice particle and the gravitational pull on it are balanced and the ice particle reaches the top of its journey and begins to fall to the ground in the form of hail, collecting more mass along the way. As it falls, it travels into warmer air.

Hail develops in most mid-latitude thunderstorms, often melting before reaching the ground. Severe hail is officially defined as being 1 inch or more in diameter. Even sub-severe hail may damage crops, which can be destroyed even by very small, wind-driven hail. Extremely severe hailstones can damage cars, ruin roofs, break windows, kill animals, and seriously hurt or kill humans. The largest hailstones can reach 6" in diameter, weigh 3.5 pounds, and hit the ground at 110 mph. The costliest thunderstorms in history have been supercells producing very large hail over metropolitan areas, such as the 1995 storm in Fort Worth, Texas.

Straight-line winds: Severe convective systems often produce straight-line winds. Straight-line winds include downbursts, microbursts, squall lines, and derechos. Downbursts form when rain-cooled air spreads in all directions after reaching the ground. A downburst concentrated over a smaller area is known as a microburst and can produce up to EF1 damage in a concentrated area. Squall lines are a collection of thunderstorms that often form along cold fronts and drylines and produce high winds. A derecho is a type of squall line that often forms bow patterns on radar and produces sustained winds of at least 58 mph. Derechos are more severe than other squall-lines. Straight-line winds cover much larger areas than tornadoes, but their winds are weaker (usually less than 85 mph).

This document describes the methodology used to modify the U.S. SCS model in CoreLogic's RQE (Risk Quantification & Engineering) catastrophe risk modeling software to reflect climate change impacts from the latest nationwide expansion project. The climate-coupled U.S. SCS model is used to generate the climate change versions of the future hazard data sets to assess climate change-related financial risks.

Proprietary. This material may not be reproduced in any form without the express written permission of CoreLogic.

Hazard Modeling

CoreLogic's U.S. Severe Convective Storm (SCS) Model is a probabilistic tornado/hail risk analysis model designed to estimate damage and insured losses to properties subjected to tornado, hail, and straight-line wind in the contiguous United States. Our U.S. Severe Convective Model uses radar data, upper atmospheric data, historical observations, and historical tornado/hail/straight-line wind data to develop the stochastic event set.

Stochastic Event Set: The foundation of the stochastic event set is a comprehensive reconstruction of observed events based on idealized tornado, hail, and wind footprints that are generated from the SPC (Storm Prediction Center) report database. The WVS (Weather Verification Services) forensic data-based footprints are used to guide and calibrate the idealized footprint generation process. The idealized footprints include centroids of hail/wind streaks, maximum hail size/wind speed, orientation of the streaks, and the width and length of the streaks. Regression functions are fitted to compute the magnitude of hail size or wind speed at distances from the centroid location. The relationships between maximum intensity and distance from storm center are based on climatology of storms in the forensic hail and wind database. Annually, hail and wind footprints show close agreement on a national scale with areas derived from the forensic models.

Development of the Stochastic Event Set: The radar data, upper atmospheric data, historical observations, and historical tornado/hail/straight-line wind data are used as a starting point to develop the frequency and severity distributions needed for modeling the peril. The completeness and reasonableness of the stochastic event set are the foundation of any stochastic model. The U.S. Severe Convective Storm Model stochastically simulates occurrences, location, severity, areal extent, and clustering of tornado, wind, and/or hail events. Tornado parameters such as width and path length are simulated and assigned to each tornado. Frequencies of stochastic events are assigned based on touchdown/swath locations, severity of hail/wind/tornadoes, and severe convective climatology derived from climate-conforming variables. These simulations result in local severe convective frequencies to be consistent with climatology and to have locally smooth variations of severe convective risk. More details on frequency and severity distribution methodology are provided below.

Frequency Distribution: CoreLogic has implemented a distinctive, rational approach to building the frequency distribution for events in the model. Rather than building the frequency distributions directly from the stochastic event set, location-specific target frequency distributions are built upon historical tornado touchdown characteristics from SPC reports (1955–2016) and eight years of high-resolution hail and wind footprints from CoreLogic's industry leading WVS group (2009–2016).

The underlying data was smoothed due to the limited spatial extent of individual storms and gaps in the database in terms of events location. Severity and frequency needed to be filled due to the sparseness of tornado/hail/wind historical data and since historical events may not be a good representation of future risk (i.e., future events may be different from the historical ones in terms of location, severity, and frequency). Traditionally, an isotropic filter is used to spatially smooth the underlying data with weights that are directionally uniform, irrespective of natural gradients in behavior. Although necessary, smoothing the observed frequency was done in a way that is physically consistent with long-term risk so as not to introduce locally unphysical severe storm risk characteristics.

The underlying frequency distributions for tornado, hail, and wind are smoothed using a novel technique called *Environmental-Conforming Smoothing*. The methodology identifies and preserves regions with naturally strong gradients in storm behavior while also sufficiently smoothing regions with naturally high variability using environmental atmospheric data at seven different altitudes and the historical severe weather reports. It is assumed that storms in similar environments have similar behaviors. The environment-conforming smoothing technique produces substantially more realistic zones of similar long-term risk than traditional isotropic spatial filters, especially in regions with complex terrain.

Proprietary. This material may not be reproduced in any form without the express written permission of CoreLogic.

Severity Distribution: Severity of tornadoes is usually defined in terms of its EF-scale, which determines the potential damage severity. The tornado EF-Scale distributions, gust wind speed distributions and hail size distributions are defined on a fine granular grid system covering the entire U.S., taking local effects into consideration. These distributions are smoothed spatially at the grid level. The modeled wind speed is defined as a 2-second averaged peak gust. A 200m-by-200m grid system is used to define tornado severity distributions to maximize geographical resolution of the hazard, consistency with physical events, and minimize model run-time/performance. Hail and wind events are modeled using calculated hazard at a point.

Vulnerability Modeling

The U.S. SCS vulnerability module calculates damage ratios for a given hazard intensity. Vulnerability curves, also known as damage functions, are defined separately for each different structure type and contain, for each value of intensity, a damage ratio value, and a corresponding coefficient of variation (COV).

Output of the vulnerability module is damage, typically expressed as a ratio, or percent, of the full replacement value. Damage is also known as "ground-up loss," because it represents losses before applying insurance policy structures, terms, and conditions. The vulnerability module significantly influences model results. These results will be most reliable when the input data most closely matches actual exposures. Vulnerability calculations are particularly sensitive to the classification of structure type, occupancy, height, age, cladding, and secondary structure modifiers (SSMs). Next, the vulnerability calculations are sensitive to the total insured value because it is the denominator for the calculation of damage as a ratio.

CoreLogic defines separate sets of vulnerability curves for each of three types of insurance coverage: building, contents, and time element.

Building vulnerability curves capture damage to non-movable elements of the building including but not limited to the structure, architecture, finishes, permanent equipment including ceilings, lights, windows, ductwork, etc. Thus, building vulnerability implicitly includes damage to those components which structural engineers historically classify as "nonstructural."

Contents vulnerability curves capture damage to components that could be removed from a building including but not limited to inventory, furniture, and specialty equipment such as fabrication machines.

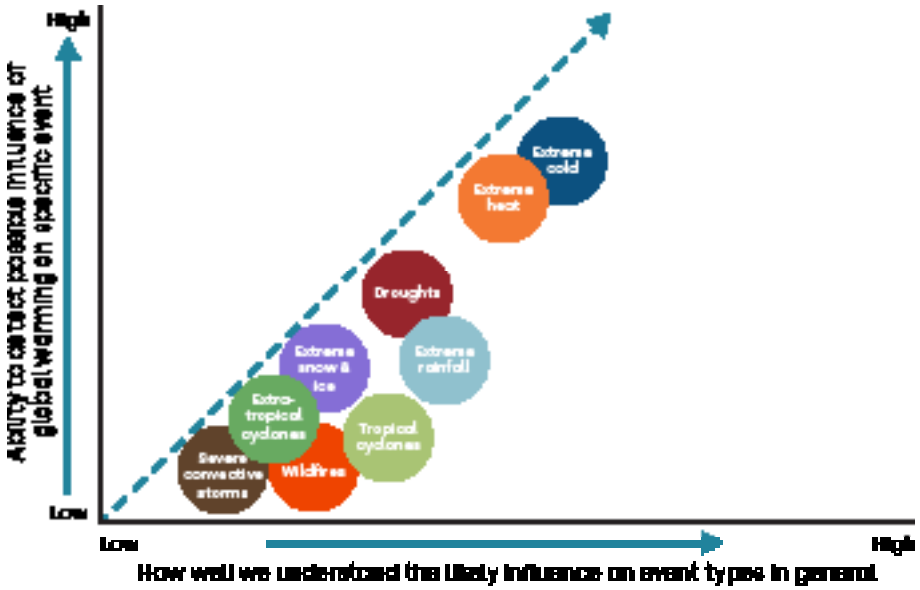
Damage to the contents housed in a building is estimated using vulnerability functions. Contents damage occurs because of breaches in the building's envelope or collapse. The contents vulnerability functions are defined for the same parameters that define building vulnerability functions, namely, occupancy, height, building material, age, and cladding.

Proprietary. This material may not be reproduced in any form without the express written permission of CoreLogic.

Climate Change Background

Although SCS events are widespread, evaluating their characteristics in the U.S during climate change is complex. Figure 9 below shows our general ability to detect climate change's impact on any weather extreme. As we see, the SCS events are one of the complex weather phenomena and to evaluate the effects of climate change on SCS is embedded with a lot of uncertainty Although SCS events are widespread, evaluating their characteristics in the U.S during climate change is complex. Figure 9 below shows our general ability to detect climate change's impact on any weather extreme. As we see, the SCS events are one of the complex weather phenomena and to evaluate the effects of climate change on SCS is embedded with a lot of uncertainty.

Relative confidence in attribution of different extreme events



NOAA Climate.gov, adapted from NAS 2016

Figure 9: Weather extremes and climate change attribution

However, recent developments in our physical understanding of SCS response to global warming and use of convection permitting models allowed us to quantity the changes in SCS favorable environment days in the future for different RCP scenarios. Because the SCSs are formed due to land surface heating, severity and frequency of these events are also projected to increase in a warmer world. Hoogewind et al. (2017) projects an increase in the frequency of hazardous convective weather (HCW) including tornadoes, hail, and wind gusts in the US by the end of this century. They also project an increase in the HCW season by more than a month by the end of the century. The frequency of large hailstorms (> 35 mm in diameter) is expected to increase across the US, with an increase in frequency of very large hailstorms (> 50mm diameter) in the Central US (Trapp et al., 2019). Environmental conditions favoring the formation of SCSs are also expected to increase the frequency of events in the order of 5–20% with 1°C rise in global temperature, with some regional differences (Lepore et al., 2021). Climate models project intense summertime mesoscale storm frequency to triple by the end of the century across much of North America (Prein et al., 2017). The combination of extreme precipitation and significant spreading of regions impacted by heavy rainfall is projected to increase the total volume of precipitation from mesoscale storms by 80%.

Climate Change Modeling

In our AR5 version of the climate change risk analytics, we modeled changes in the number of SCS days using high-resolution data from convection-permitting dynamical downscaling models. The current modeling approach involves the implementation of SCS frequency and severity changes at the regional level. Furthermore, our current modeling includes the implementation of seasonal changes in SCSs. Our current SCS modeling involves implementing improved climate change data with partnerships from different scientific groups across the U.S.

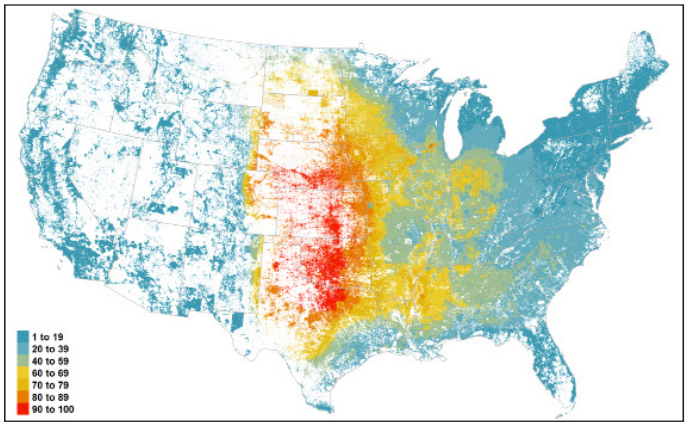
Proprietary. This material may not be reproduced in any form without the express written permission of CoreLogic.

Model Validation

Based on the WRF downscaled GCM data, we estimated the percentage change in the number of SCS days for six different regions and for four different seasons. Our projections cover three different time horizons and RCP scenarios. It is projected that the main regions of Southern Great Plains, Northern Great Plains and Midwest will see a minimum of 48% increase in number of severe convective days in the June, July, August (JJA) season. Under climate change, it is projected that the convective season will be longer, resulting in an increase in the total number of severe convective days in a year.

Our projections show that the number of SCS events increase in the future over every region in the U.S. This increase in hazard translates to varying losses by region. Figure 10 shows comparison of the risk score generated by CoreLogic for SCS peril. The risk from SCS events is projected to increase for the Central to Midwest regions in the U.S incurring more losses in the future worst-case climate scenario.

STTH–SFR–base



STTH–SFR–rcp85_2050

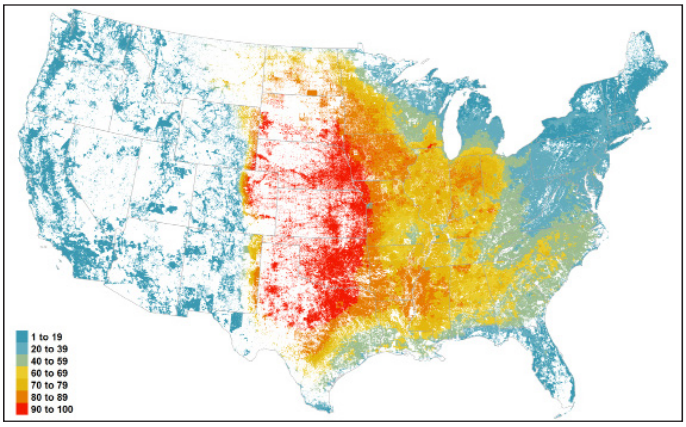


Figure 10: Comparison of risk scores from SCS peril for base case and RCP8.5 2050 scenarios for single-family residential properties.

Proprietary. This material may not be reproduced in any form without the express written permission of CoreLogic.

References

Hoogewind et al., 2017. The Impact of Climate Change on Hazardous Convective Weather in the United States: Insight from High-Resolution Dynamical Downscaling. *Journal of Climate*, 30: 10081–10100.

Prein et al., 2017. Increases rainfall volume from the future convective storms in the US. Nature Climate Change, 7: 880–884.

Lepore, C., Abernathey, R., Henderson, N., Allen, J. T., & Tippett, M. K. (2021). Future global convective environments in CMIP6 models. *Earth's Future*, 9(12), e2021EF002277.

Trapp, R. J., Hoogewind, K. A., & Lasher-Trapp, S. (2019). Future changes in hail occurrence in the United States determined through convection-permitting dynamical downscaling. *Journal of Climate*, 32(17), 5493– 5509.

Proprietary. This material may not be reproduced in any form without the express written permission of CoreLogic.

Winter Storms

Introduction

In the United States, each year, from November to April, the northern branch of the jet stream dips to the south, bringing cold polar air into the Midwest and Southern Great Plains states. The counter-clockwise rotation around a low-pressure center allows warm, moist air from the south to flow northward on the eastern side of the low. Frigid air from the north is drawn southward, behind the low-pressure center. Sufficiently cold air and abundant moisture are two ingredients necessary to fuel a winter storm system, which normally covers thousands of miles.

The types of precipitation that can fall from a winter storm include snow, sleet, freezing rain, and rain. The precipitation type that reaches the ground depends on the air mass structure through which the precipitation falls, with the depth of the warm layer and temperature at ground level affecting the proportions of liquid and frozen precipitation, as well as the density of the frozen material. This is important to note, as the weight of 1 inch of ice can be greater than 10 inches of new fallen snow. Many types of weather-related damage can occur depending on the rate of precipitation and its composition.

Hazard Modeling

The U.S. Winter Storm Model uses a stochastic event set of more than 11,500 events. This event set includes an extensive catalog of winter storm historical events from various sources, such as the Solar and Meteorological Surface Observation Network and hourly stations, Historical Climatology Network (HCN) and COOP stations. Three hazard parameters are incorporated in the model: 1) snow depth (major structural damage), 2) snow and ice thickness (light to minor damage), and 3) wind speed (wind damage).

Vulnerability Modeling

The stochastic event set of historical winter storms currently accounts for a composite of weather related damage, including roof and other direct structural damage from wind and heavy snow and ice, as well as interior damage from water leaks and burst pipes. The vulnerability functions for the different structural and occupancy types are based on extensive claims data collected from the re/insurance industry and observation data. Multiple damage types are represented in the U.S. Winter Storm Model.

Roof damage due to snow accumulation: Sheltered snow may not slide off roofs, while wind-blown snow can quickly accumulate in drifts exceeding multiple times the local precipitation. In both cases the weight load surpasses the structural capacity of the roof. Additionally, certain types of roof construction are more susceptible to damage from snow accumulation, including "lean-tos," shingled roofs, and roofs with valleys in their architecture.

Frozen and ruptured pipes: Prolonged freezing events and inadequate insulation of a home's extremities can lead to pipes bursting, which will flood the home in areas such as crawl spaces and outside walls. This flood water can also enter the living space, causing damage to floors, walls, and décor.

Ice dam / eave icing: Ice formation on roofs and in gutters can prevent melting snow from draining. When temperatures drop, melted snow can re-freeze on eaves and create ice dams or icicles, which can block drainage and cause water to seep into the home, resulting in interior damage to floors and furniture, as well as rot and mold within walls.

Proprietary. This material may not be reproduced in any form without the express written permission of CoreLogic.

Climate Change Background

Winter storms cause over $3 billion of insured damage to structures annually at present, however the total economic losses for individual storms can be an order of magnitude higher when they occur in regions ill equipped to handle winter weather. With climate change, climate extremes can be enhanced at both ends of the temperature spectrum. While the lower latitudes are expected to see large drops in days below freezing over the next few decades, northern regions will retain freezing conditions in the wintertime, even as wintertime average temperatures moderate. In addition, precipitation rates are expected to increase for all U.S. regions, as a warmer atmosphere can hold more moisture (Douville et al., 2021). More extreme precipitation in the wintertime may make severe winter storms more likely for certain regions. Additionally, southern excursions of the polar jet stream that bring winter storm conditions to the U.S. may be enhanced by atmospheric circulation changes, allowing for far-reaching impacts that extend down to the Southern Great Plains.

Climate Change Modeling

The climate change versions of the CoreLogic winter storm model incorporate the effects of expected changes in storm frequency by examining heavy frozen precipitation in regional climate models under the guidelines of U.S. National Weather Service (NWS) standards. CORDEX regional modeling (Giorgi et al., 2009) using WRF, RegCM4, canRCM4, CRCM5, REMO, and RCA4 downscaled global circulation model variables from CMIP5 over North America. All CORDEX models specified by the Intergovernmental Panel on climate change's (IPCC) Interactive Atlas were considered in the ensemble average of daily precipitation and temperature.

The observed number of frost days, where temperatures dip below freezing, was calculated directly from the CORDEX data, while daily historical observed precipitation data from the Global Precipitation Climatology Centre (GPCC) (Schneider et al., 2008) was shifted to the future climate using CORDEX precipitation rates. This was done to preserve the number of wet days and only shift the magnitude of precipitation rates, as certain climate models have been found to suffer from a "drizzle effect" where they experience many days of minor precipitation. In combination, these sources allowed for an assessment in changes in extreme daily frozen precipitation for different future time horizons and carbon emissions pathways.

For each location in the U.S. and for each season, the frequency of extreme precipitation events equal to or greater than the minimum criteria set by the National Weather Service (NWS) for a severe winter storm warning were computed for the historical period using the GPCC daily data. Next these GPCC events were computed after modifying them to account for changes in the extreme precipitation modeled by the CORDEX ensemble members, leading to many U.S. regions experiencing heavier precipitation under future climate change than they do at present. The combined occurrences of a frost day and heavy precipitation beyond the NWS threshold were used to determine the locations and frequencies of severe winter storms in the CoreLogic event set under future climate change.

Model Validation

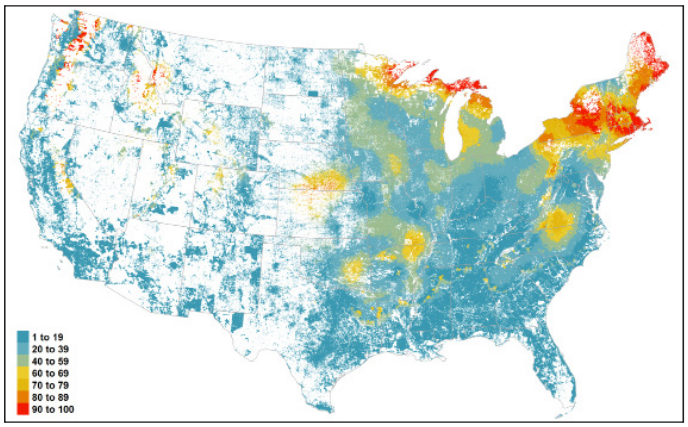
Verification of the storm detection algorithm's ability to reproduce the historical frequency of severe winter storm events was performed by comparing the annual frequency of storms in CoreLogic's RQE to the average number of storms detected using GPCC precipitation and CORDEX regional climate model days below freezing. The nationwide average over 1995–2020 from the detection algorithm of 20.0 storms per year compared favorably with the average frequency from RQE of 20.4 storms per year.

Additionally, regional patterns and magnitudes of winter storm frequency changes were found to correspond well with published studies for the Northern Hemisphere using an ensemble of CMIP5 models (Danco et al., 2016) and Eastern North America using the Geophysical Fluid Dynamics Laboratory (GFDL) Forecast-Oriented Low Ocean Resolution (FLOR) model (Janoski et al., 2018).

Proprietary. This material may not be reproduced in any form without the express written permission of CoreLogic.

These future scenarios for changes in winter storm events were then run for CoreLogic's national property portfolio to assess losses, which corresponded well with the regional frequency changes calculated for the underlying events. The nonlinear interaction between shifts in days below freezing and extreme precipitation led to declines in winter storm frequencies in some regions, as well as a delayed feedback in frequency increases for some regions, as more precipitation won out over milder temperatures in later decades.

STTH–SFR–base



STTH–SFR–rcp85_2050

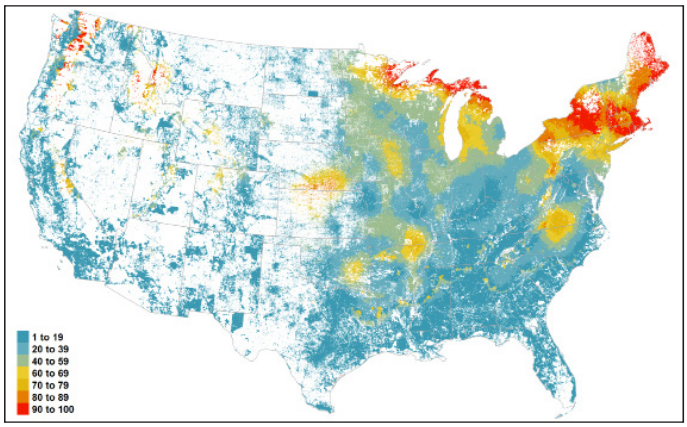


Figure 11: Comparison of risk scores from Winter Storm peril for base case and RCP8.5 2050 scenarios for single-family residential properties.

Proprietary. This material may not be reproduced in any form without the express written permission of CoreLogic.

References

Danco, J. F., DeAngelis, A. M., Raney, B. K., & Broccoli, A. J. (2016). Effects of a warming climate on daily snowfall events in the Northern Hemisphere. Journal of Climate, 29(17), 6295–6318.

Douville, H., K. Raghavan, J. Renwick, R.P. Allan, P.A. Arias, M. Barlow, ...& O. Zolina (2021). Water Cycle Changes. In Climate Change 2021: The Physical Science Basis. Contribution of Working Group I to the Sixth Assessment Report of the Intergovernmental Panel on Climate Change [Masson-Delmotte, V., P. Zhai, A. Pirani, S.L. Connors, C. Péan, S. Berger, N. Caud, Y. Chen, L. Goldfarb, M.I. Gomis, M. Huang, K. Leitzell, E. Lonnoy, J.B.R. Matthews, T.K. Maycock, T. Waterfield, O. Yelekçi, R. Yu, and B. Zhou (eds.)]. Cambridge University Press, Cambridge, United Kingdom and New York, NY, USA, pp. 1055–1210. doi:10.1017/9781009157896.010

Giorgi, F., Jones, C., & Asrar, G. R. (2009). Addressing climate information needs at the regional level: the CORDEX framework. World Meteorological Organization (WMO) Bulletin, 58(3), 175. http://wcrp.ipsl.jussieu.fr/cordex/documents/CORDEX_giorgi_WMO.pdf

Janoski, T. P., Broccoli, A. J., Kapnick, S. B., & Johnson, N. C. (2018). Effects of climate change on wind-driven heavy-snowfall events over eastern North America. Journal of climate, 31(22), 9037–9054.

Karl, T., & Koss, W. J. (1984). Regional and national monthly, seasonal, and annual temperature weighted by area, 1895–1983. https://www.ncei.noaa.gov/access/monitoring/reference-maps/us-climate-regions

Schneider, U., Fuchs, T., Meyer-Christoffer, A., & Rudolf, B. (2008). Global precipitation analysis products of the GPCC. Global Precipitation Climatology Centre (GPCC), DWD, Internet Publikation, 112.

Proprietary. This material may not be reproduced in any form without the express written permission of CoreLogic.

Wildfires

Introduction

A wildfire is a self-sustaining combustion of vegetative fuel across a landscape. Wildfires spread across the landscape in response to the fire environment—fuel, weather, and topography. The wildfire conditions we observe today are a result of previous forest disturbance centuries ago. Successful fire suppression campaigns in the past have created dense, overly vegetated forests in most of the West leading to continuous layers of thick vegetation. Pairing this with fire has led to very severe crown fires that burn large swaths of forested landscapes.

The current CoreLogic U.S. Wildfire Model is a fully probabilistic model, covering 14 states in the contiguous United States. The states covered are Arizona, California, Colorado, Florida, Idaho, Montana, Nevada, New Mexico, Oklahoma, Oregon, Texas, Utah, Washington, and Wyoming. It considers multiple ignition sources and models the spread of wildland fires into urbanized areas in the United States.

Hazard Modeling

CoreLogic's wildfire hazard model considers multiple sources of ignition. The wildfire ignition model incorporates aspects of both natural and human influences on the wildfire hazard. The ignition model is based on spatially and temporally smoothed historical wildfire ignition data. The data covers natural and man-made ignition sources, and the model generates stochastic ignitions during the simulation.

A robust definition of wildfire hazard can be based on the three components of the fire behavior triangle. Wildfire propagation is dependent on: 1) the available fuel load, 2) the topography of the area, and 3) the prevailing weather conditions, such as temperature, humidity, and winds. These conditions and others are explicitly modeled.

Vulnerability Modeling

The vulnerability module relates the hazard intensity, or severity, to the cost of repairing the ensuing damage. It does that for a specified exposure at a particular site. The module outputs the damage information, typically expressed as a ratio, or percent, of the full replacement value. CoreLogic characterizes the degree of fire vulnerability or building damage based on primary characteristics like the structure type, occupancy type, age, and number of stories, and secondary structural modifiers such as vegetation clearance, roofing fire class, and the presence of fire resistive windows or siding.

Climate Change Background

Wildfires are naturally occurring phenomena in California and most of the Western United States, though climate change is exacerbating the negative effects of wildfire. Climate change is increasing wildfire frequency and severity. Earlier spring snowmelt has lengthened the fire season and led to more wildfire activity (Westerling et al., 2006). Increases in temperature and vapor pressure deficit have enhanced fuel aridity leading to increased wildfire activity and wildfire burned area (Abatzogloud and Williams, 2011).

Changing climate conditions and human development factors have modified the risk of large wildfires for different geographic regions and dominant vegetation types in the contiguous United States. Warmer temperatures and altered wind patterns may lead to more frequent fire weather conditions. Changes in precipitation and runoff modify fuel conditions. Meteorological projections alone are a poor metric for this changing risk, as increased air temperatures are insufficient to explain the spatial changes in wildfire frequencies over the historical period or under future climate change, not accounting for crucial factors like population growth and land cover change. Since 80% of fires are human caused, human development on the wildland urban interface and encroachment into wilderness puts the main source of wildfire ignition in greater contact with available fuel stock.

Proprietary. This material may not be reproduced in any form without the express written permission of CoreLogic.

Climate Change Modeling

The climate change version of the CoreLogic wildfire model considers statistical data derived from California's Fourth Climate Change Assessment (Westerling, 2018), as well as climate-shifted data from Missoula Fire Sciences Laboratory's FSim burn probability model (Thompson et al., 2011). This data was used to determine changes in annual burn probability (ABP) for different fire intensity levels (FIL) and frequencies of large wildfires of varying size classes.

The California Fourth Assessment data were derived from a downscaling of meteorological and hydrological data using the Localized Constructed Analogs (LOCA) statistical technique (Pierce et al., 2014) for four CMIP5 climate models (CanESM2, CNRM-CM5, HadGEM2-ES, and MIROC5). These meteorological drivers were then combined with changes in vegetation and human population to derive a stochastic dataset of wildfire perimeters for the entire state.

The U.S. Forest Service FSim model simulates hundreds of thousands of large wildfire events over the course of many synthetic seasons. These seasons combine historical weather, terrain, and fuel conditions. Fire suppression is also accounted for in the model. Aggregating the fire perimeters from these synthetic seasons allows for an estimate of the annual burn APB of every grid cell in the model domain, which covers the Continental U.S. at 270m resolution. The pattern of ABP reflects the general likelihood of a fire occurrence across the landscape and can be combined with probabilities of various FIL. These intensity levels are based on categories of flame lengths calculated from the FSim model and give an estimate of the likelihood of a certain intensity of burn, assuming there is already an active fire.

Given that the FSim model produces estimates of ABP based on historical wildfire occurrence and upon calibration against observed fire distributions, the differences in ABP from one grid cell to the next can be explained by variations in regional climate and human activities, as well as by terrain and land cover. In this methodology, climate and human drivers of present-day fire occurrence are isolated and used to construct a surrogate model of APB for three separate classes of FIL. The surrogated approach developed here by CoreLogic leverages statistical models trained on present conditions to produce shifted FSim burn probability fields using future meteorological variables from CORDEX and human development variables from NASA's SEDAC following the IPCC's Shared Socioeconomic Pathways (Samir and Lutz, 2017).

Model Validation

The four models employed in the California Fourth Climate Assessment, the CanESM2, CNRM-CM5, HadGEM2-ES, and MIROC5, were all previously selected due to their good regional performance across the state (Pierce et. al. 2018). In addition, the Measuring Trends in Burn Severity (MTBS) dataset, a multiagency effort to consistently document historical wildfire occurrence, was used to validate trends and patterns for the state, in both wildfire frequency and annual acres burned.

Similarly, for the contiguous U.S. the MTBS dataset was considered nationwide for the 128 pyromes, regions with unique wildfire regimes as defined by the U.S. Forest Service. These were compared with the surrogate model's outputs when climate shifted to the period 1986–2005, finding good agreement in the spatial patterns. Future projections of annual acres burned from the climate-shifted Fsim model were also compared to the California Fourth Assessment projections (Westerling, 2018), as well as regional projections for the Greater Yellowstone region (Westerling et al., 2011), to ensure consistency between this product and existing climate change projections.

Proprietary. This material may not be reproduced in any form without the express written permission of CoreLogic.

FIXX–SFR–base

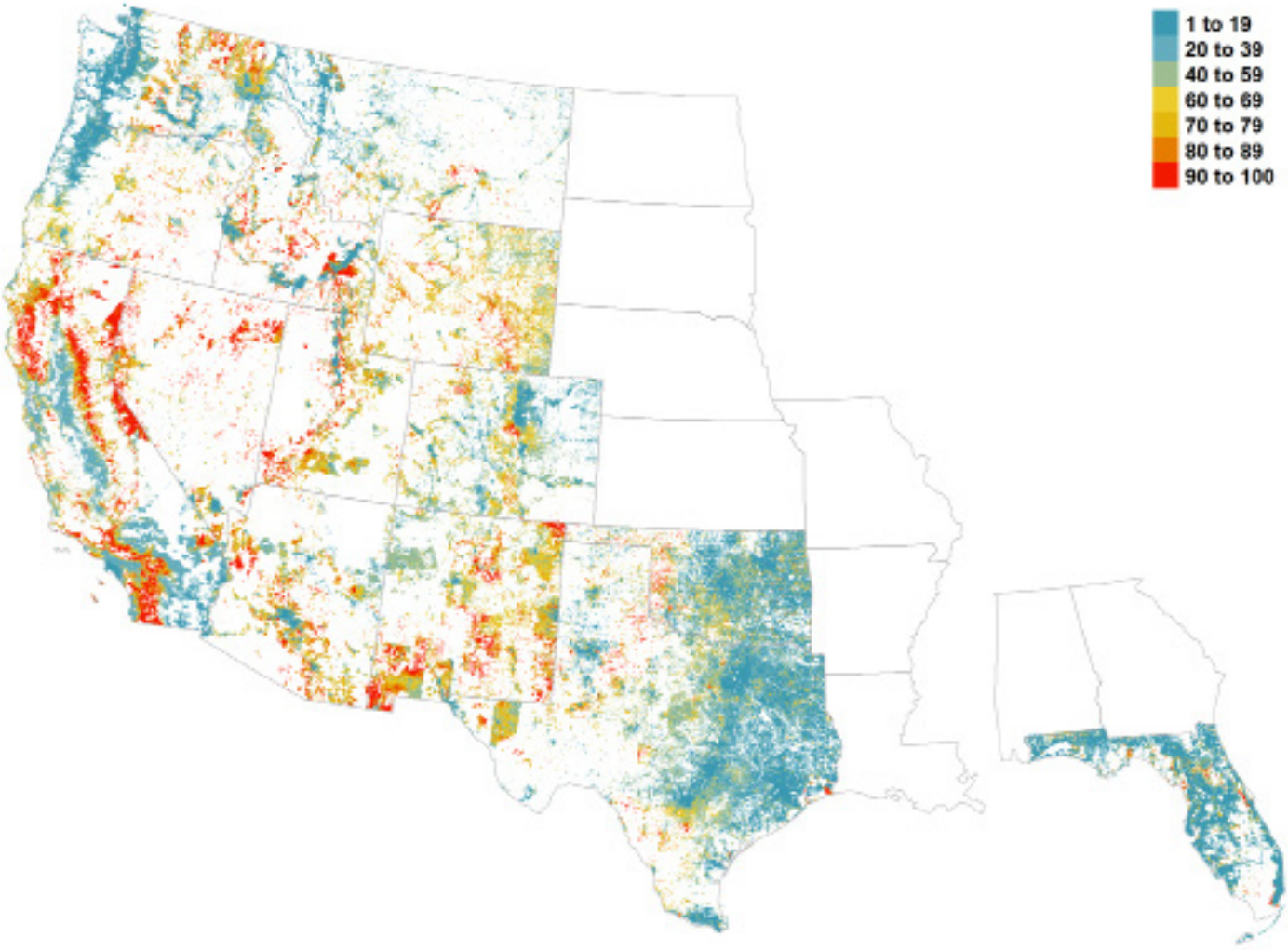


Figure 12: Baseline risk scores for Single-Family Residential (SFR) properties from Wildfire peril.

Proprietary. This material may not be reproduced in any form without the express written permission of CoreLogic.

FIXX–SFR–rcp85_2050

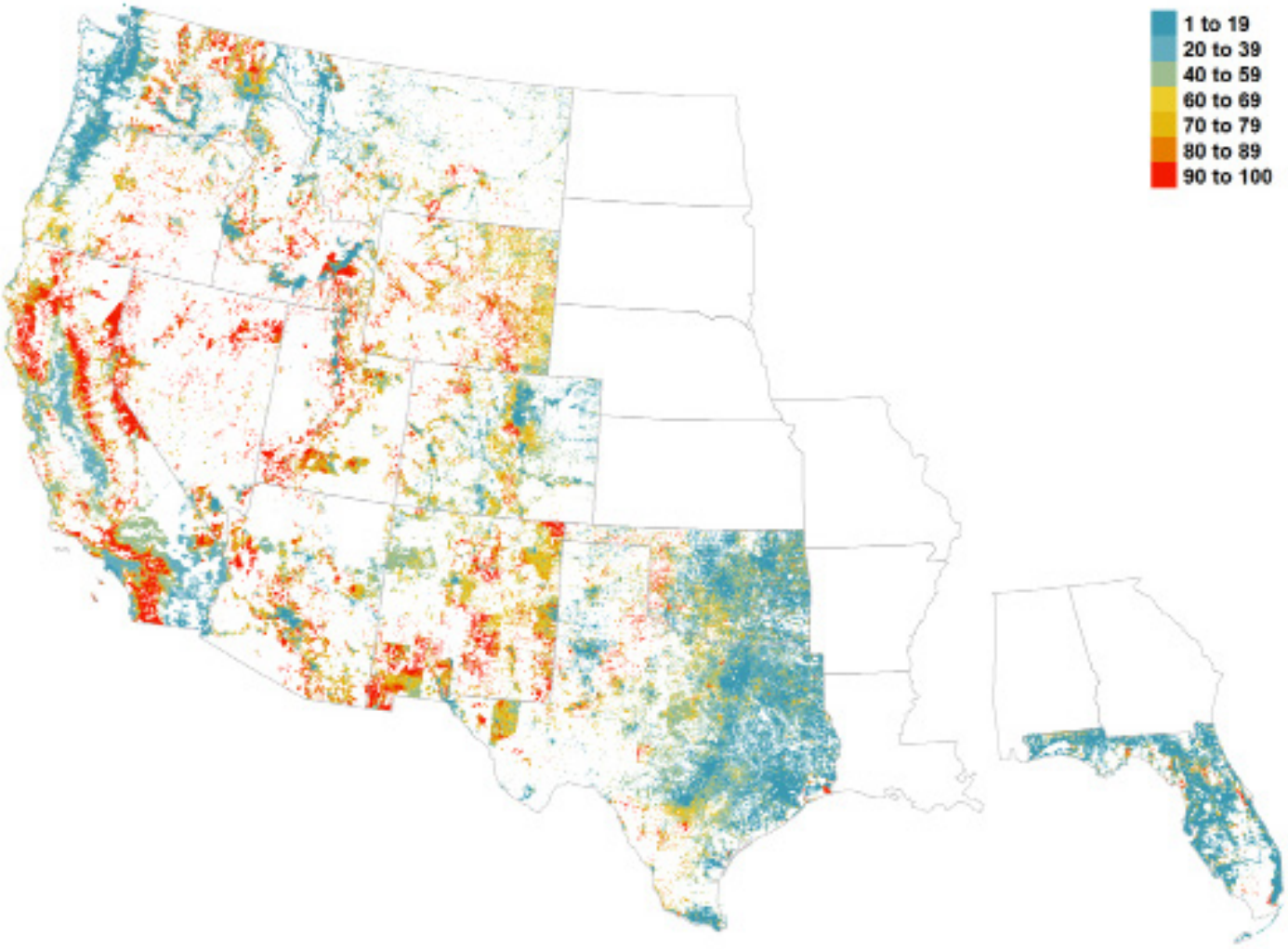


Figure 13: RCP8.5 risk scores at 2050 for Single-Family Residential (SFR) properties from Wildfire peril.

Proprietary. This material may not be reproduced in any form without the express written permission of CoreLogic.

References

Abatzoglou, J. T., & Williams, A. P. (2016). Impact of anthropogenic climate change on wildfire across western US forests. Proceedings of the National Academy of Sciences, 113(42), 11770–11775. doi:10.1073/pnas.1607171113

Giorgi, F., Jones, C., & Asrar, G. R. (2009). Addressing climate information needs at the regional level: the CORDEX framework. World Meteorological Organization (WMO) Bulletin, 58(3), 175. http://wcrp.ipsl.jussieu.fr/cordex/documents/CORDEX_giorgi_WMO.pdf

Hansen, M. C., DeFries, R. S., Townshend, J. R., & Sohlberg, R. (2000). Global land cover classification at 1 km spatial resolution using a classification tree approach. International journal of remote sensing, 21(6–7), 1331–1364. doi:10.1080/014311600210209

Pierce, D.W., D.R. Cayan and B.L. Thrasher, (2014). Statistical Downscaling Using Localized Constructed Analogs (LOCA). Journal of Hydrometeorology, 15,2558–2585. doi:10.1175/JHM-D-14-0082.1

Samir, K. C., & Lutz, W. (2017). The human core of the shared socioeconomic pathways: Population scenarios by age, sex, and level of education for all countries to 2100. Global Environmental Change, 42, 181–192. doi:10.1016/j.gloenvcha.2014.06.004

Thompson, M. P., Calkin, D. E., Finney, M. A., Ager, A. A., & Gilbertson-Day, J. W. (2011). Integrated national-scale assessment of wildfire risk to human and ecological values. Stochastic Environmental Research and Risk Assessment, 25(6), 761–780. doi: 10.1007/s00477-011-0461-0

Westerling, A. L., Hidalgo, H. G., Cayan, D. R., & Swetnam, T. W. (2006). Warming and earlier spring increase western US forest wildfire activity. science, 313(5789), 940–943. doi:10.1126/science.1128834

Westerling, A. L., Turner, M. G., Smithwick, E. A., Romme, W. H., & Ryan, M. G. (2011). Continued warming could transform Greater Yellowstone fire regimes by mid-21st century. Proceedings of the National Academy of Sciences, 108(32), 13165–13170. doi:10.1073/pnas.111019910

Westerling, A. L. (2018). Wildfire Simulations for California's Fourth Climate Change Assessment: Projecting Changes in Extreme Wildfire Events with a Warming Climate: a Report for California's Fourth Climate Change Assessment (p. 57). Sacramento, CA: California Energy Commission. http://ibecproject.com/PREDEIR_0002479.pdf

Proprietary. This material may not be reproduced in any form without the express written permission of CoreLogic.

About CoreLogic

CoreLogic is a leading provider of property insights and innovative solutions, working to transform the property industry by putting people first. Using its network, scale, connectivity and technology, CoreLogic delivers faster, smarter, more human-centered experiences, that build better relationships, strengthen businesses, and ultimately create a more resilient society. For more information, please visit www.corelogic.com.

40 Pacifica, Ste. 900
Irvine, CA 92618

For more information, please call 866.774.3282.

©2024 CoreLogic, Inc. All Rights Reserved.

CoreLogic, the CoreLogic logo and RQE are trademarks of CoreLogic, Inc. and/or its subsidiaries.
All other trademarks are the property of their respective holders.

References for Supplemental Sections

37. National Centers for Environmental Information. *Storm Data* www.ncdc.noaa.gov/IPS/sd/sd.html.

38. Arizona State University Center for Emergency Management and Homeland Security. *SHELDUS Metadata* cemhs.asu.edu/sheldus/metadata.

39. Wiese, P. *Trends in Normalized Weather-Related Property Losses in the United States: 1960–2018* (Society of Actuaries, 2020).

40. Gall, M., Borden, K. A. & Cutter, S. L. When Do Losses Count?: Six Fallacies of Natural Hazards Loss Data. *Bulletin of the American Meteorological Society* **90,** 799–810 (2009).

41. First Street. *Models and Methodlogy* Accessed April 2024. https://firststreet.org/methodology.

42. Discussion with representatives from First Street. 2022.

43. Emrich, C. T. & Cutter, S. L. Social Vulnerability to Climate-Sensitive Hazards in the Southern United States. *Weather, Climate, and Society* **3,** 193–208 (2011).

44. Leichenko, R. & Silva, J. A. Climate change and poverty: vulnerability, impacts, and alleviation strategies. *WIREs Climate Change* **5,** 539–556 (2014).

45. Hallegatte, S. & Rozenberg, J. Climate change through a poverty lens. *Nature Climate Change* **7,** 250–256 (2017).

46. Cutter, S. L. & Finch, C. Temporal and spatial changes in social vulnerability to natural hazards. *Proceedings of the National Academy of Sciences* **105,** 2301–2306 (2008).